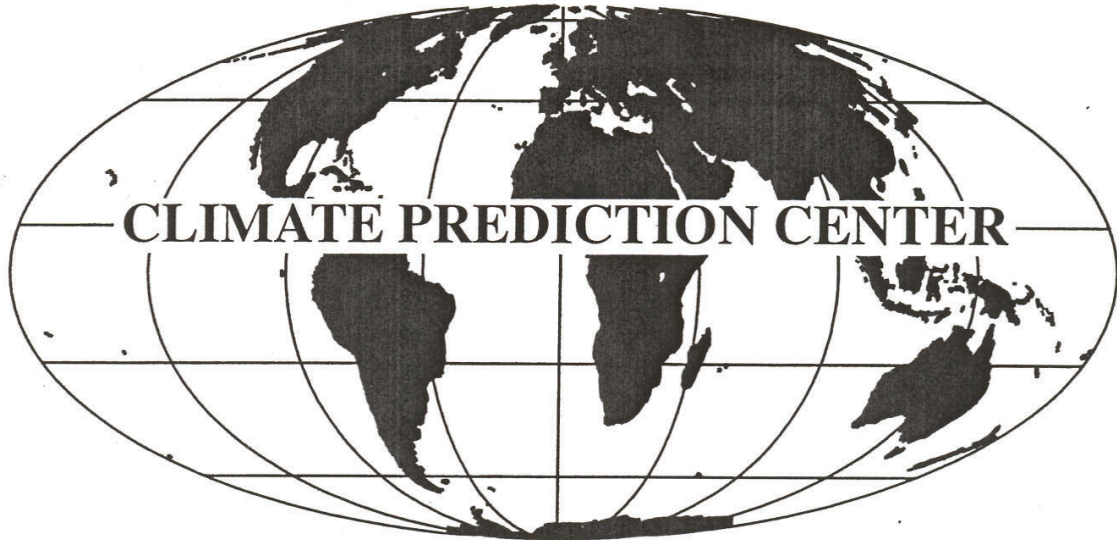


# CLIMATE DIAGNOSTICS BULLETIN



## SEPTEMBER 2018

NEAR REAL-TIME OCEAN / ATMOSPHERE

Monitoring, Assessments, and Prediction

**U.S. DEPARTMENT OF COMMERCE**  
**National Oceanic and Atmospheric Administration**  
**National Weather Service**  
**National Centers for Environmental Prediction**

## CLIMATE DIAGNOSTICS BULLETIN



**CLIMATE PREDICTION CENTER**  
**Attn: Climate Diagnostics Bulletin**  
**Room 3116, NCWCP**  
**5830 University Research Court**  
**College Park, MD 20740**

**Chief Editor:** Gerald D. Bell

**Editors:** Wei Shi, Michelle L'Heureux, and Michael Halpert

**Bulletin Production:** Wei Shi

**External Collaborators:**

Center for Ocean-Atmospheric Prediction Studies (COAPS)  
Cooperative Institute for Research in the Atmosphere (CIRA)  
Earth & Space Research  
International Research Institute for Climate and Society (IRI)  
Joint Institute for the Study of the Atmosphere and Ocean (JISAO)  
Lamont-Doherty Earth Observatory (LDEO)  
NOAA-CIRES, Climate Diagnostics Center  
NOAA-AOML, Atlantic Oceanographic and Meteorological Laboratory  
NOAA-NESDIS-STAR, Center for Satellite Applications and Research  
NOAA-NDBC, National Data Buoy Center  
Scripps Institution of Oceanography

**Software:** Most of the bulletin figures generated at CPC are created using the Grid Analysis and Display System (GrADS).

**- Climate Diagnostics Bulletin available on the World Wide Web**

The CDB is available on the World Wide Web. The address of the online version of the CDB is:

**<http://www.cpc.ncep.noaa.gov/products/CDB>**

If you have any problems accessing the bulletin, contact Dr. Wei Shi by E-mail:

*Wei.Shi@noaa.gov*

# Table of Contents

## TROPICS

Highlights . . . . . page 6  
 Table of Atmospheric Indices . . . . . page 7  
 Table of Oceanic Indices . . . . . page 8

## FIGURE

|  |           |
|--|-----------|
| Time Series                                    |           |
| Southern Oscillation Index (SOI)               | T1        |
| Tahiti and Darwin SLP Anomalies                | T1        |
| OLR Anomalies                                  | T1        |
| CDAS/Reanalysis SOI & Equatorial SOI           | T2        |
| 200-hPa Zonal Wind Anomalies                   | T3        |
| 500-hPa Temperature Anomalies                  | T3        |
| 30-hPa and 50-hPa Zonal Wind Anomalies         | T3        |
| 850-hPa Zonal Wind Anomalies                   | T4        |
| Equatorial Pacific SST Anomalies               | T5        |
| Time-Longitude Sections                        |           |
| Mean and Anomalous Sea Level Pressure          | T6        |
| Mean and Anomalous 850-hPa Zonal Wind          | T7        |
| Mean and Anomalous OLR                         | T8        |
| Mean and Anomalous SST                         | T9        |
| Pentad SLP Anomalies                           | T10       |
| Pentad OLR Anomalies                           | T11       |
| Pentad 200-hPa Velocity Potential Anomalies    | T12       |
| Pentad 850-hPa Zonal Wind Anomalies            | T13       |
| Anomalous Equatorial Zonal Wind                | T14       |
| Mean and Anomalous Depth of the 20°C Isotherm  | T15       |
| Mean & Anomaly Fields                          |           |
| Depth of the 20°C Isotherm                     | T16       |
| Subsurface Equatorial Pacific Temperatures     | T17       |
| SST  | T18       |
| SLP  | T19       |
| 850-hPa Vector Wind                            | T20       |
| 200-hPa Vector Wind                            | T21       |
| 200-hPa Streamfunction                         | T22       |
| 200-hPa Divergence                             | T23       |
| 200-hPa Velocity Potential and Divergent Wind  | T24       |
| OLR  | T25       |
| SSM/I Tropical Precipitation Estimates         | T26       |
| Cloud Liquid Water                             | T27       |
| Precipitable Water                             | T28       |
| Divergence & E-W Divergent Circulation         | T29 - T30 |
| Pacific Zonal Wind & N-S Divergent Circulation | T31 - T32 |
| Appendix 1: Outside Contributions              |           |
| Tropical Drifting Buoys                        | A1.1      |

## FIGURE

|                       |   |             |
|-----------------------|---|-------------|
|                       | Pacific Wind Stress and Anomalies                   | A1.2        |
|                       | Satellite-Derived Surface Currents                  | A1.3 - A1.4 |
| <b>FORECAST FORUM</b> |   |             |
|                       | Discussion . . . . .                                | page 49     |
|                       | Canonical Correlation Analysis Forecasts            | F1 - F2     |
|                       | NCEP Coupled Model Forecasts                        | F3 - F4     |
|                       | NCEP Markov Model Forecasts                         | F5 - F6     |
|                       | LDEO Model Forecasts                                | F7 - F8     |
|                       | Linear Inverse Modeling Forecasts                   | F9 - F10    |
|                       | ENSO-CLIPER Model Forecast                          | F11         |
|                       | Model Forecasts of Niño 3.4                         | F12         |
| <b>EXTRATROPICS</b>   |   |             |
|                       | Highlights . . . . .                                | page 64     |
|                       | Table of Teleconnection Indices . . . . .           | page 66     |
|                       | Global Surface Temperature                          | E1          |
|                       | Temperature Anomalies (Land Only)                   | E2          |
|                       | Global Precipitation                                | E3          |
|                       | Regional Precipitation Estimates                    | E4 - E5     |
|                       | U. S. Precipitation                                 | E6          |
|                       | Northern Hemisphere                                 |             |
|                       | Teleconnection Indices                              | E7          |
|                       | Mean and Anomalous SLP                              | E8          |
|                       | Mean and Anomalous 500-hPa heights                  | E9          |
|                       | Mean and Anomalous 300-hPa Wind Vectors             | E10         |
|                       | 500-hPa Persistence                                 | E11         |
|                       | Time-Longitude Sections of 500-hPa Height Anomalies | E12         |
|                       | 700-hPa Storm Track                                 | E13         |
|                       | Southern Hemisphere                                 |             |
|                       | Mean and Anomalous SLP                              | E14         |
|                       | Mean and Anomalous 500-hPa heights                  | E15         |
|                       | Mean and Anomalous 300-hPa Wind Vectors             | E16         |
|                       | 500-hPa Persistence                                 | E17         |
|                       | Time-Longitude Sections of 500-hPa Height Anomalies | E18         |
|                       | Stratosphere  |             |
|                       | Height Anomalies                                    | S1 - S2     |
|                       | Temperatures  | S3 - S4     |
|                       | Ozone   | S5 - S6     |
|                       | Vertical Component of EP Flux                       | S7          |
|                       | Ozone Hole  | S8          |
|                       | Appendix 2: Additional Figures                      |             |
|                       | Arctic Oscillation and 500-hPa Anomalies            | A2.1        |
|                       | Snow Cover  | A2.2        |

## Tropical Highlights - September 2018

Sea surface temperatures (SSTs) remained above-average across the equatorial Pacific during September 2018 (Fig. T18, Table T2). The latest monthly Niño indices were  $+0.5^{\circ}\text{C}$  for the Niño 4 region, and  $+0.3^{\circ}\text{C}$  for the Niño 3.4 and Niño 3 regions (Table T2, Fig. T5). The depth of the oceanic thermocline (measured by the depth of the  $20^{\circ}\text{C}$  isotherm) was above-average across the equatorial Pacific (Figs. T15, T16), and the corresponding sub-surface temperatures were  $1\text{-}3^{\circ}\text{C}$  above average (Fig. T17).

Also during September, the lower-level easterly winds were weaker-than-average (indicated by westerly anomalies) across most of the equatorial Pacific (Table T1, Fig. T20), while the upper-level winds anomalies were easterly over the central and east-central equatorial Pacific (Fig. T21). Meanwhile, convection was suppressed over Indonesia and the central equatorial Pacific (Figs. T25, E3). Collectively, these oceanic and atmospheric anomalies reflect ENSO-neutral conditions with a tendency towards a developing El Niño.

For the latest status of the ENSO cycle see the ENSO Diagnostic Discussion at:  
[http://www.cpc.ncep.noaa.gov/products/analysis\\_monitoring/enso\\_advisory/index.html](http://www.cpc.ncep.noaa.gov/products/analysis_monitoring/enso_advisory/index.html)

| Month  | SLP Anomalies |        | Tahiti minus Darwin SOI | 850-hPa Zonal Wind Index |                 |                 | 200-hPa Wind Index | OLR Index       |
|--------|---------------|--------|-------------------------|--------------------------|-----------------|-----------------|--------------------|-----------------|
|        | Tahiti        | Darwin |                         | 5N-5S 135E-180           | 5N-5S 175W-140W | 5N-5S 135W-120W |                    |                 |
| SEP 18 | -1.6          | 0.1    | -0.9                    | -1.1                     | -0.7            | -0.5            | 5N-5S 165W-110W    | 5N-5S 160E-160W |
| AUG 18 | -0.9          | -0.3   | -0.3                    | -0.4                     | -0.6            | -0.2            |                    |                 |
| JUL 18 | -0.2          | -0.6   | 0.2                     | 0.4                      | 0.1             | -0.3            |                    |                 |
| JUN 18 | 0.5           | 0.8    | -0.1                    | 0.2                      | -0.9            | -0.9            |                    |                 |
| MAY 18 | 1.4           | 0.7    | 0.4                     | 0.3                      | 0.1             | -0.1            |                    |                 |
| APR 18 | 0.6           | -0.4   | 0.5                     | -0.3                     | 0.8             | 0.4             |                    |                 |
| MAR 18 | 0.4           | -2.2   | 1.5                     | -0.8                     | 1.4             | 1.1             |                    |                 |
| FEB 18 | -0.8          | 0.2    | -0.5                    | -1.2                     | -0.3            | 0.1             |                    |                 |
| JAN 18 | 0.1           | -1.9   | 1.1                     | 1.4                      | 0.8             | 0.1             |                    |                 |
| DEC 17 | -0.3          | -0.1   | -0.1                    | 0.5                      | 0.4             | -0.1            |                    |                 |
| NOV 17 | 0.2           | -1.5   | 0.9                     | 0.8                      | 0.9             | 0.2             |                    |                 |
| OCT 17 | 0.3           | -1.4   | 0.9                     | 0.6                      | 0.3             | -0.4            |                    |                 |
| SEP 17 | 1.2           | 0.1    | 0.6                     | 1.2                      | 0.2             | 0.0             |                    |                 |

TABLE T1 - Atmospheric index values for the most recent 12 months. Indices are standardized by the mean annual standard deviation, except for the Tahiti and Darwin SLP anomalies which are in units of hPa. Positive (negative) values of 200-hPa zonal wind index imply westerly (easterly) anomalies. Positive (negative) values of 850-hPa zonal wind indices imply easterly (westerly) anomalies. Anomalies are departures from the 1981-2010 base period means.

| Month  | PACIFIC SST                  |                             |                                |                              | ATLANTIC SST               |                            | GLOBAL |      |      |      |      |      |      |      |
|--------|------------------------------|-----------------------------|--------------------------------|------------------------------|----------------------------|----------------------------|--------|------|------|------|------|------|------|------|
|        | Niño 1+2<br>0-10S<br>90W-80W | Niño 3<br>5N-5S<br>150W-90W | Niño 3.4<br>5N-5S<br>170W-120W | Niño 4<br>5N-5S<br>160E-150W | N.ATL<br>5N-20N<br>60W-30W | S. ATL<br>0-20S<br>30W-10E |        |      |      |      |      |      |      |      |
| SEP 18 | -0.1                         | 20.3                        | 0.3                            | 25.2                         | 0.3                        | 27.1                       | 0.5    | 29.1 | 0.1  | 28.2 | -0.1 | 22.9 | 0.2  | 27.4 |
| AUG 18 | 0.1                          | 20.7                        | 0.2                            | 25.2                         | 0.3                        | 27.1                       | 0.5    | 29.2 | -0.3 | 27.5 | -0.2 | 22.9 | 0.1  | 27.3 |
| JUL 18 | -0.2                         | 21.4                        | 0.4                            | 26.1                         | 0.3                        | 27.5                       | 0.3    | 29.1 | -0.5 | 26.7 | 0.1  | 23.8 | 0.1  | 27.6 |
| JUN 18 | -0.6                         | 22.2                        | 0.3                            | 26.7                         | 0.2                        | 27.9                       | 0.3    | 29.2 | -0.7 | 26.1 | 0.2  | 25.2 | 0.1  | 28.1 |
| MAY 18 | -0.5                         | 23.7                        | -0.2                           | 26.9                         | -0.1                       | 27.7                       | 0.2    | 29.0 | -0.5 | 25.9 | -0.1 | 26.2 | 0.0  | 28.5 |
| APR 18 | -1.0                         | 24.6                        | -0.4                           | 27.1                         | -0.4                       | 27.4                       | 0.1    | 28.6 | -0.3 | 25.7 | -0.0 | 27.0 | -0.0 | 28.6 |
| MAR 18 | -0.8                         | 25.8                        | -0.8                           | 26.4                         | -0.7                       | 26.5                       | -0.1   | 28.1 | 0.1  | 25.7 | -0.4 | 26.7 | -0.1 | 28.2 |
| FEB 18 | -0.6                         | 25.6                        | -1.0                           | 25.4                         | -0.9                       | 25.8                       | -0.2   | 27.9 | -0.0 | 25.6 | -0.3 | 26.3 | -0.1 | 27.7 |
| JAN 18 | -0.8                         | 23.7                        | -1.1                           | 24.5                         | -0.8                       | 25.8                       | -0.3   | 28.0 | 0.3  | 26.3 | -0.1 | 25.6 | -0.1 | 27.5 |
| DEC 17 | -1.5                         | 21.3                        | -1.1                           | 24.0                         | -0.8                       | 25.8                       | -0.3   | 28.2 | 0.6  | 27.4 | -0.3 | 24.4 | -0.1 | 27.6 |
| NOV 17 | -1.2                         | 20.4                        | -1.0                           | 23.9                         | -0.9                       | 25.8                       | -0.2   | 28.5 | 0.2  | 27.9 | 0.0  | 24.0 | 0.1  | 27.7 |
| OCT 17 | -1.3                         | 19.5                        | -0.6                           | 24.3                         | -0.5                       | 26.2                       | -0.1   | 28.6 | 0.2  | 28.3 | 0.2  | 23.6 | 0.1  | 27.5 |
| SEP 17 | -0.7                         | 19.7                        | -0.7                           | 24.2                         | -0.4                       | 26.3                       | 0.0    | 28.7 | 0.4  | 28.5 | 0.1  | 23.2 | 0.1  | 27.4 |

TABLE T2. Mean and anomalous sea surface temperature (°C) for the most recent 12 months. Anomalies are departures from the 1981–2010 adjusted OI climatology (Smith and Reynolds 1998, *J. Climate*, **11**, 3320–3323).



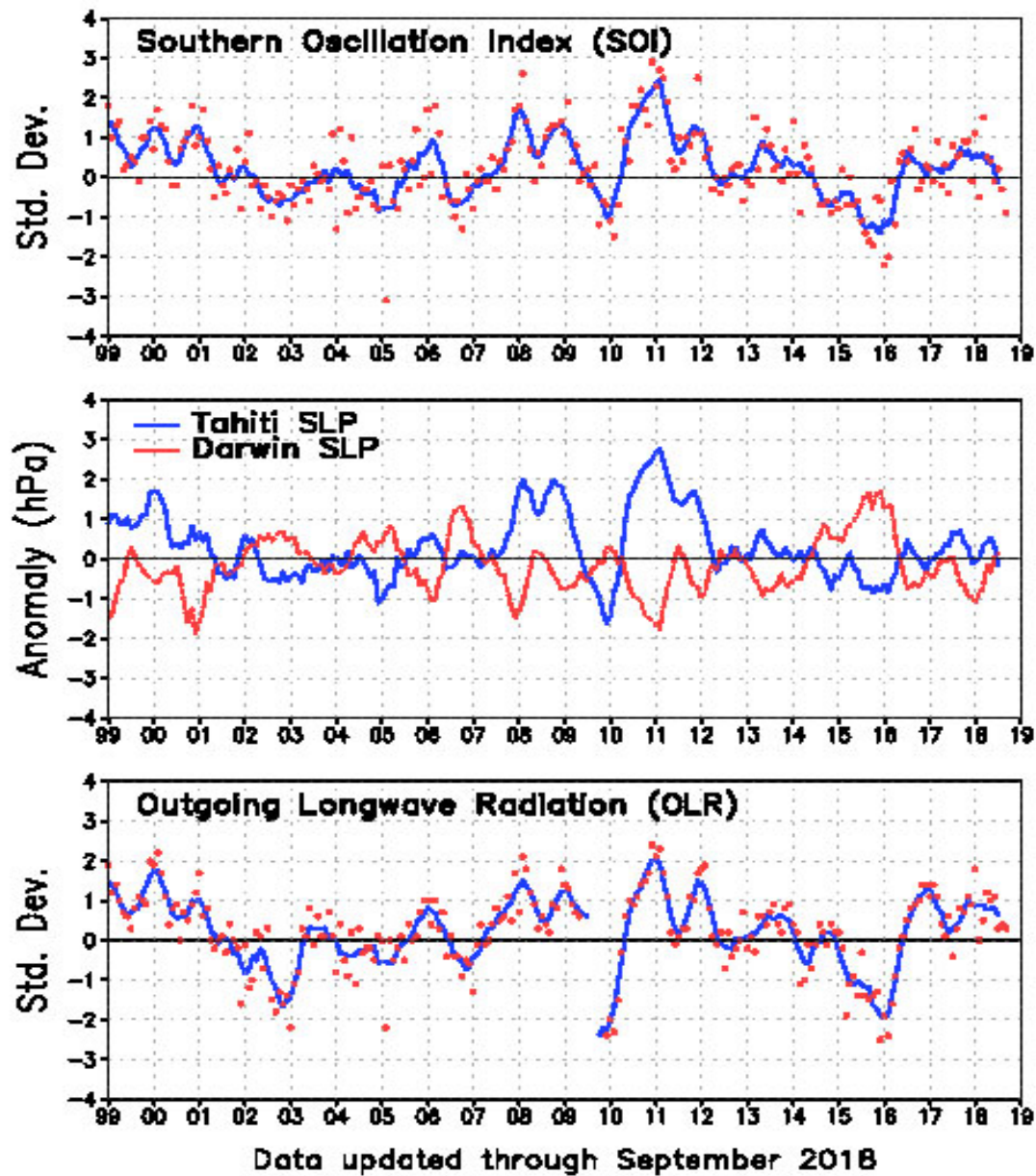


FIGURE T1. Five-month running mean of the Southern Oscillation Index (SOI) (top), sea-level pressure anomaly (hPa) at Darwin and Tahiti (middle), and outgoing longwave radiation anomaly (OLR) averaged over the area 5N-5S, 160E-160W (bottom). Anomalies in the top and middle panels are departures from the 1981-2010 base period means and are normalized by the mean annual standard deviation. Anomalies in the bottom panel are departures from the 1981-2010 base period means. Individual monthly values are indicated by “x”s in the top and bottom panels. The x-axis labels are centered on July.

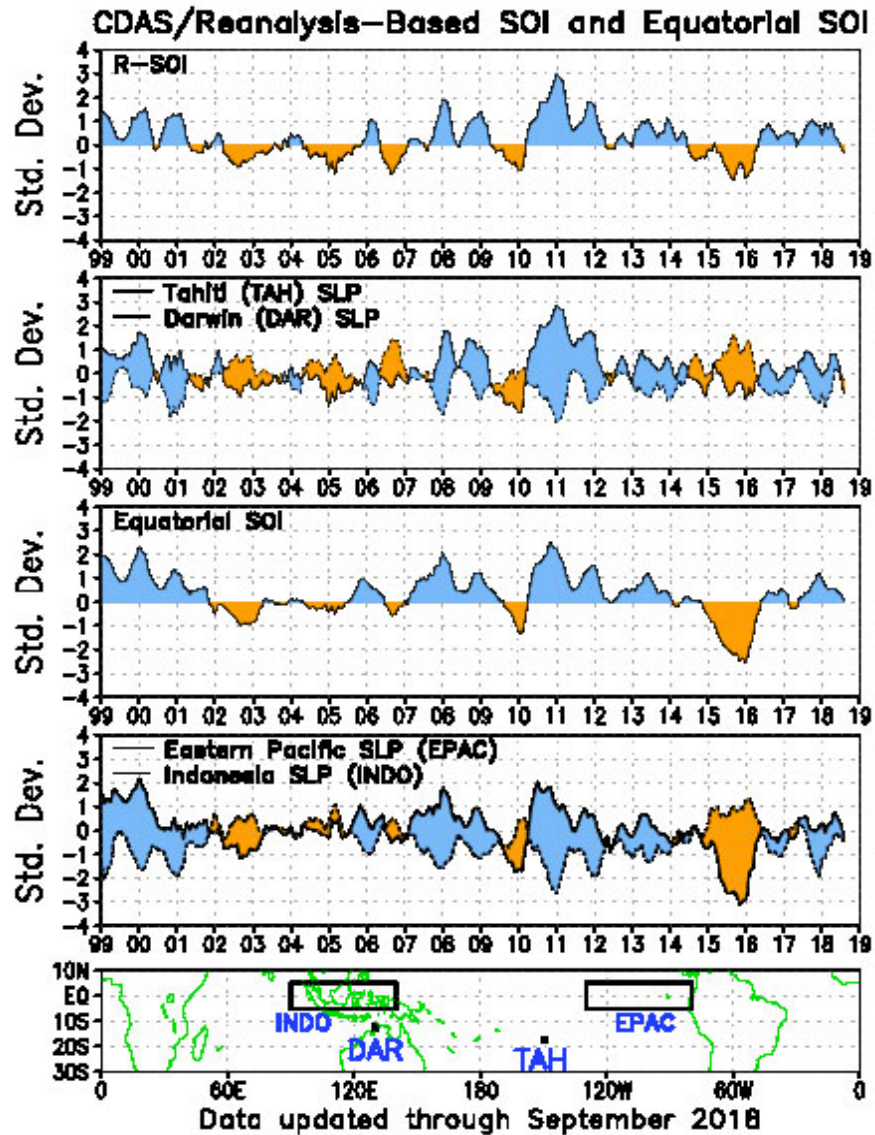


FIGURE T2. Three-month running mean of a CDAS/Reanalysis-derived (a) Southern Oscillation Index (RSOI), (b) standardized pressure anomalies near Tahiti (solid) and Darwin (dashed), (c) an equatorial SOI ([EPAC] - [INDO]), and (d) standardized equatorial pressure anomalies for (EPAC) (solid) and (INDO) (dashed). Anomalies are departures from the 1981-2010 base period means and are normalized by the mean annual standard deviation. The equatorial SOI is calculated as the normalized difference between the standardized anomalies averaged between 5°N–5°S, 80°W–130°W (EPAC) and 5°N–5°S, 90°E–140°E (INDO).

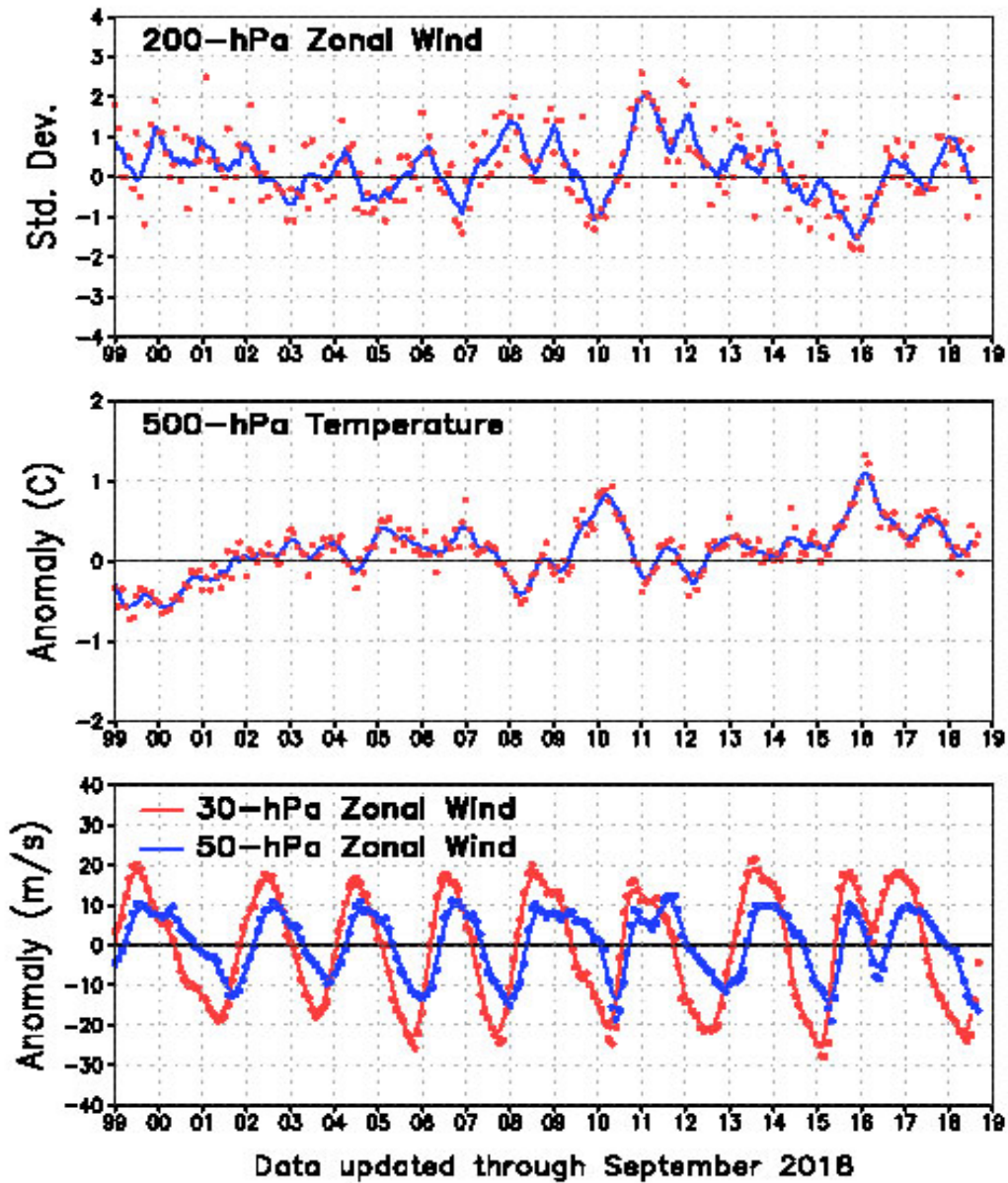


FIGURE T3. Five-month running mean (solid lines) and individual monthly mean (dots) of the 200-hPa zonal wind anomalies averaged over the area 5N-5S, 165W-110W (top), the 500-hPa virtual temperature anomalies averaged over the latitude band 20N-20S (middle), and the equatorial zonally-averaged zonal wind anomalies at 30-hPa (red) and 50-hPa (blue) (bottom). In the top panel, anomalies are normalized by the mean annual standard deviation. Anomalies are departures from the 1981-2010 base period means. The x-axis labels are centered on January.

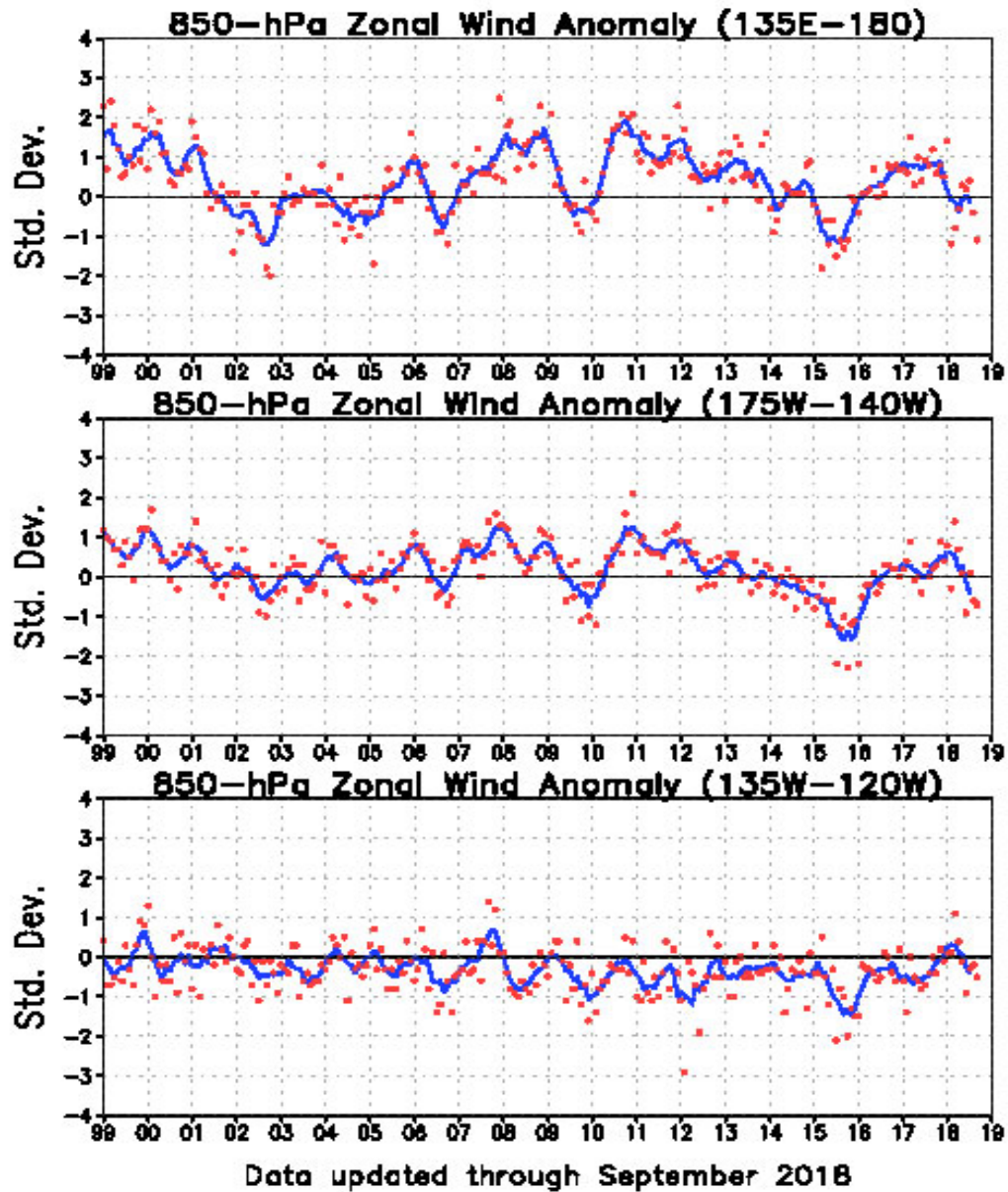


FIGURE T4. Five-month running mean (solid line) and individual monthly mean (dots) of the standardized 850-hPa zonal wind anomaly index in the latitude belt 5N-5S for 135E-180 (top), 175W-140W (middle) and 135W-120W (bottom). Anomalies are departures from the 1981-2010 base period means and are normalized by the mean annual standard deviation. The x-axis labels are centered on January. Positive (negative) values indicate easterly (westerly) anomalies.

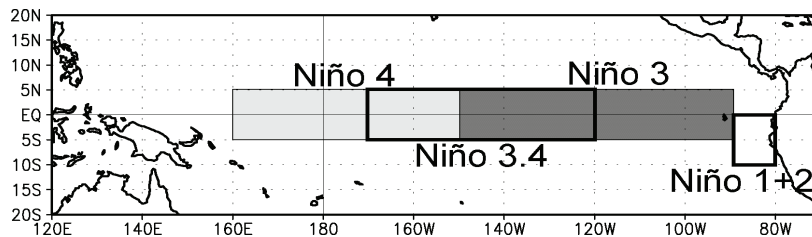
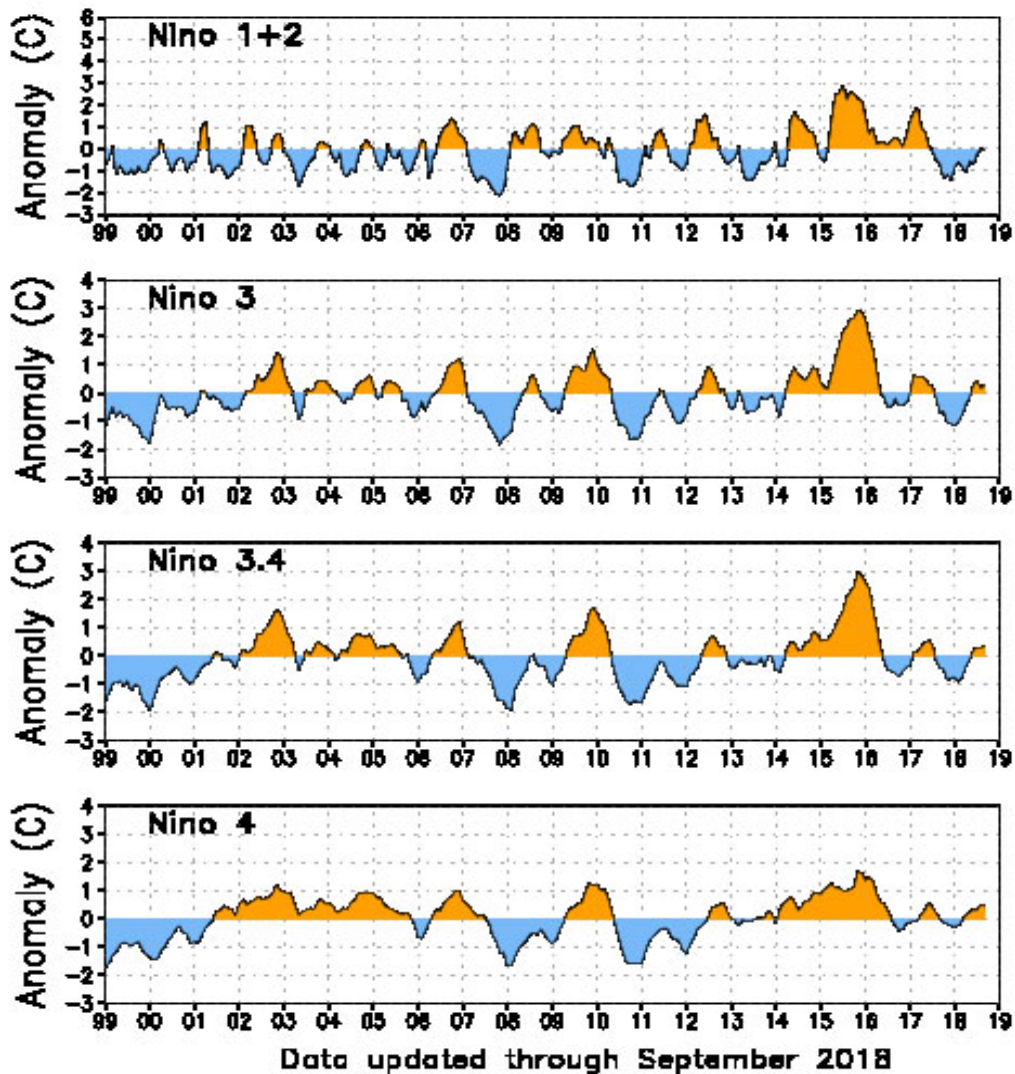


FIGURE T5. Niño region indices, calculated as the area-averaged sea surface temperature anomalies (C) for the specified region. The Niño 1+2 region (top) covers the extreme eastern equatorial Pacific between 0-10S, 90W-80W. The Niño-3 region (2nd from top) spans the eastern equatorial Pacific between 5N-5S, 150W-90W. The Niño 3.4 region (3rd from top) spans the east-central equatorial Pacific between 5N-5S, 170W-120W. The Niño 4 region (bottom) spans the date line and covers the area 5N-5S, 160E-150W. Anomalies are departures from the 1981-2010 base period monthly means (*Smith and Reynolds 1998, J. Climate, 11, 3320-3323*). Monthly values of each index are also displayed in [Table 2](#).

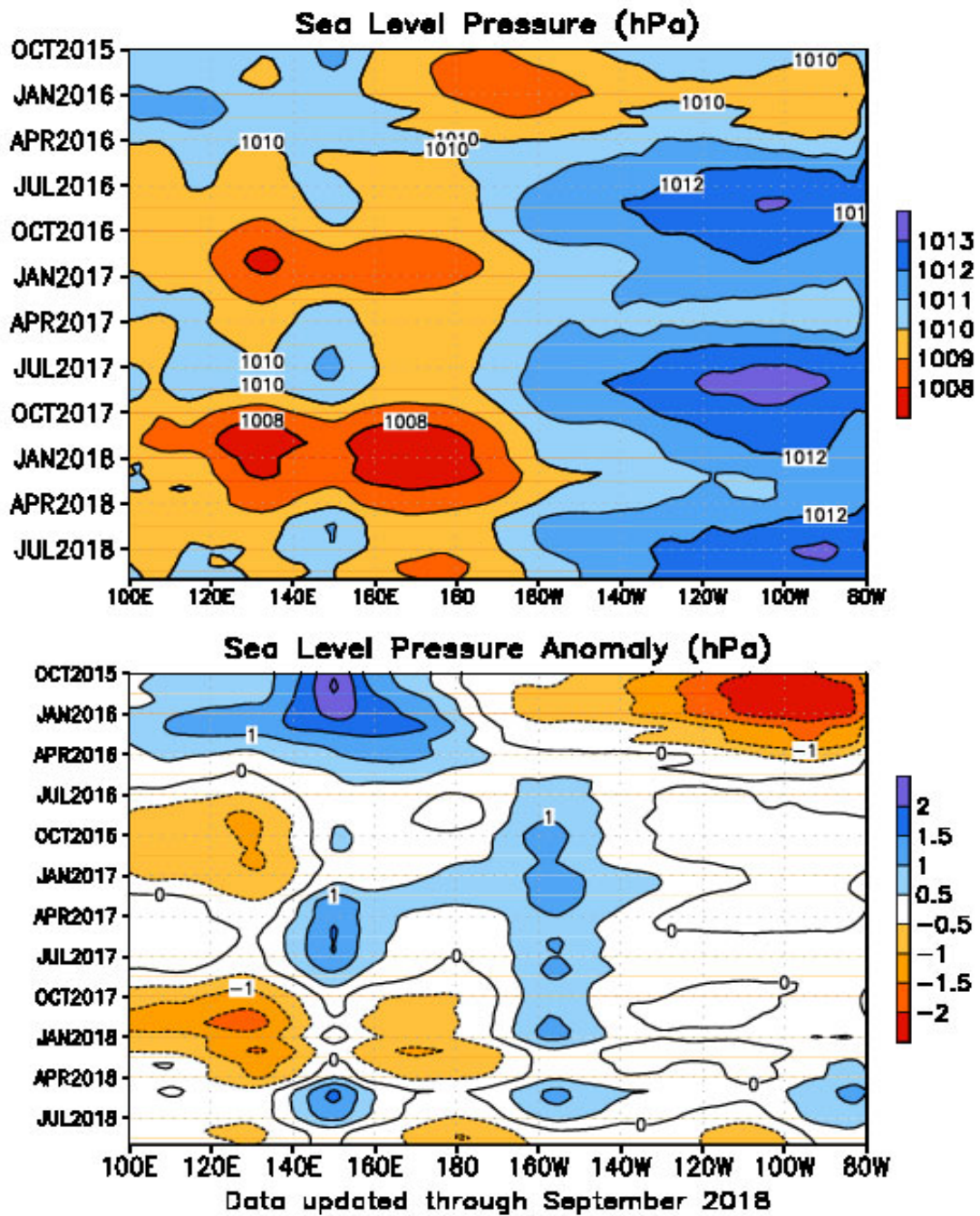


FIGURE T6. Time-longitude section of mean (top) and anomalous (bottom) sea level pressure (SLP) averaged between 5N-5S (CDAS/Reanalysis). Contour interval is 1.0 hPa (top) and 0.5 hPa (bottom). Dashed contours in bottom panel indicate negative anomalies. Anomalies are departures from the 1981-2010 base period monthly means. The data are smoothed temporally using a 3-month running average.

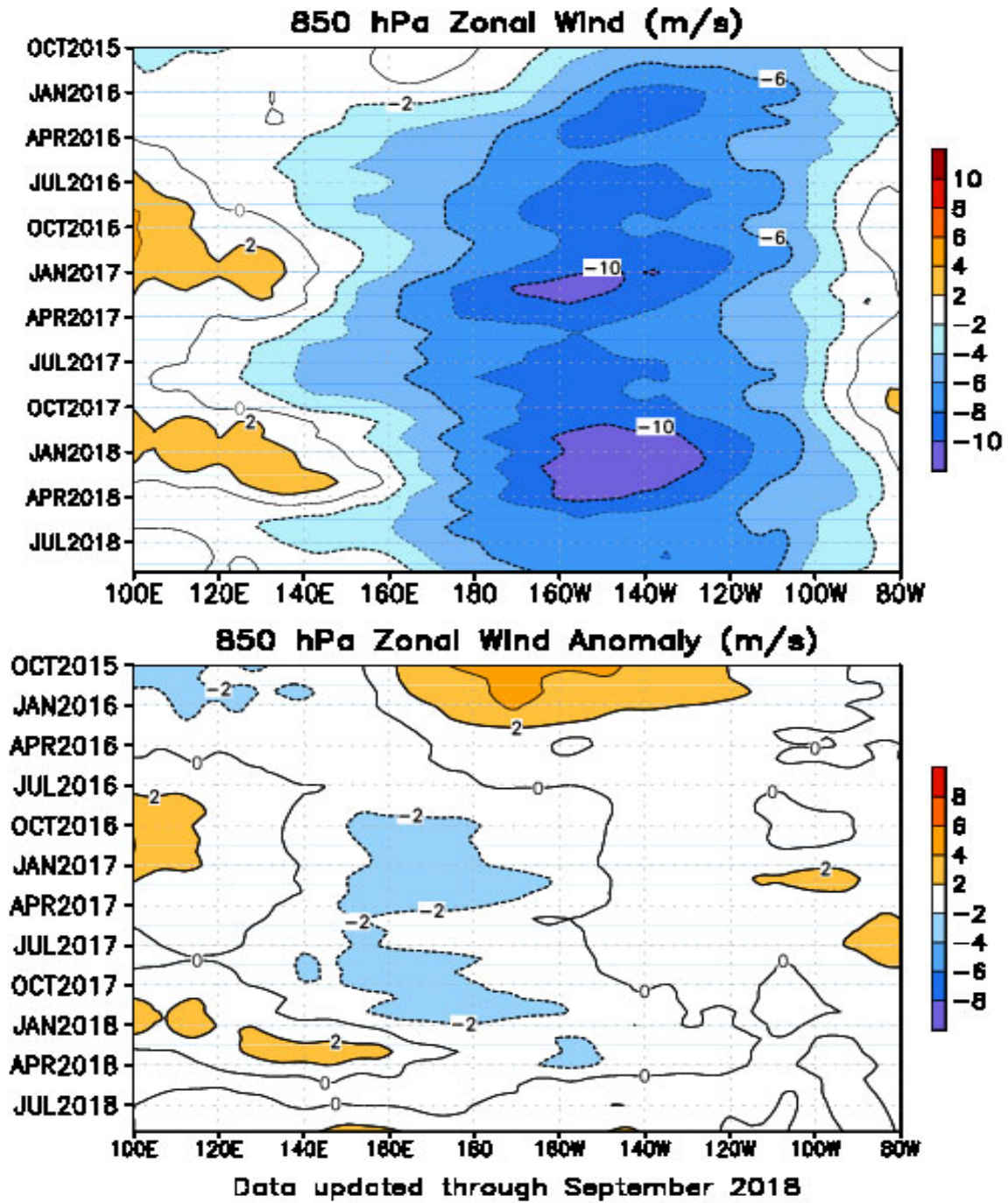


FIGURE T7. Time-longitude section of mean (top) and anomalous (bottom) 850-hPa zonal wind averaged between 5N-5S (CDAS/Reanalysis). Contour interval is  $2 \text{ ms}^{-1}$ . Blue shading and dashed contours indicate easterlies (top) and easterly anomalies (bottom). Anomalies are departures from the 1981-2010 base period monthly means. The data are smoothed temporally using a 3-month running average.

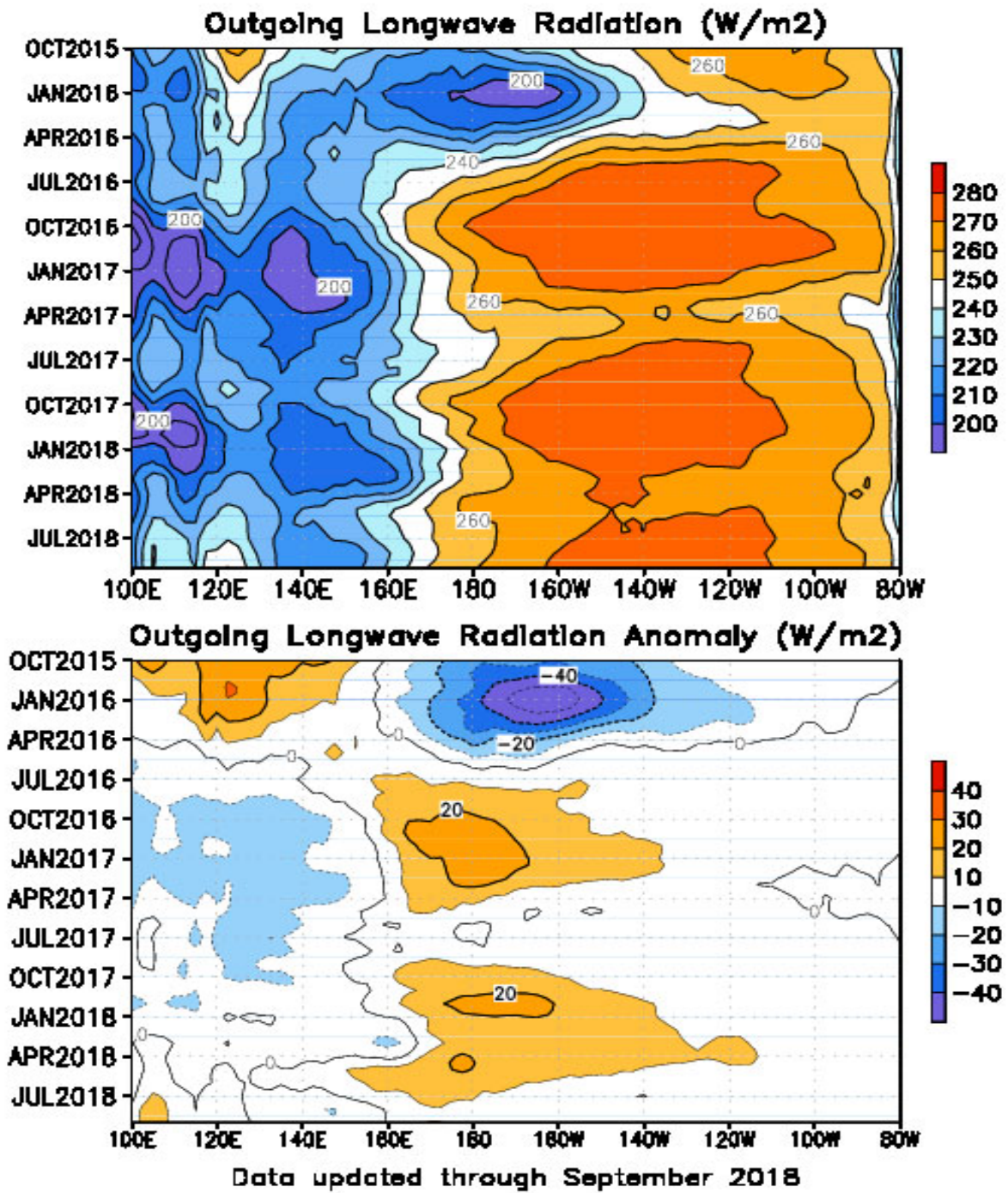


FIGURE T8. Time-longitude section of mean (top) and anomalous (bottom) outgoing longwave radiation (OLR) averaged between 5N-5S. Contour interval is 10 Wm<sup>-2</sup>. Dashed contours in bottom panel indicate negative OLR anomalies. Anomalies are departures from the 1981-2010 base period monthly means. The data are smoothed temporally using a 3-month running average.



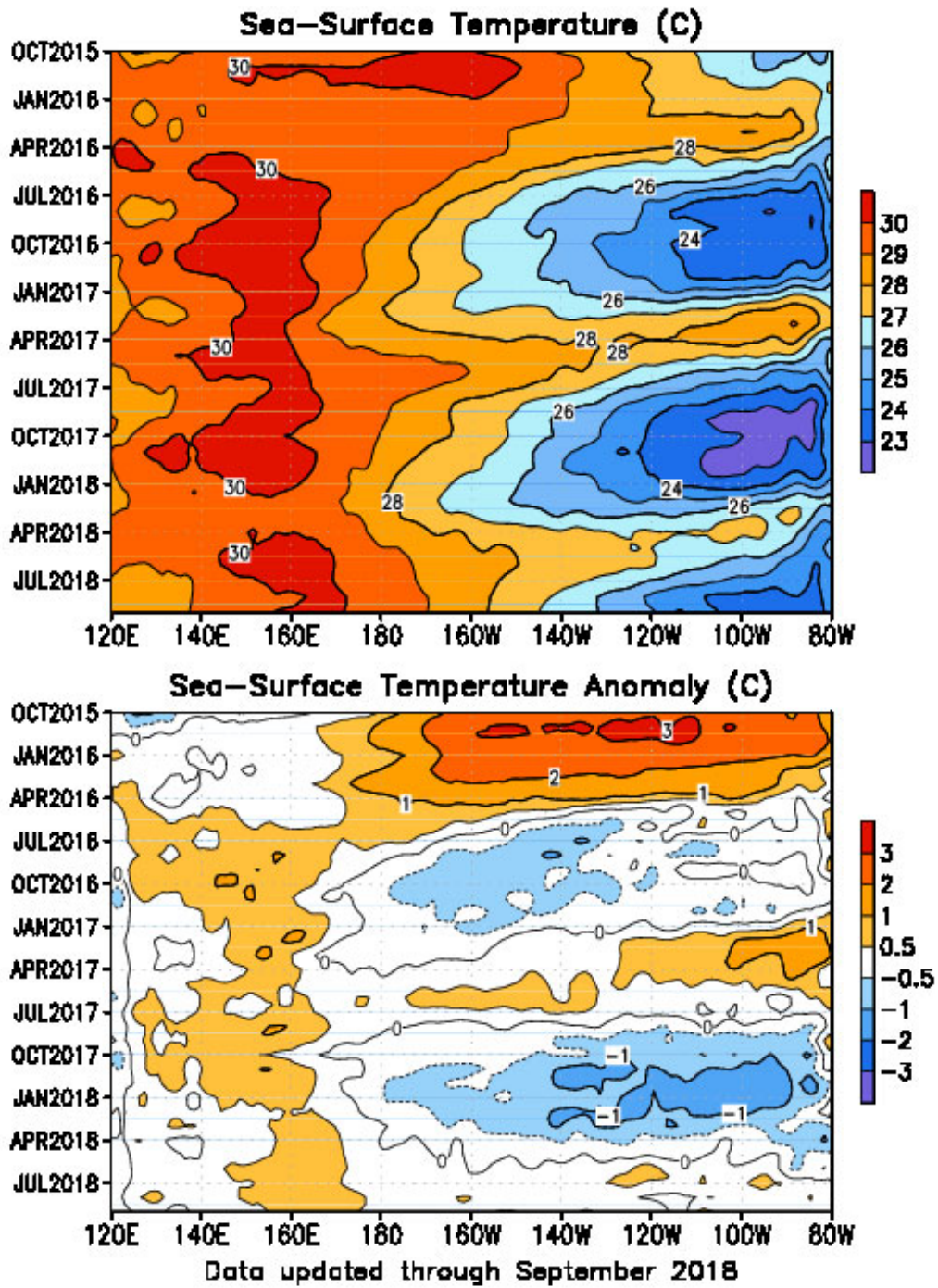


FIGURE T9. Time-longitude section of monthly mean (top) and anomalous (bottom) sea surface temperature (SST) averaged between 5N-5S. Contour interval is 1C (top) and 0.5C (bottom). Dashed contours in bottom panel indicate negative anomalies. Anomalies are departures from the 1981-2010 base period means (Smith and Reynolds 1998, *J. Climate*, 11, 3320-3323).

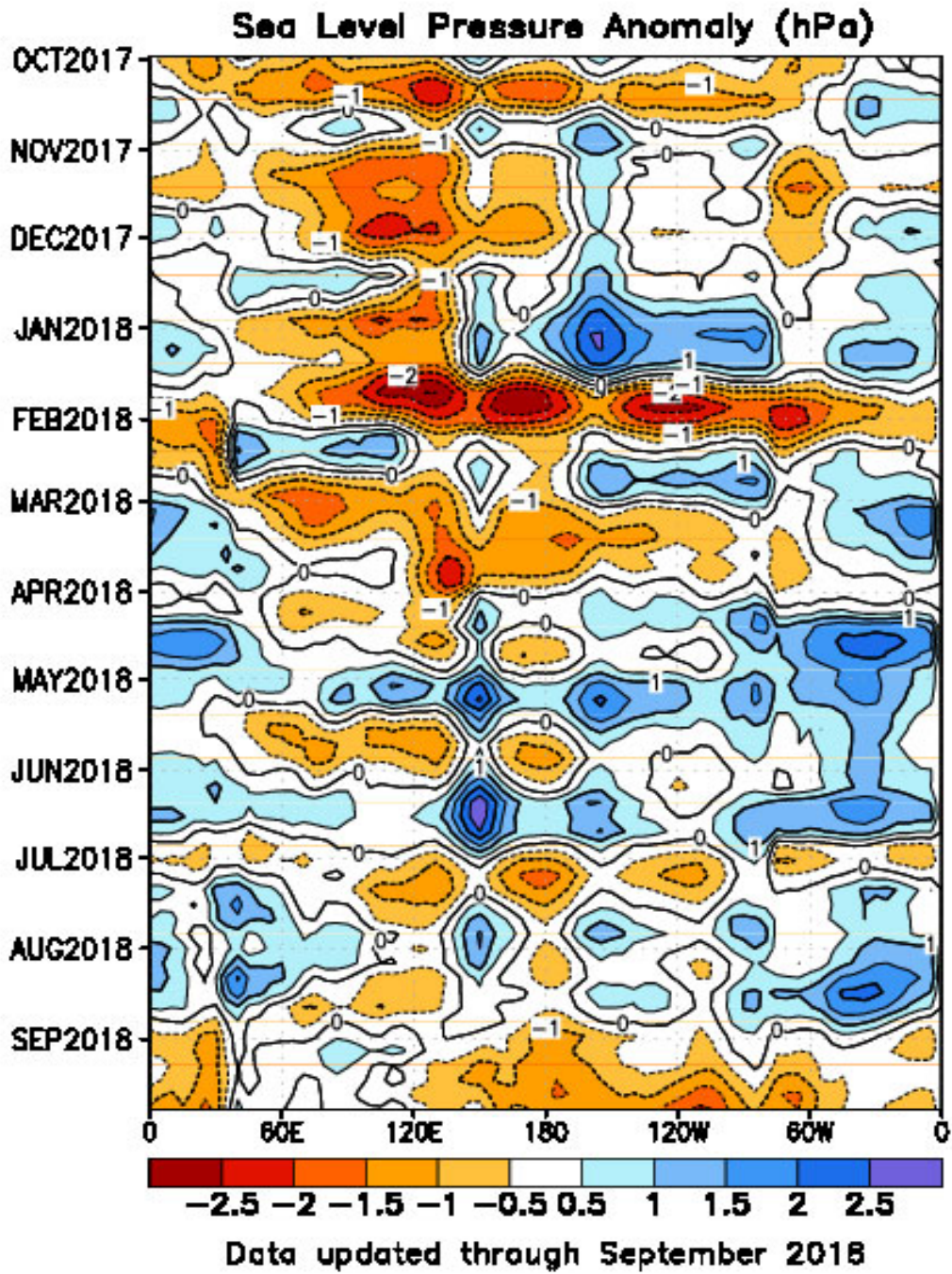


FIGURE T10. Time-longitude section of anomalous sea level pressure (hPa) averaged between 5N-5S (CDAS/Re-analysis). Contour interval is 1 hPa. Dashed contours indicate negative anomalies. Anomalies are departures from the 1981-2010 base period pentad means. The data are smoothed temporally using a 3-point running average.

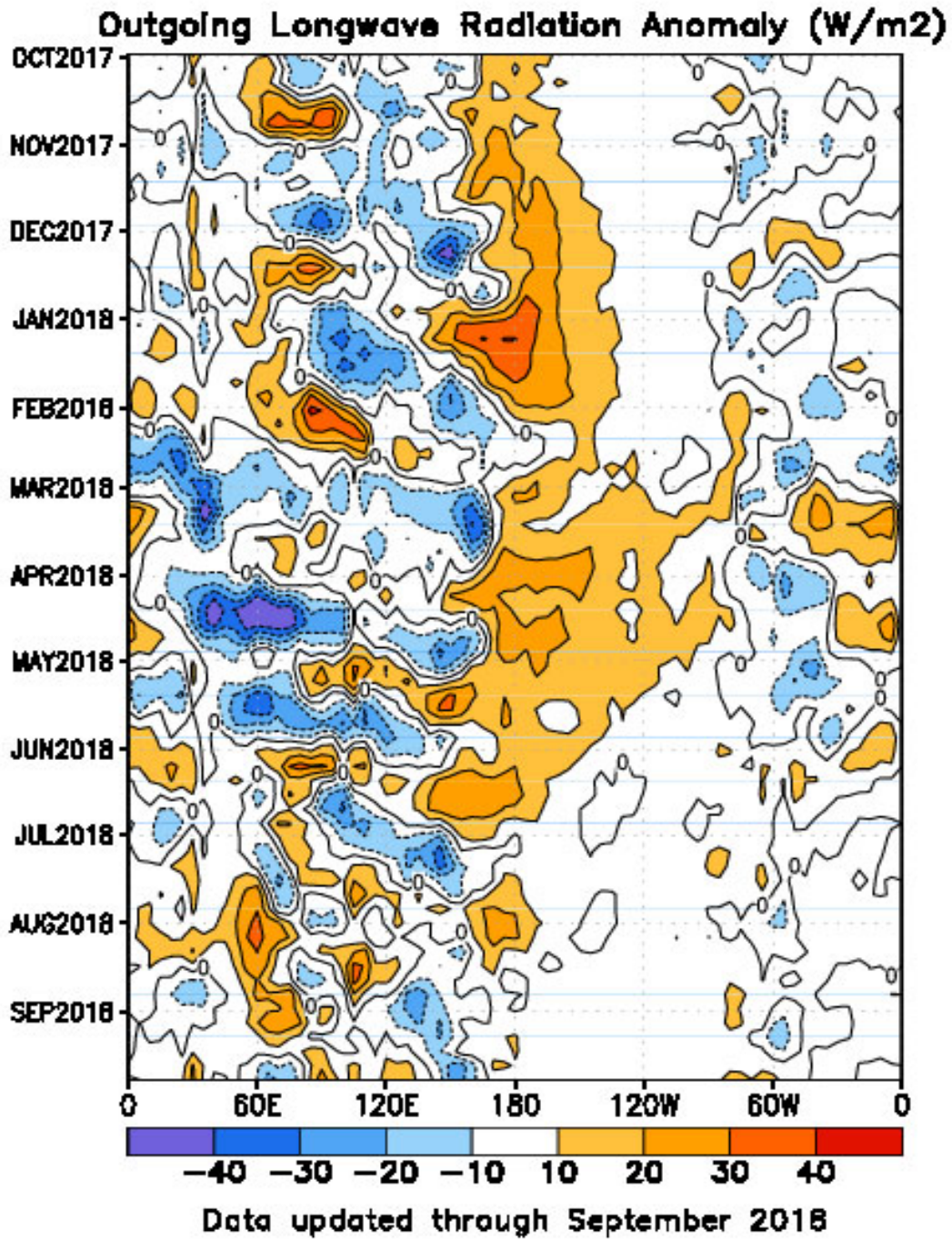


FIGURE T11. Time-longitude section of anomalous outgoing longwave radiation averaged between 5N-5S. Contour interval is  $15 Wm^{-2}$ . Dashed contours indicate negative anomalies. Anomalies are departures from the 1981-2010 base period pentad means. The data are smoothed temporally using a 3-point running average.

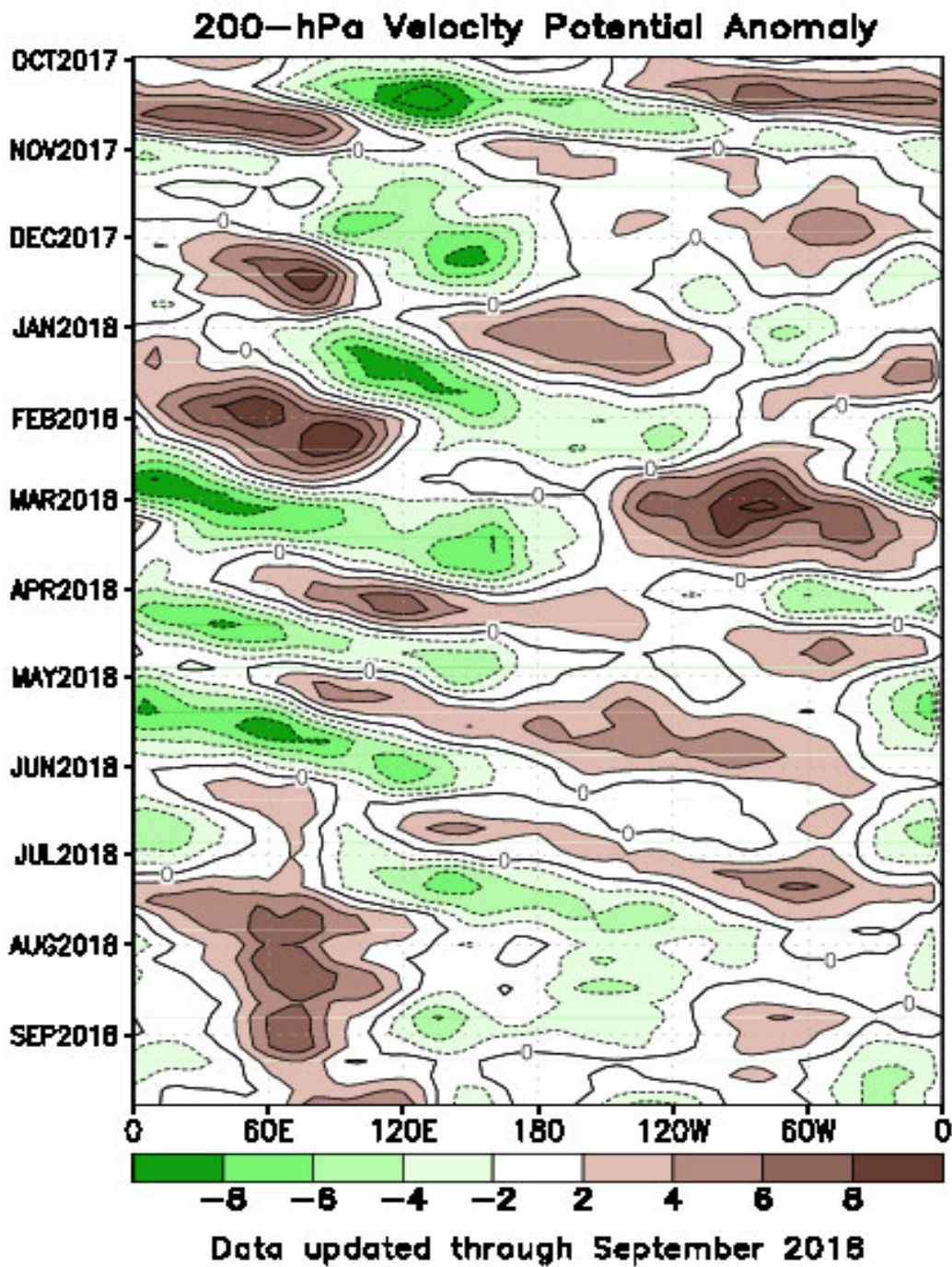


FIGURE T12. Time-longitude section of anomalous 200-hPa velocity potential averaged between 5N-5S (CDAS/Re-analysis). Contour interval is  $3 \times 10^6 \text{ m}^2\text{s}^{-1}$ . Dashed contours indicate negative anomalies. Anomalies are departures from the 1981-2010 base period pentad means. The data are smoothed temporally using a 3-point running average.

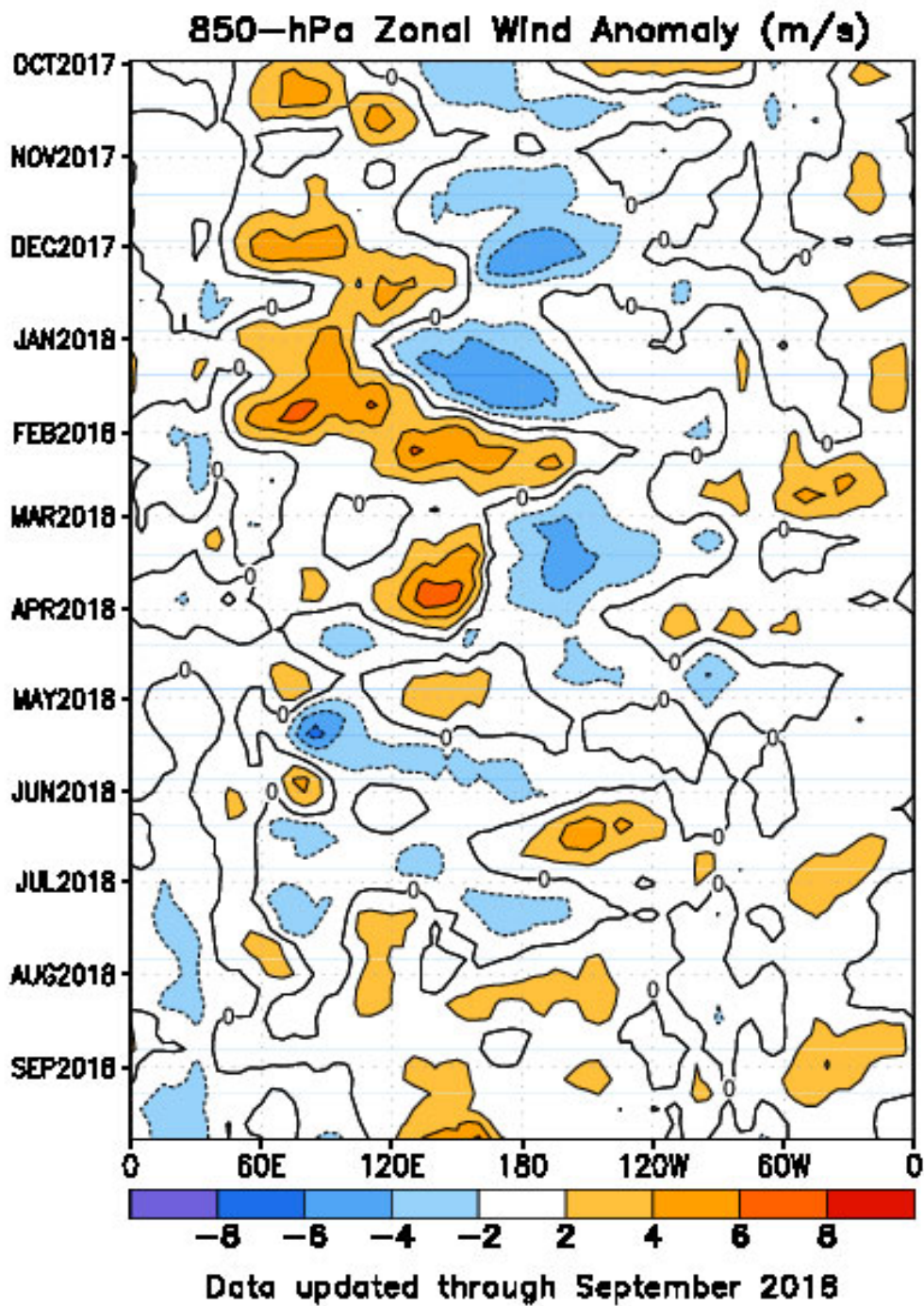


FIGURE T13. Time-longitude section of anomalous 850-hPa zonal wind averaged between 5N-5S (CDAS/Reanalysis). Contour interval is  $2 \text{ m s}^{-1}$ . Dashed contours indicate negative anomalies. Anomalies are departures from the 1981-2010 base period pentad means. The data are smoothed temporally by using a 3-point running average.

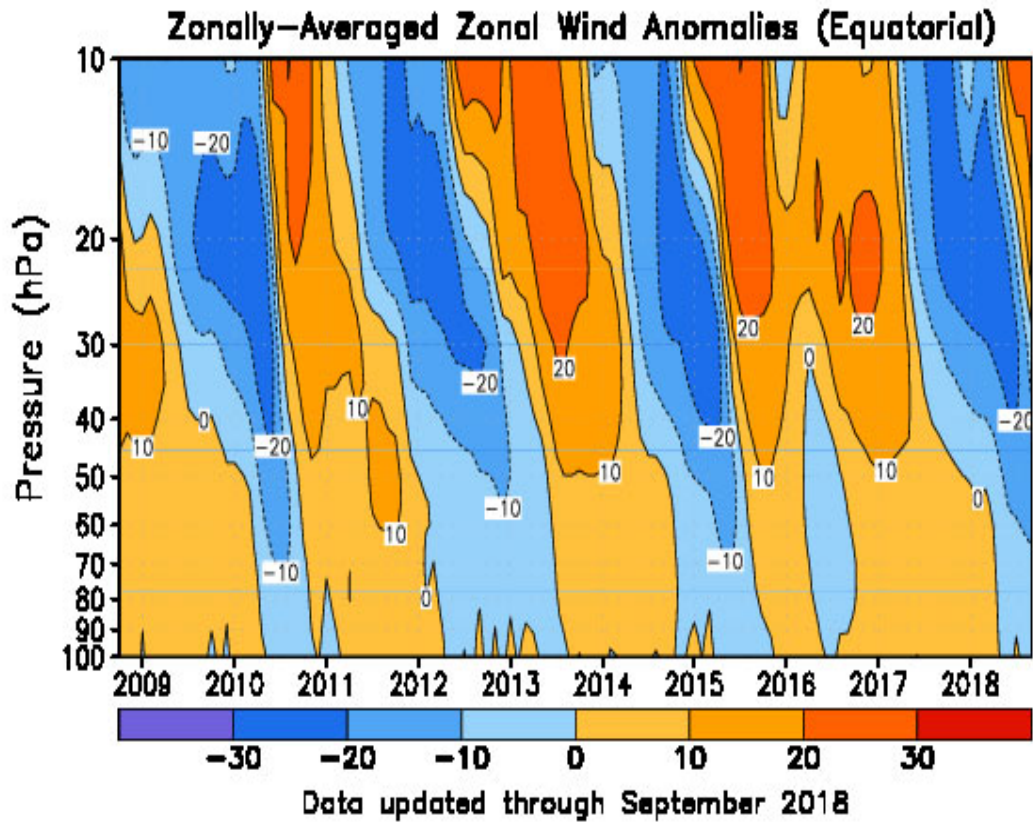


FIGURE T14. Equatorial time-height section of anomalous zonally-averaged zonal wind ( $\text{m s}^{-1}$ ) (CDAS/Reanalysis). Contour interval is  $10 \text{ m s}^{-1}$ . Anomalies are departures from the 1981-2010 base period monthly means.

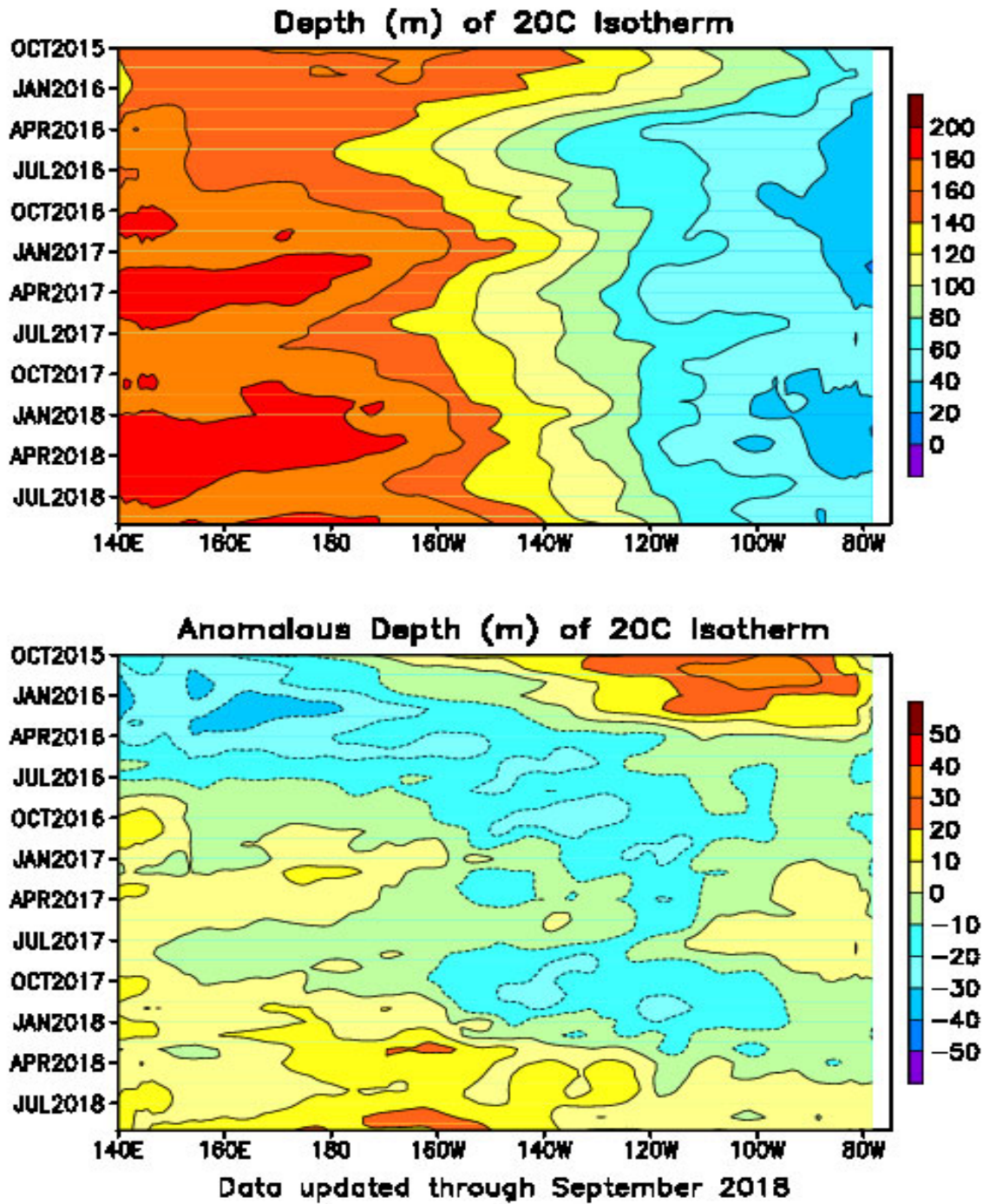


FIGURE T15. Mean (top) and anomalous (bottom) depth of the 20C isotherm averaged between 5N-5S in the Pacific Ocean. Data are derived from the NCEP's global ocean data assimilation system which assimilates oceanic observations into an oceanic GCM (Behringer, D. W., and Y. Xue, 2004: Evaluation of the global ocean data assimilation system at NCEP: The Pacific Ocean. AMS 84th Annual Meeting, Seattle, Washington, 11-15). The contour interval is 10 m. Dashed contours in bottom panel indicate negative anomalies. Anomalies are departures from the 1981-2010 base period means.

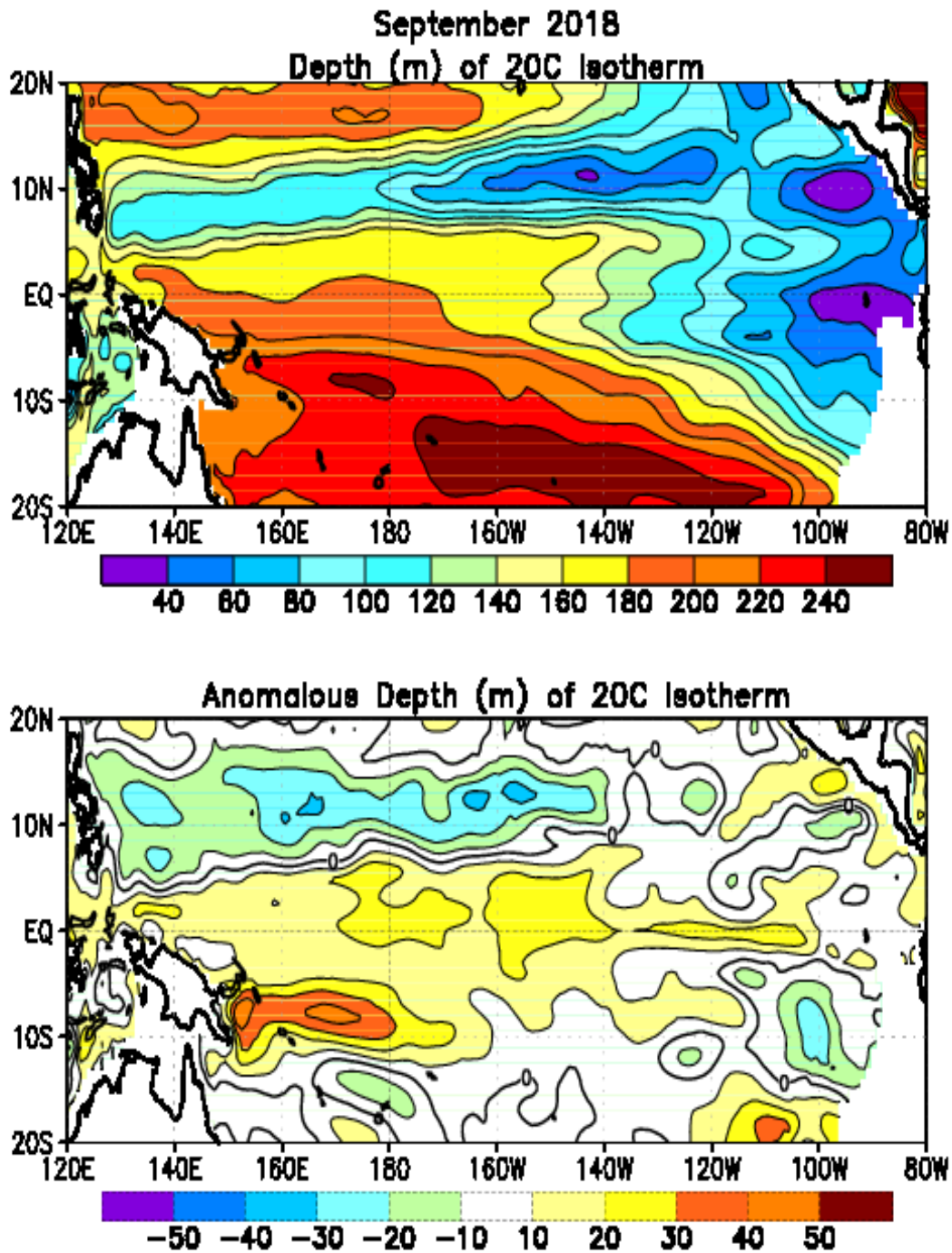
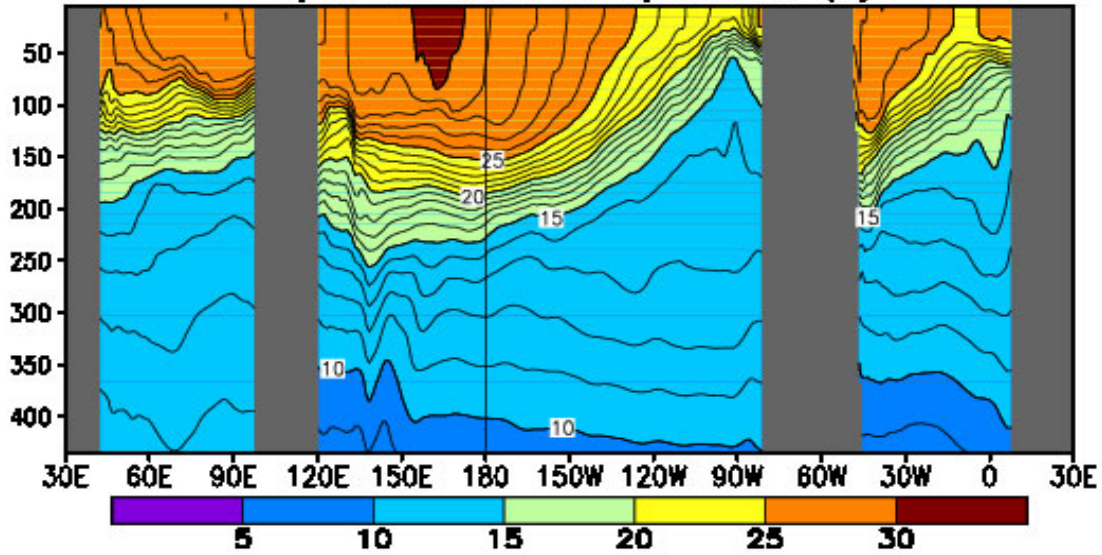


FIGURE T16. Mean (top) and anomalous (bottom) depth of the 20°C isotherm for SEP 2018. Contour interval is 40 m (top) and 10 m (bottom). Dashed contours in bottom panel indicate negative anomalies. Data are derived from the NCEP’s global ocean data assimilation system version 2 which assimilates oceanic observations into an oceanic GCM (Xue, Y. and Behringer, D.W., 2006: Operational global ocean data assimilation system at NCEP, to be submitted to BAMS). Anomalies are departures from the 1981–2010 base period means.



**September 2018: Depth–Longitude Section  
Equatorial Ocean Temperatures (C)**



**Equatorial Ocean Temperature Anomalies (C)**

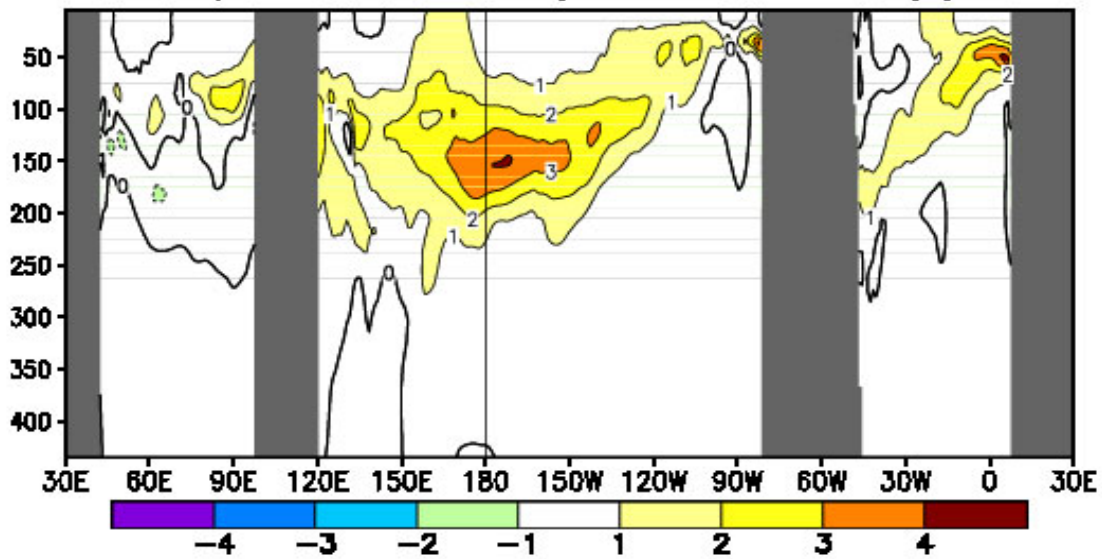


FIGURE T17. Equatorial depth–longitude section of ocean temperature (top) and ocean temperature anomalies (bottom) for SEP 2018. Contour interval is 1°C. Dashed contours in bottom panel indicate negative anomalies. Data are derived from the NCEP’s global ocean data assimilation system version 2 which assimilates oceanic observations into an oceanic GCM (Xue, Y. and Behringer, D.W., 2006: Operational global ocean data assimilation system at NCEP, to be submitted to BAMS). Anomalies are departures from the 1981–2010 base period means.

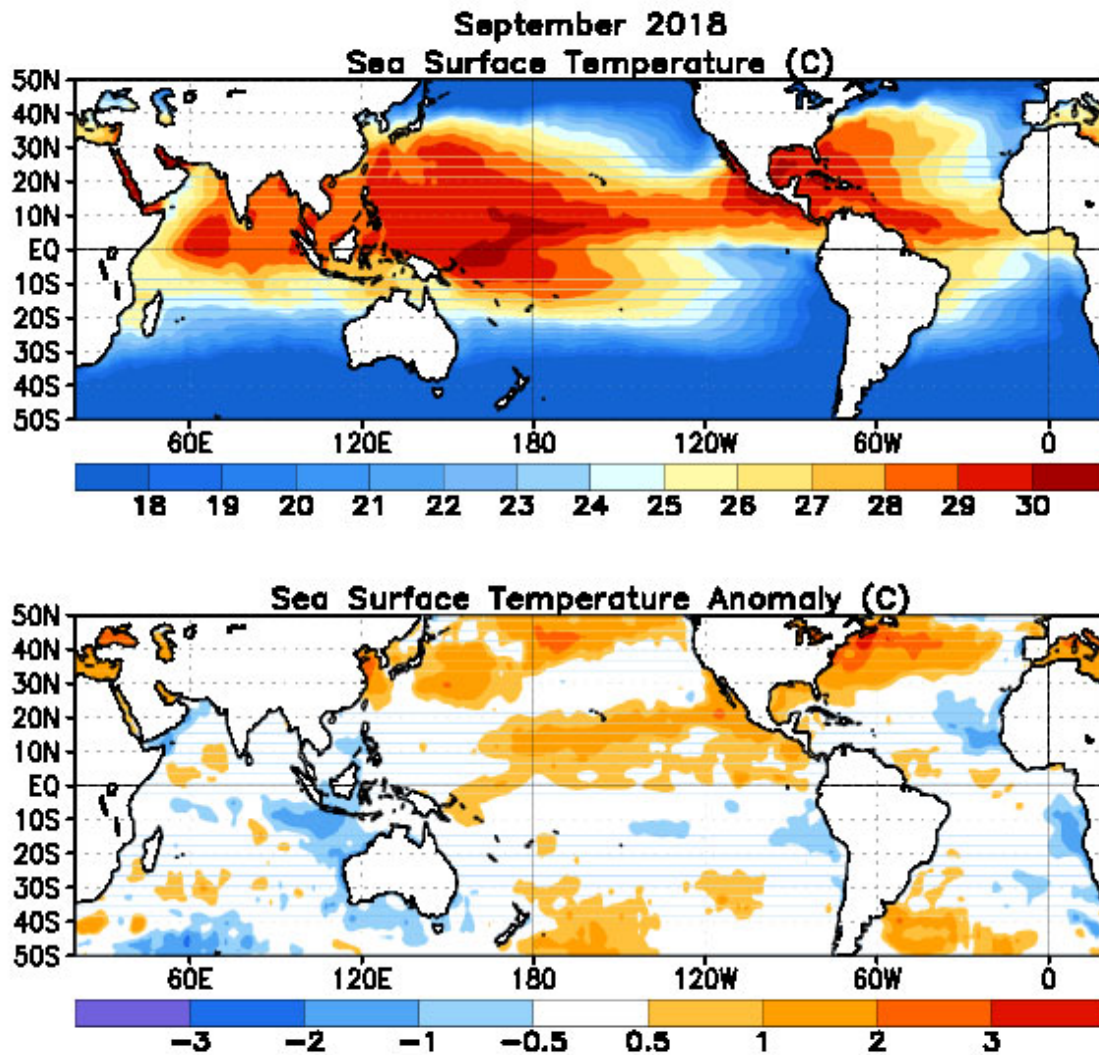


FIGURE T18. Mean (top) and anomalous (bottom) sea surface temperature (SST). Anomalies are departures from the 1981-2010 base period monthly means (Smith and Reynolds 1998, *J. Climate*, 11, 3320-3323).

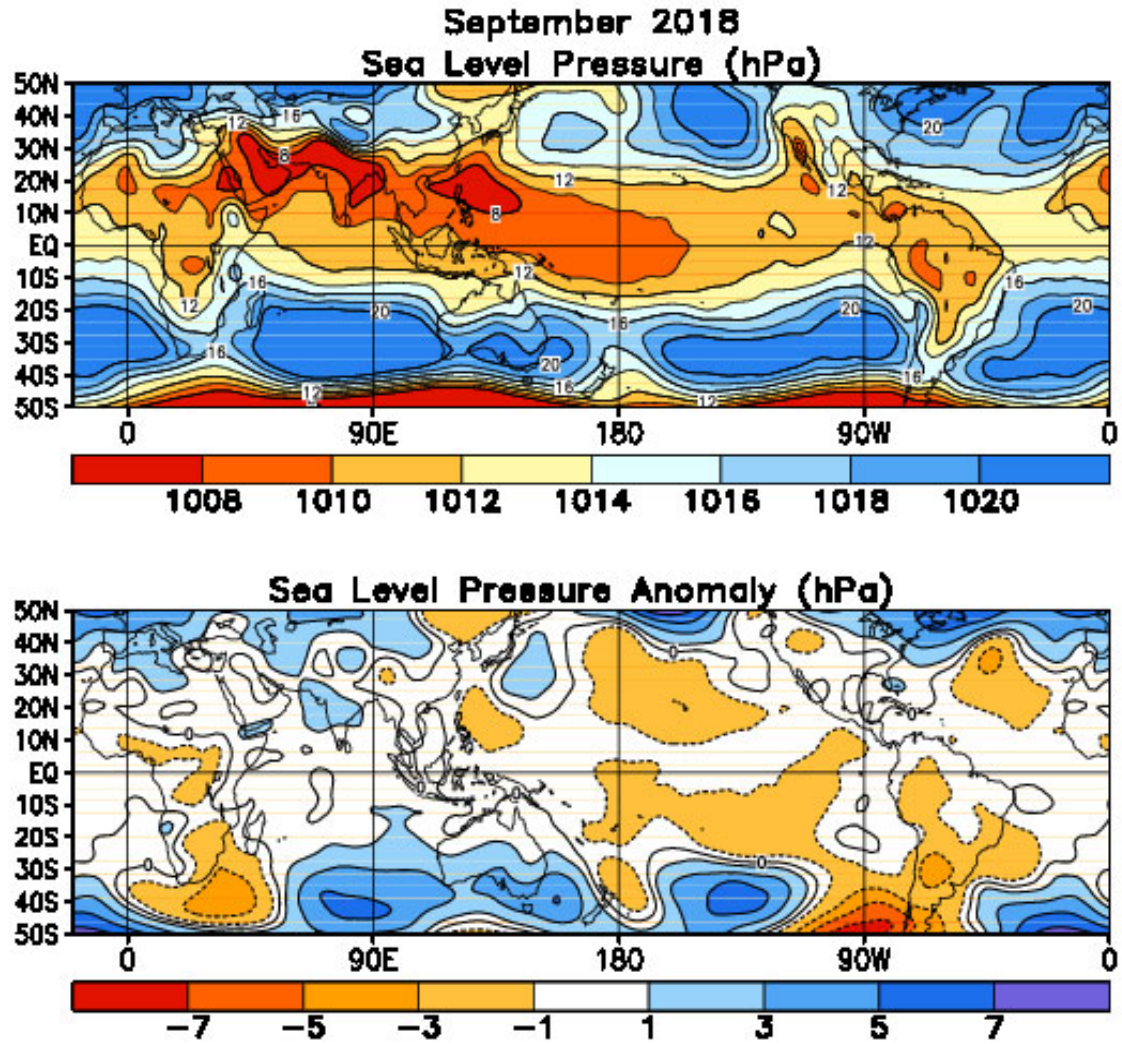


FIGURE T19. Mean (top) and anomalous (bottom) sea level pressure (SLP) (CDAS/Reanalysis). In top panel, 1000 hPa has been subtracted from contour labels, contour interval is 2 hPa, and values below 1000 hPa are indicated by dashed contours. In bottom panel, anomaly contour interval is 1 hPa and negative anomalies are indicated by dashed contours. Anomalies are departures from the 1981-2010 base period monthly means.

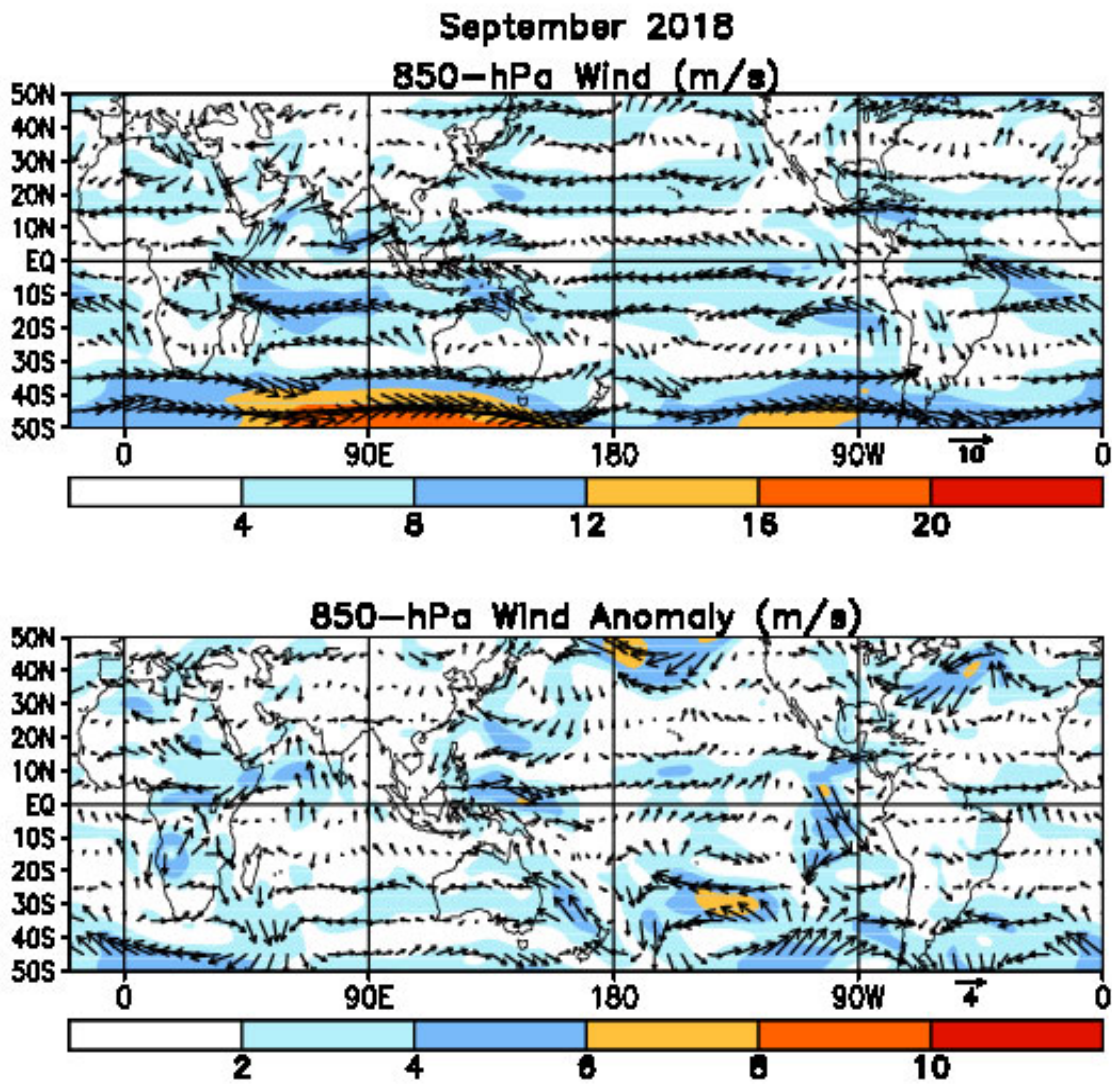


FIGURE T20. Mean (top) and anomalous (bottom) 850-hPa vector wind (CDAS/Reanalysis) for SEP 2018. Contour interval for isotachs is  $4 \text{ ms}^{-1}$  (top) and  $2 \text{ ms}^{-1}$  (bottom). Anomalies are departures from the 1981-2010 base period monthly means.

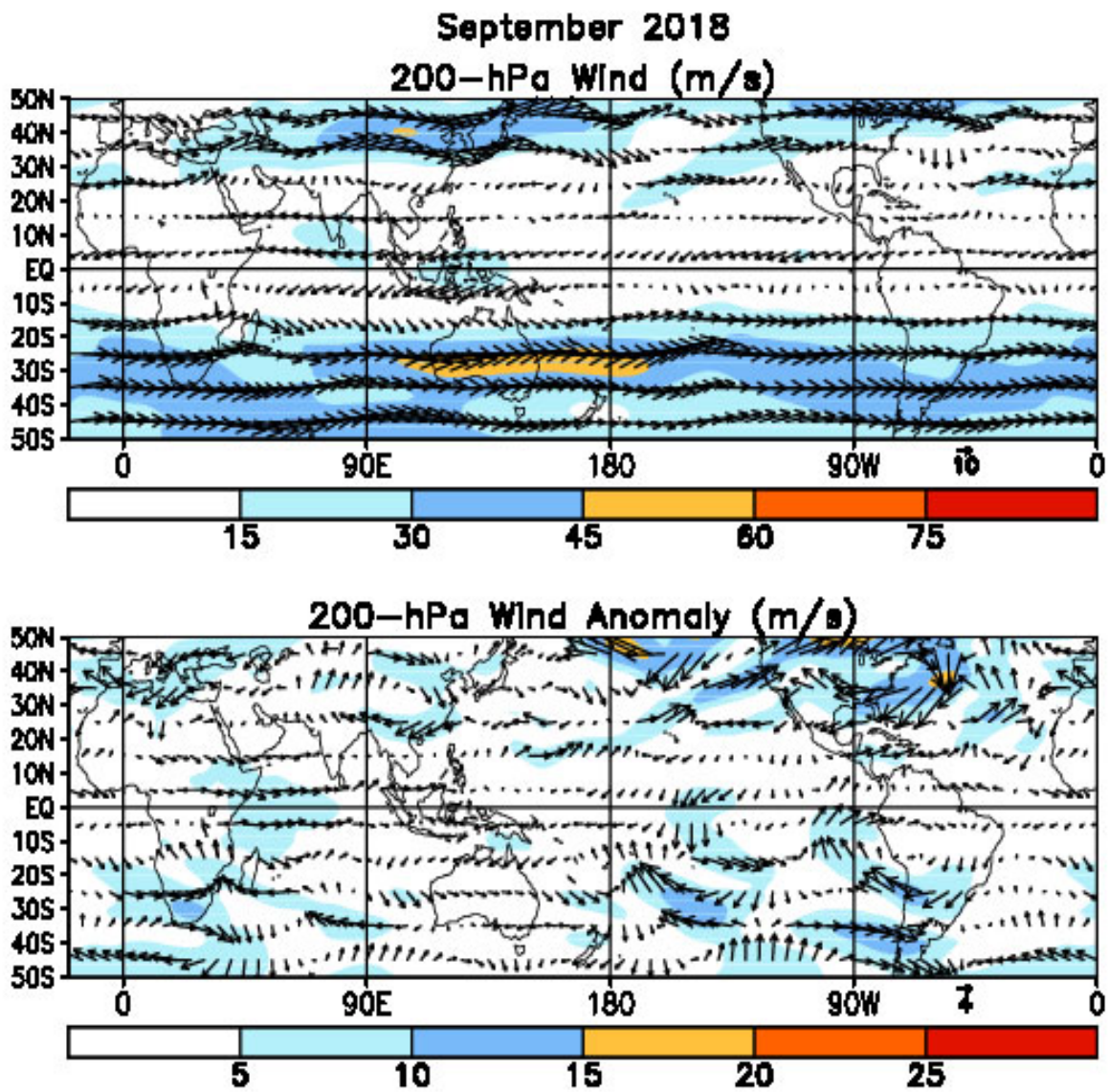


FIGURE T21. Mean (top) and anomalous (bottom) 200-hPa vector wind (CDAS/Reanalysis) for SEP 2018. Contour interval for isotachs is  $15 \text{ ms}^{-1}$  (top) and  $5 \text{ ms}^{-1}$  (bottom). Anomalies are departures from 1981-2010 base period monthly means.

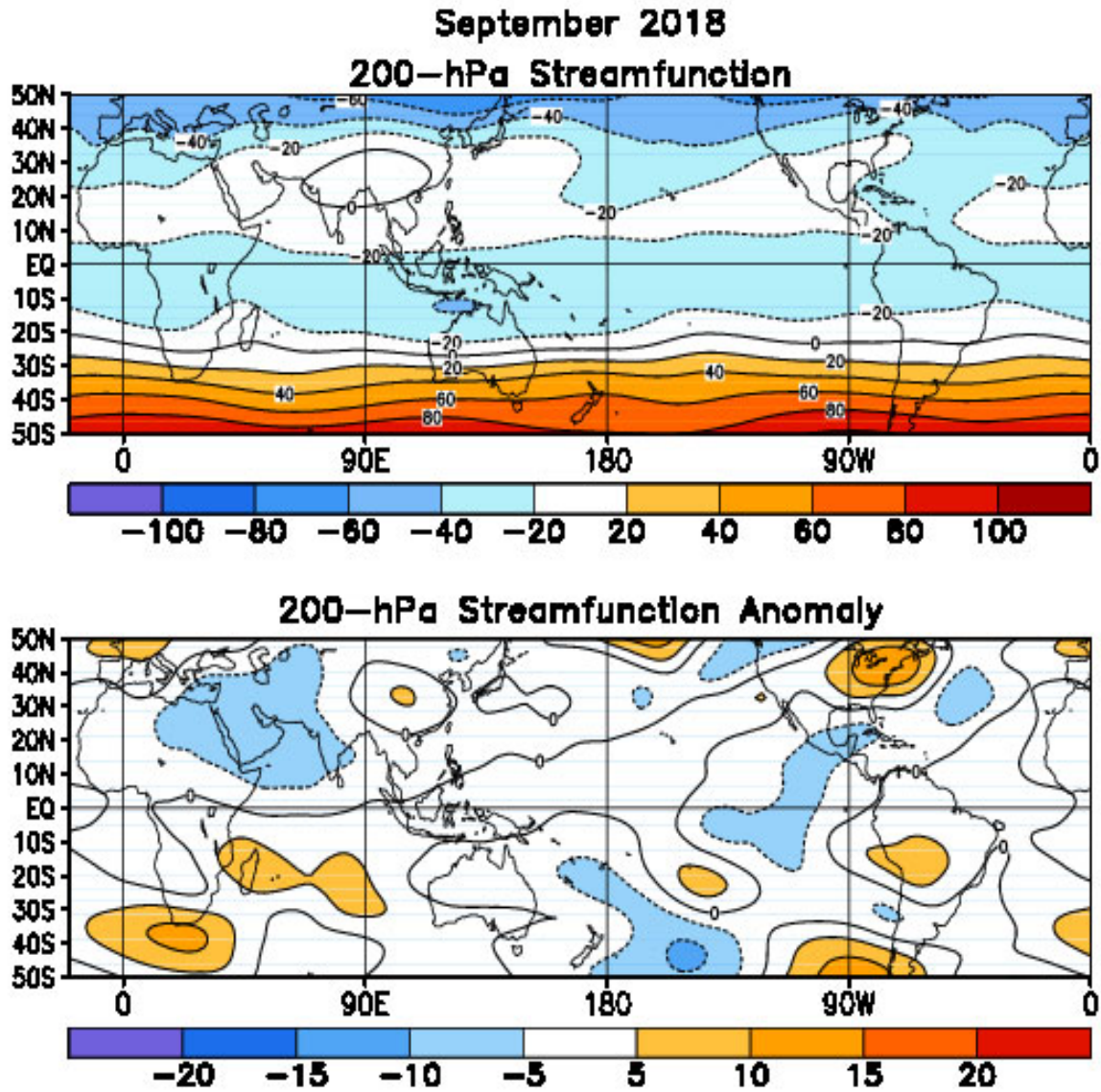


FIGURE T22. Mean (top) and anomalous (bottom) 200-hPa streamfunction (CDAS/Reanalysis). Contour interval is  $20 \times 10^6 \text{ m}^2\text{s}^{-1}$  (top) and  $5 \times 10^6 \text{ m}^2\text{s}^{-1}$  (bottom). Negative (positive) values are indicated by dashed (solid) lines. The non-divergent component of the flow is directed along the contours with speed proportional to the gradient. Thus, high (low) stream function corresponds to high (low) geopotential height in the Northern Hemisphere and to low (high) geopotential height in the Southern Hemisphere. Anomalies are departures from the 1981-2010 base period monthly means.

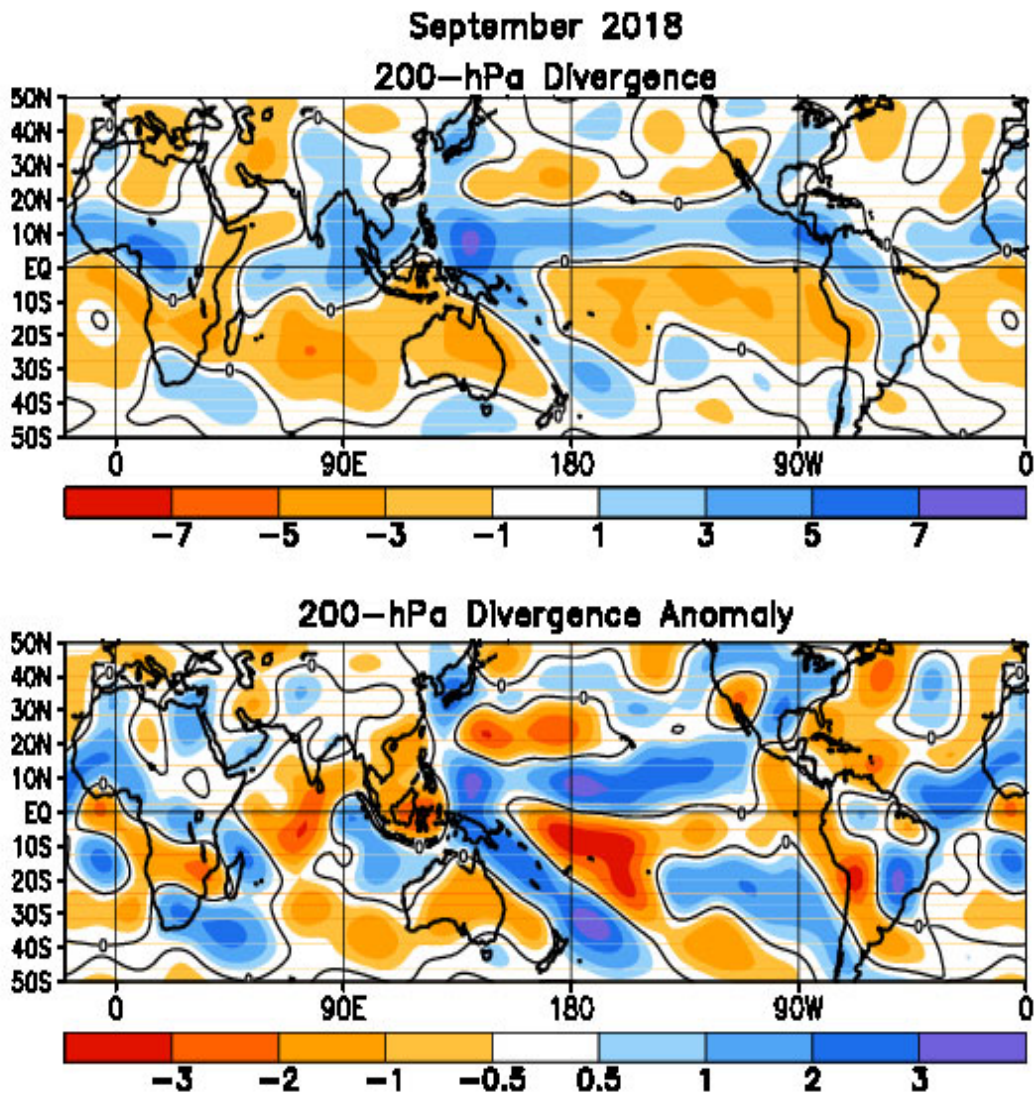


FIGURE T23. Mean (top) and anomalous (bottom) 200-hPa divergence (CDAS/Reanalysis). Divergence and anomalous divergence are shaded blue. Convergence and anomalous convergence are shaded orange. Anomalies are departures from the 1981-2010 base period monthly means.

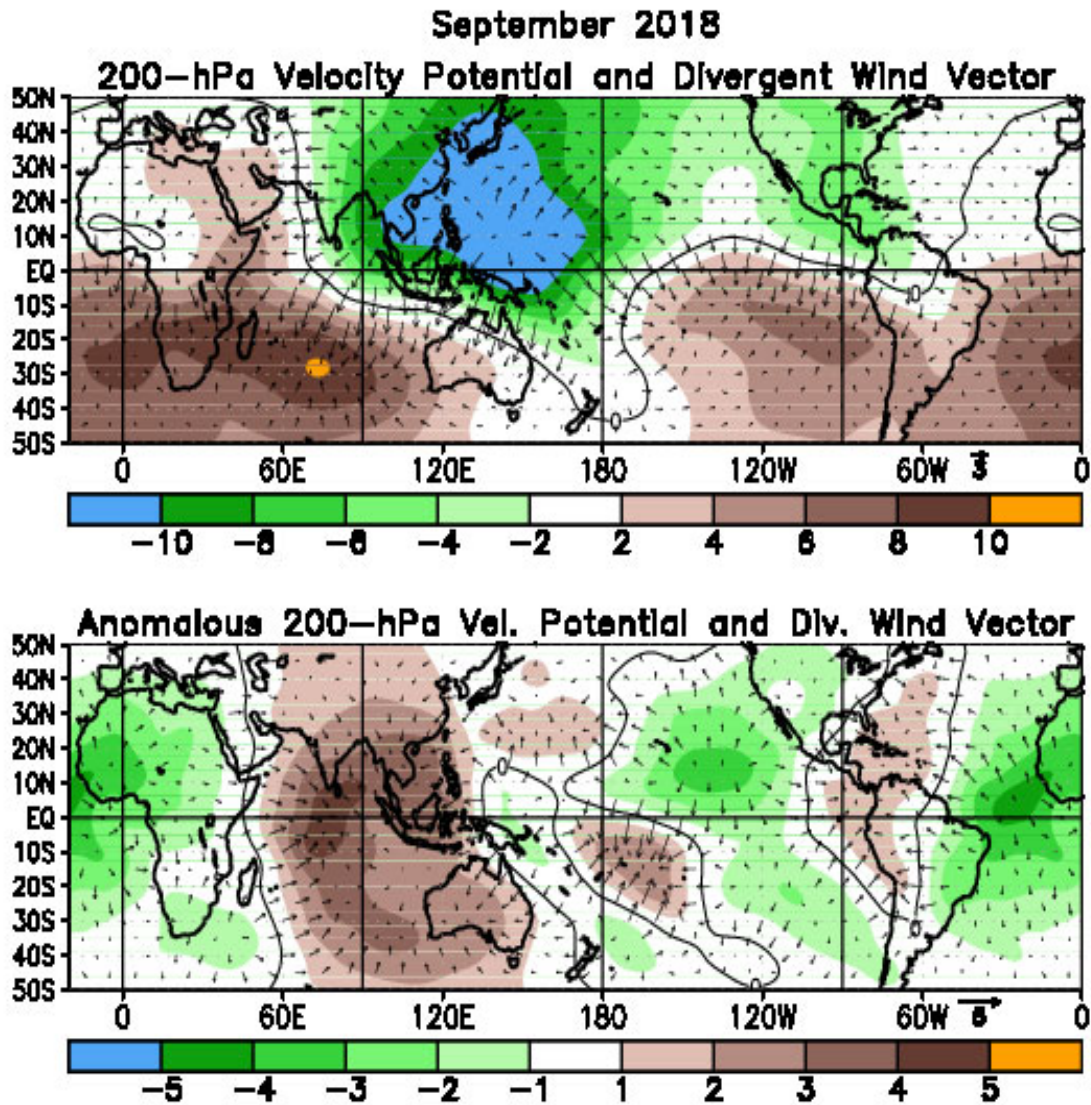


FIGURE T24. Mean (top) and anomalous (bottom) 200-hPa velocity potential ( $10^6\text{m}^2\text{s}$ ) and divergent wind (CDAS/Reanalysis). Anomalies are departures from the 1981-2010 base period monthly means.



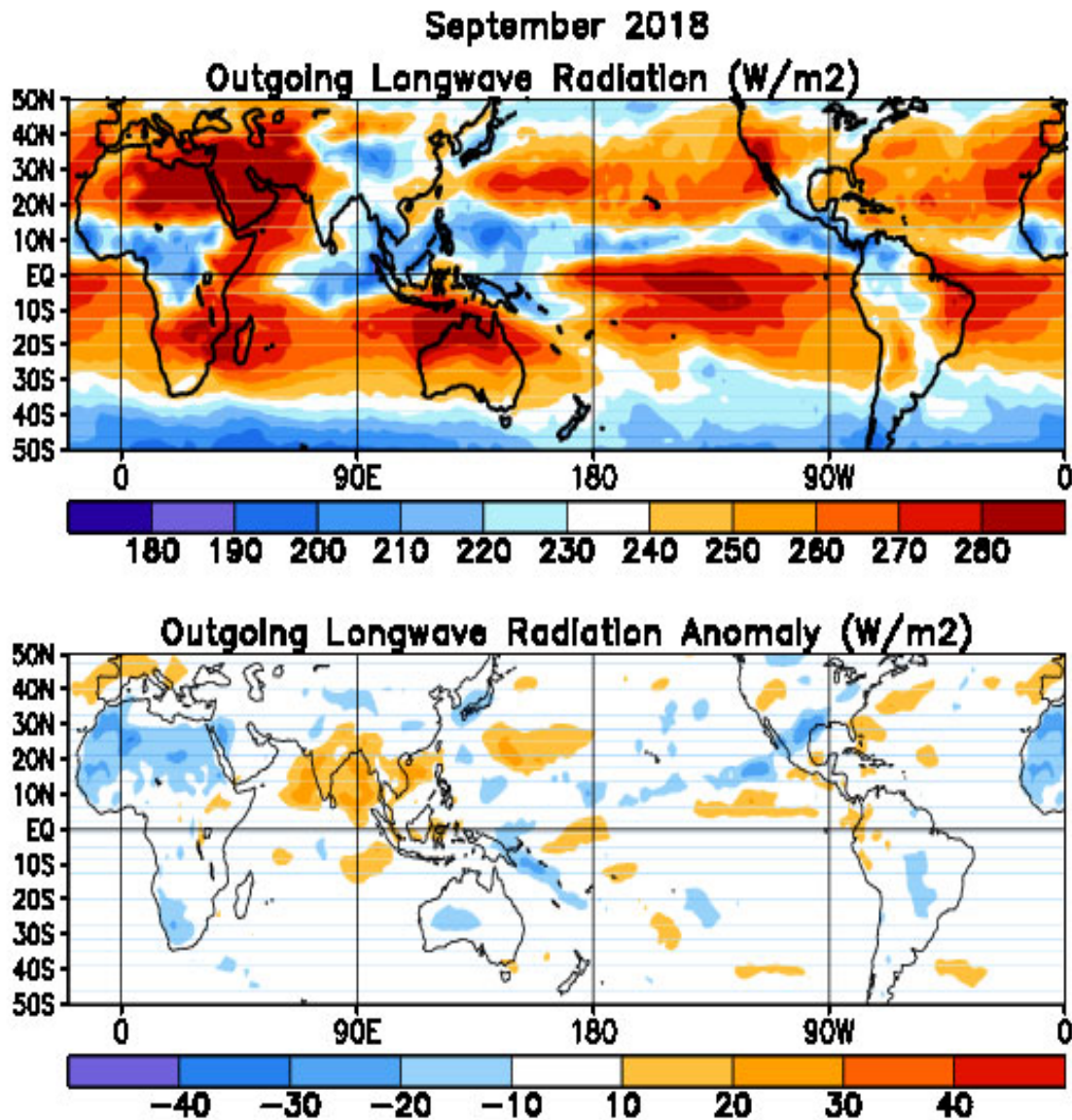


FIGURE T25. Mean (top) and anomalous (bottom) outgoing longwave radiation for SEP 2018 (NOAA 18 AVHRR IR window channel measurements by NESDIS/ORA). OLR contour interval is  $20 Wm^{-2}$  with values greater than  $280 Wm^{-2}$  indicated by dashed contours. Anomaly contour interval is  $15 Wm^{-2}$  with positive values indicated by dashed contours and light shading. Anomalies are departures from the 1981-2010 base period monthly means.

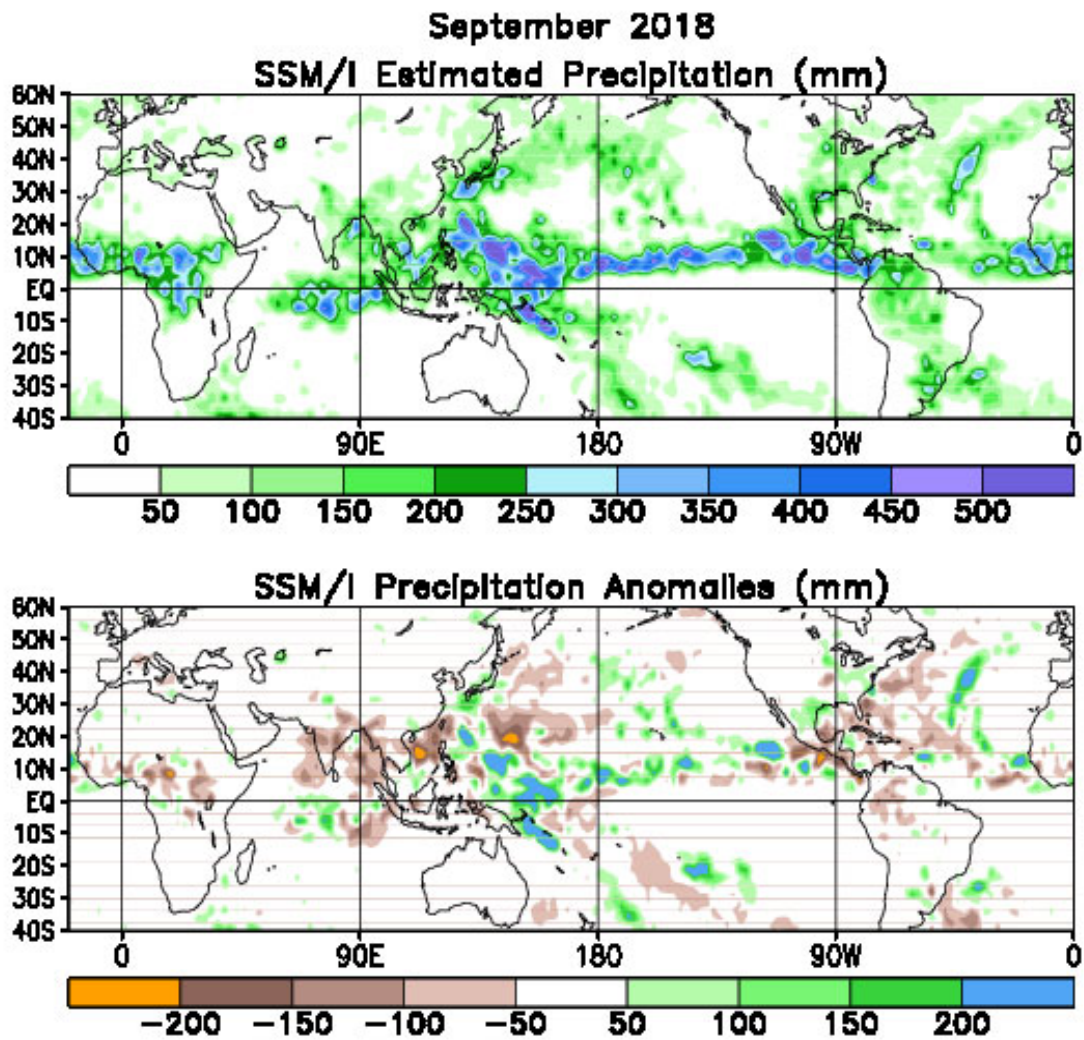


FIGURE T26. Estimated total (top) and anomalous (bottom) rainfall (mm) based on the Special Sensor Microwave/Imager (SSM/S) precipitation index (Ferraro 1997, *J. Geophys. Res.*, **102**, 16715-16735). Anomalies are computed from the SSM/I 1987-2010 base period monthly means. Anomalies have been smoothed for display purposes.

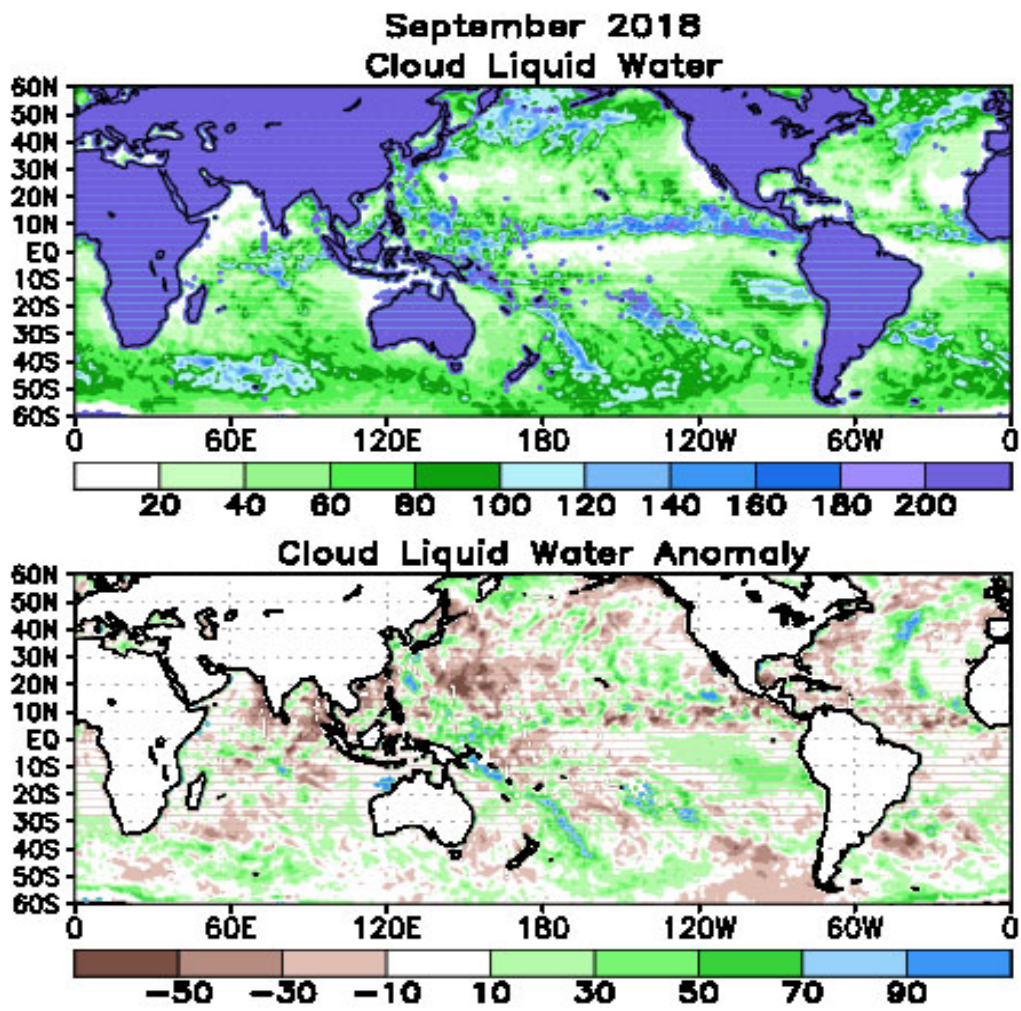


FIGURE T27. Mean (top) and anomalous (bottom) cloud liquid water ( $\text{g m}^{-2}$ ) based on the Special Sensor Microwave/Imager (SSM/I) (Weng et al 1997: *J. Climate*, **10**, 1086-1098). Anomalies are calculated from the 1987-2010 base period means.

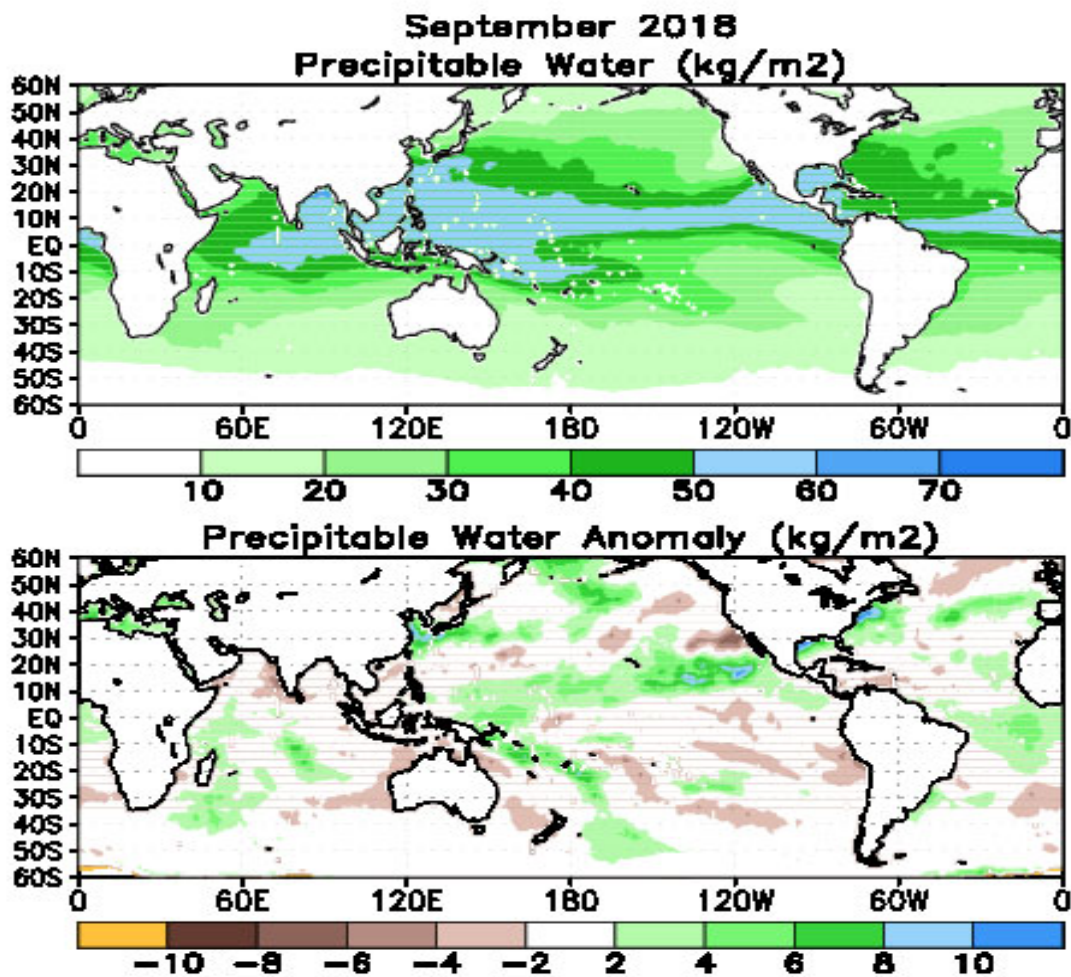


FIGURE T28. Mean (top) and anomalous (bottom) vertically integrated water vapor or precipitable water ( $\text{kg m}^{-2}$ ) based on the Special Sensor Microwave/Imager (SSM/I) (Ferraro et. al, 1996: *Bull. Amer. Meteor. Soc.*, 77, 891-905). Anomalies are calculated from the 1987-2010 base period means.

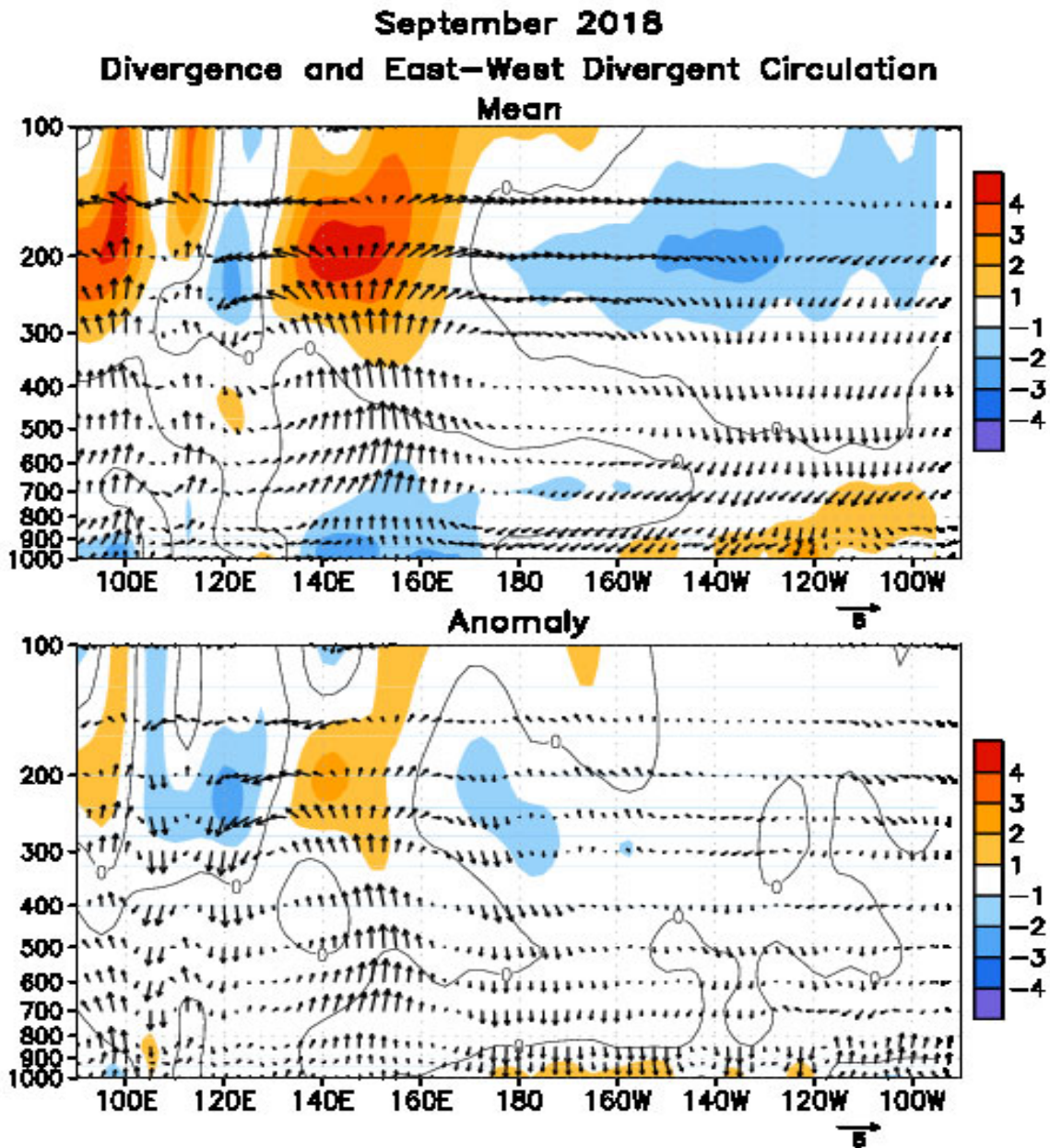


FIGURE T29. Pressure-longitude section (100E–80W) of the mean (top) and anomalous (bottom) divergence (contour interval is  $1 \times 10^{-6} \text{ s}^{-1}$ ) and divergent circulation averaged between 5N–5S. The divergent circulation is represented by vectors of combined pressure vertical velocity and the divergent component of the zonal wind. Red shading and solid contours denote divergence (top) and anomalous divergence (bottom). Blue shading and dashed contours denote convergence (top) and anomalous convergence (bottom). Anomalies are departures from the 1981–2010 base period monthly means.

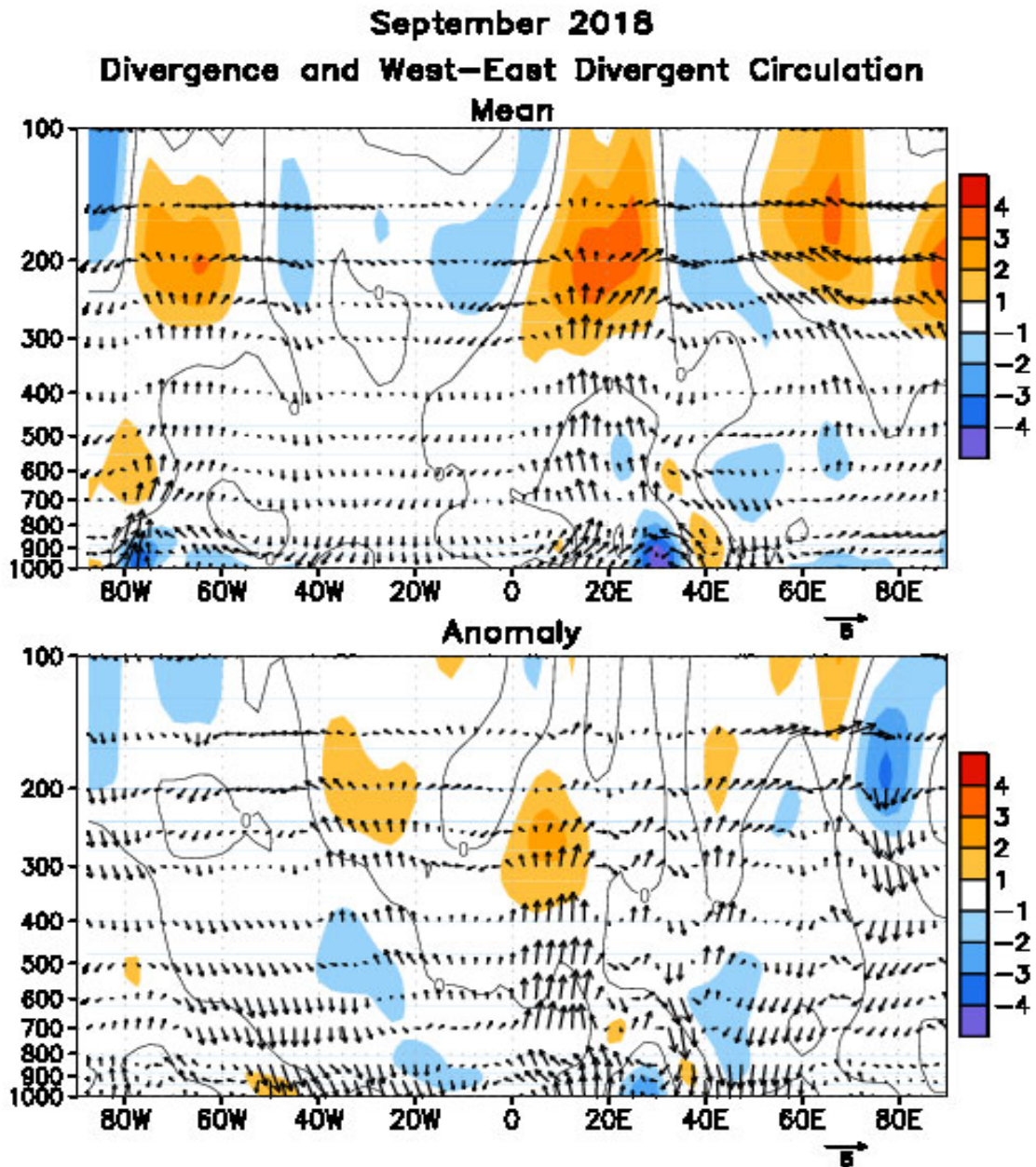


FIGURE T30. Pressure-longitude section (80W-100E) of the mean (top) and anomalous (bottom) divergence (contour interval is  $1 \times 10^{-6} \text{ s}^{-1}$ ) and divergent circulation averaged between 5N-5S. The divergent circulation is represented by vectors of combined pressure vertical velocity and the divergent component of the zonal wind. Red shading and solid contours denote divergence (top) and anomalous divergence (bottom). Blue shading and dashed contours denote convergence (top) and anomalous convergence (bottom). Anomalies are departures from the 1981-2010 base period monthly means.

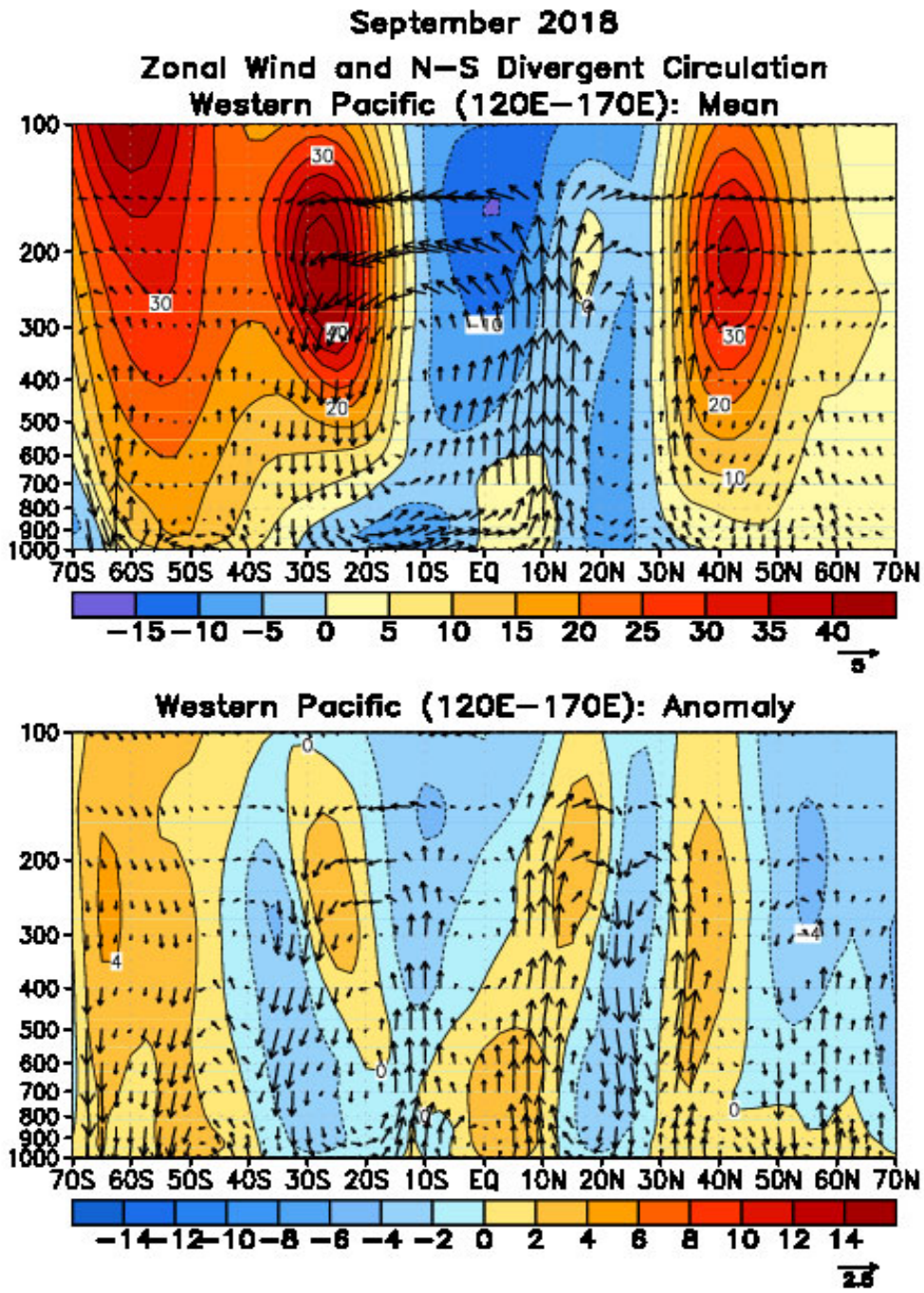


FIGURE T31. Pressure-latitude section of the mean (top) and anomalous (bottom) zonal wind ( $\text{m s}^{-1}$ ) and divergent circulation averaged over the west Pacific sector (120E–170E). The divergent circulation is represented by vectors of combined pressure vertical velocity and the divergent component of the meridional wind. Red shading and solid contours denote a westerly (top) or anomalous westerly (bottom) zonal wind. Blue shading and dashed contours denote an easterly (top) or anomalous easterly (bottom) zonal wind. Anomalies are departures from the 1981–2010 base period monthly means.

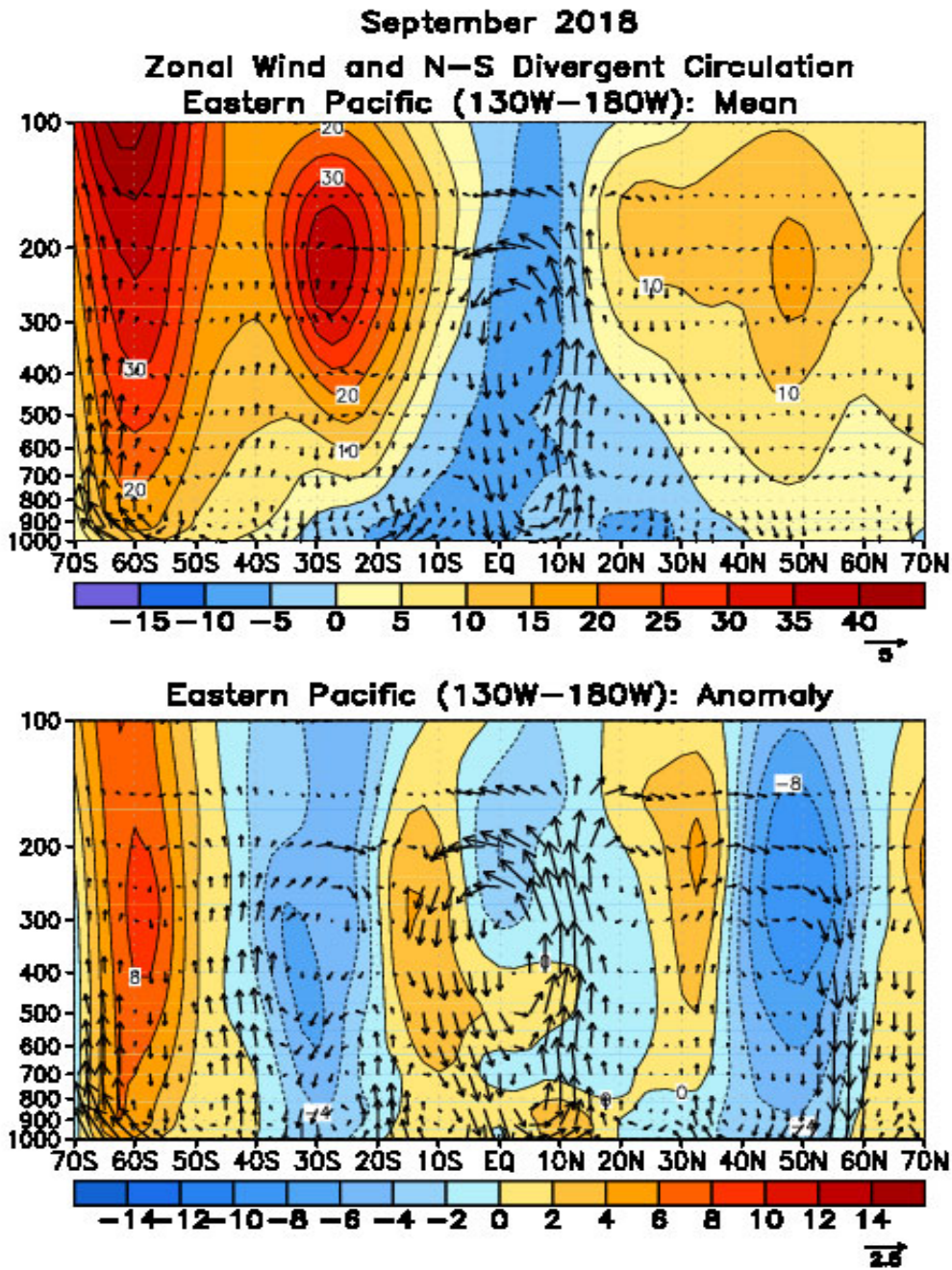
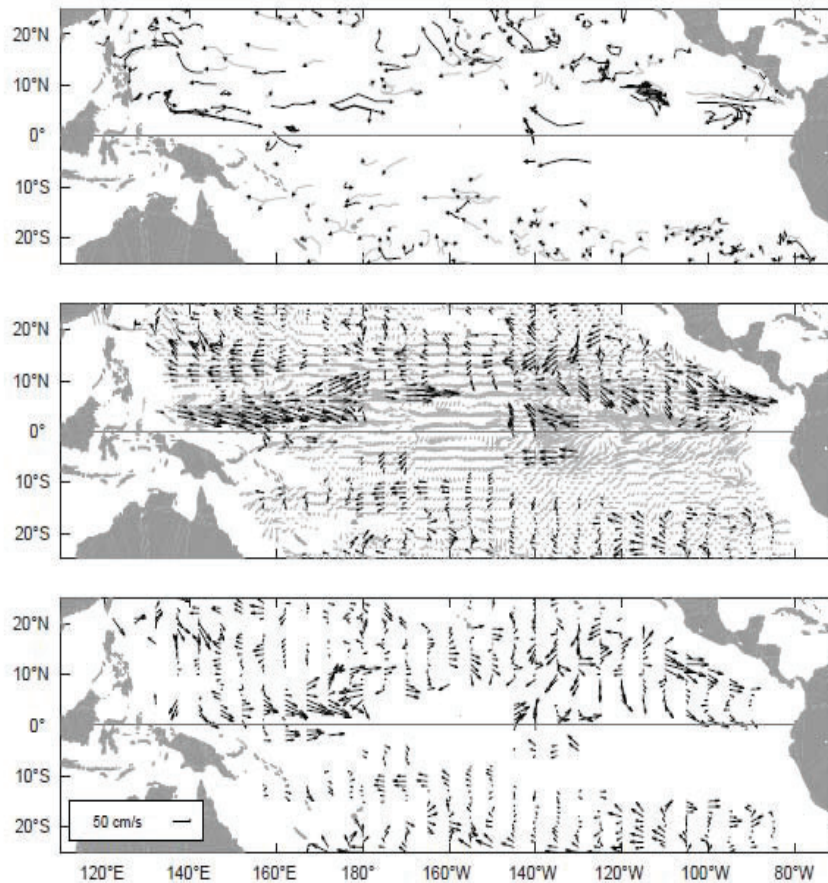


FIGURE T32. Pressure-latitude section of the mean (top) and anomalous (bottom) zonal wind ( $\text{m s}^{-1}$ ) and divergent circulation averaged over the central Pacific sector (130W-180W). The divergent circulation is represented by vectors of combined pressure vertical velocity and the divergent component of the meridional wind. Red shading and solid contours denote a westerly (top) or anomalous westerly (bottom) zonal wind. Blue shading and dashed contours denote an easterly (top) or anomalous easterly (bottom) zonal wind. Anomalies are departures from the 1981-2010 base period monthly means.



Tropical Pacific Drifting Buoys R. Lumpkin/M. Pazos, AOML, Miami

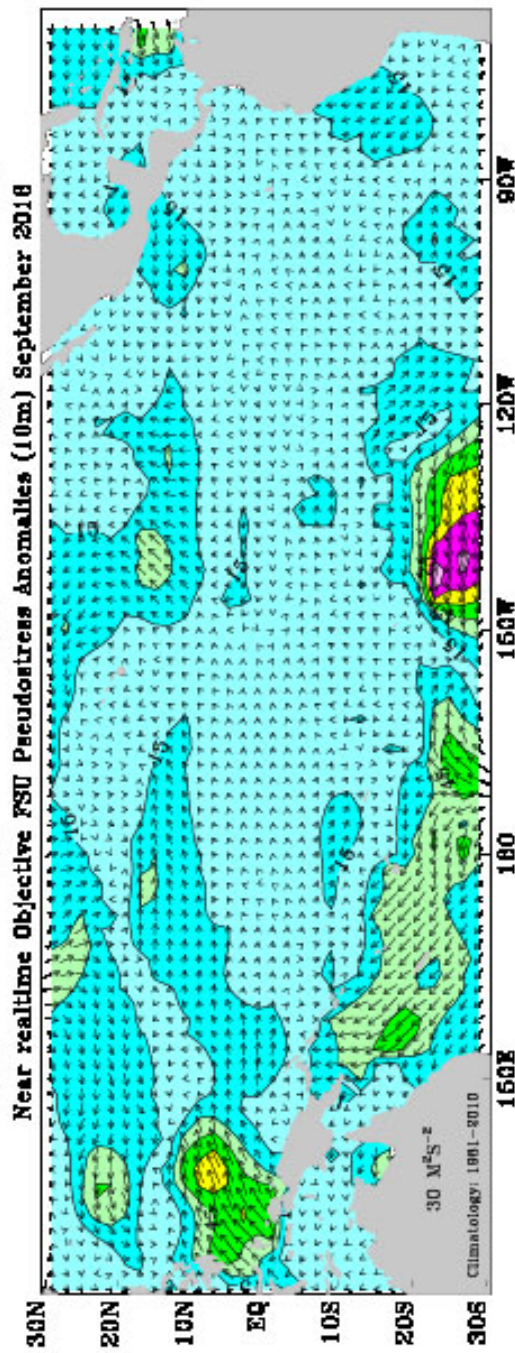
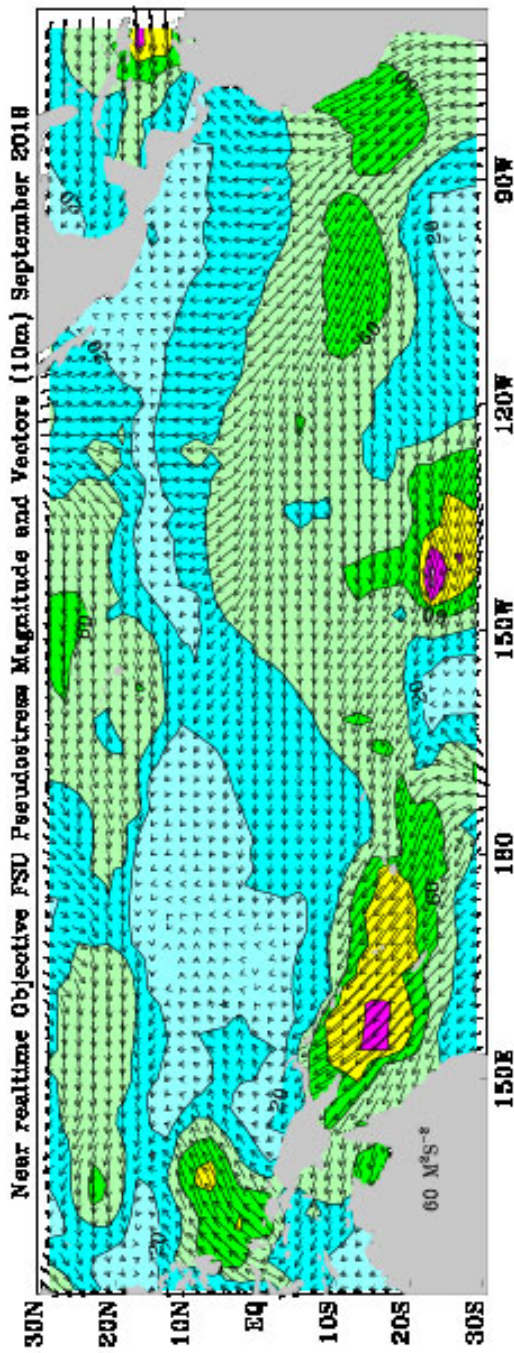
During September 2018, 272 satellite-tracked surface drifting buoys were reporting from the tropical Pacific. Several drifters indicated extremely strong (1 m/s) eastward anomalies in the far western Pacific, centered at 2-3°N. Elsewhere, the drifter array indicated that large-scale currents were close to their climatological September strengths across the basin.



**Figure A1.1 Top:** Movements of drifting buoys in the tropical Pacific Ocean during October 2018. The linear segments of each trajectory represent a one week displacement. Trajectories of buoys which have lost their subsurface drogues are gray; those with drogues are black.

**Middle:** Monthly mean currents calculated from all buoys 1993-2002 (gray), and currents measured by the drogued buoys this month (black) smoothed by an optimal filter.

**Bottom:** Anomalies from the climatological monthly mean currents for this month.



**FSU SURFACE PSEUDO-STRESS VECTORS AND ANOMALIES: September 2018.** Pseudo-stress vectors (top) are objectively analyzed from ship and buoy winds on a 2° grid. Ship and buoy data are independently weighted and the background field is created from the data. Contour interval of the vector magnitudes is  $20 \text{ M}^2\text{S}^{-2}$ . Anomalies (bottom) are departures from 1981-2010 mean. The contour interval is  $16 \text{ M}^2\text{S}^{-2}$ . For more information, please visit our web site at <http://www.coaps.fsu.edu/EVSMDC/html/winds.shtml>. Produced by Jeremy Kalish, Mark A. Bourassa, and Shawn R. Smith, Center for Ocean-Atmospheric Prediction Studies, Florida State University, Tallahassee, FL 32306-2640, USA.

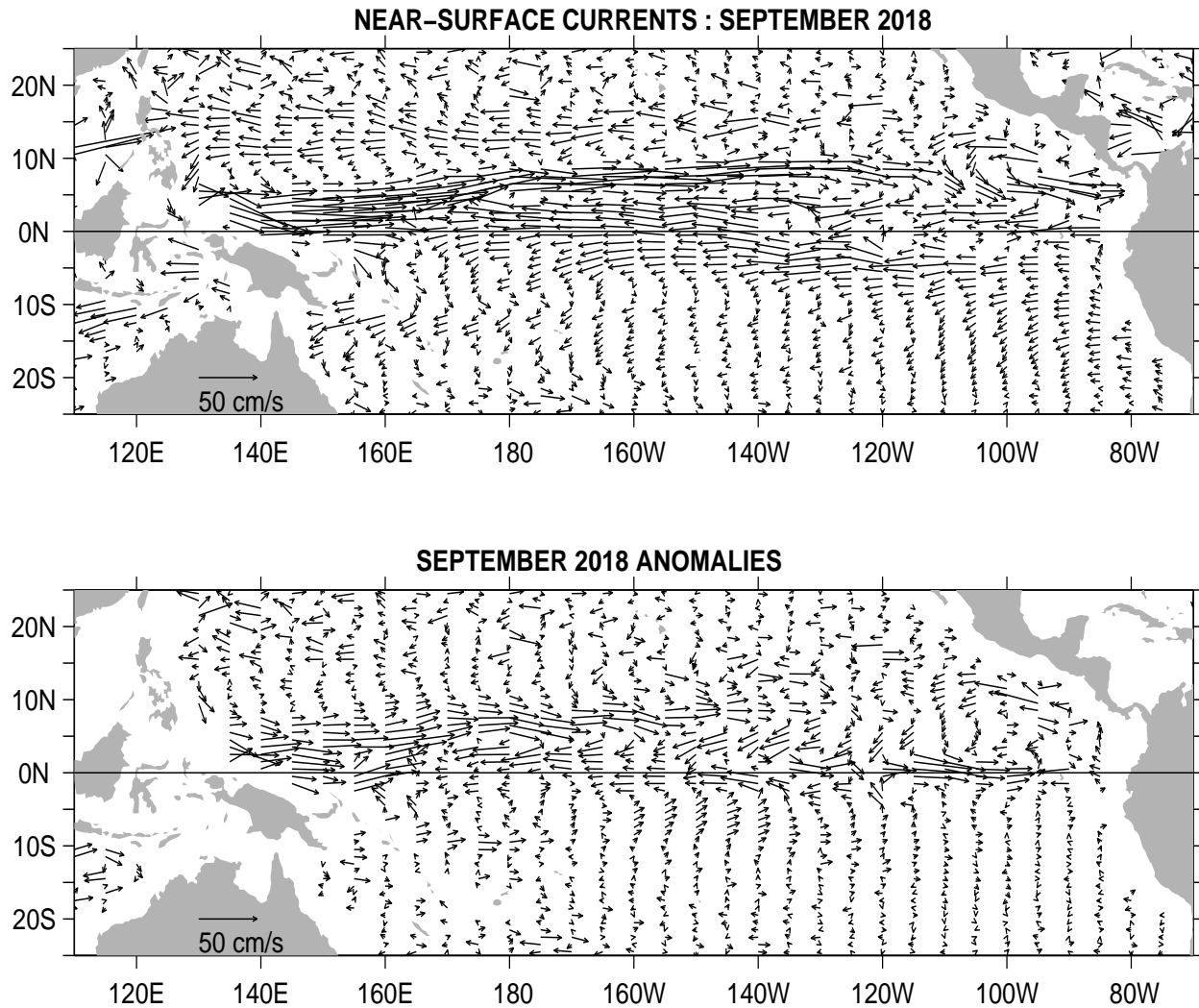


FIGURE A1.3. Ocean Surface Current Analysis-Real-time (OSCAR) for SEP 2018 (Bonjean and Lagerloef 2002, *J. Phys. Oceanogr.*, Vol. 32, No. 10, 2938-2954; Lagerloef et al. 1999, *JGR-Oceans*, 104, 23313-23326). (top) Total velocity. Surface currents are calculated from satellite data including Jason sea level anomalies and NCEP winds. (bottom) Velocity anomalies. The subtracted climatology was based on SSM/I and QuickScat winds and Topex/Poseidon and Jason from 1993-2003. See also <http://www.oscar.noaa.gov>.

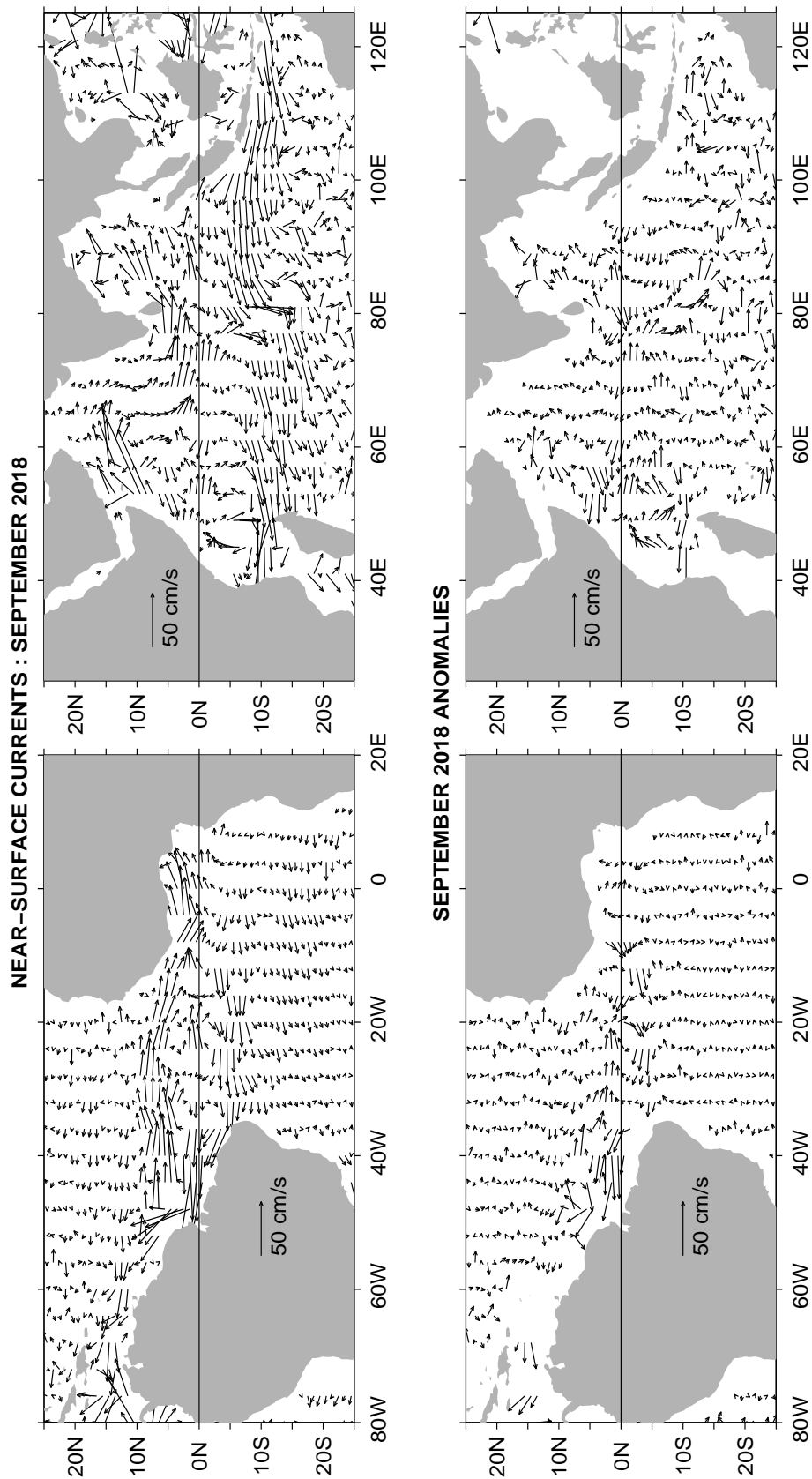


FIGURE A1.4. Ocean Surface Current Analysis-Real-time (OSCAR) for SEP 2018 (Bonjean and Lagerloef 2002, *J. Phys. Oceanogr.*, Vol. 32, No. 10, 2938-2954; Lagerloef et al. 1999, *JGR-Oceans*, 104, 23313-23326). (top) Total velocity. Surface currents are calculated from satellite data including Jason sea level anomalies and NCEP winds. (bottom) Velocity anomalies. The subtracted climatology was based on SSM/I and QuickScat winds and Topex/Poseidon and Jason from 1993-2003. See also <http://www.oscar.noaa.gov>.

## Forecast Forum

The canonical correlation analysis (CCA) forecast of SST in the central Pacific (Barnett et al. 1988, *Science*, **241**, 192196; Barnston and Ropelewski 1992, *J. Climate*, **5**, 13161345), is shown in **Figs. F1 and F2**. This forecast is produced routinely by the Prediction Branch of the Climate Prediction Center. The predictions from the National Centers for Environmental Prediction (NCEP) Coupled Forecast System Model (CFS03) are presented in **Figs. F3 and F4a, F4b**. Predictions from the Markov model (Xue, et al. 2000: *J. Climate*, **13**, 849871) are shown in **Figs. F5 and F6**. Predictions from the latest version of the LDEO model (Chen et al. 2000: *Geophys. Res. Lett.*, **27**, 25852587) are shown in **Figs. F7 and F8**. Predictions using linear inverse modeling (Penland and Magorian 1993: *J. Climate*, **6**, 10671076) are shown in **Figs. F9 and F10**. Predictions from the Scripps / Max Planck Institute (MPI) hybrid coupled model (Barnett et al. 1993: *J. Climate*, **6**, 15451566) are shown in **Fig. F11**. Predictions from the ENSOCLIPER statistical model (Knaff and Landsea 1997, *Wea. Forecasting*, **12**, 633652) are shown in **Fig. F12**. Niño 3.4 predictions are summarized in **Fig. F13**, provided by the Forecasting and Prediction Research Group of the IRI.

The CPC and the contributors to the **Forecast Forum** caution potential users of this predictive information that they can expect only modest skill.

## ENSO Alert System Status: [El Niño Watch](#)

### Outlook

El Niño is favored to form in the next couple of months and continue through the Northern Hemisphere winter 2018-19 (70-75% chance).

### Discussion

ENSO-neutral continued during September, but with increasingly more widespread regions of above-average sea surface temperatures (SSTs) across the equatorial Pacific Ocean (Fig. T18). During September, the Niño-3.4 and Niño-3 index values were +0.3C, while the Niño-4 index value was at +0.5C (Table T2). Positive subsurface temperature anomalies (averaged across 180°-100°W) increased during the last month, due to the expansion and strengthening of above-average temperatures at depth across the equatorial Pacific (Fig. T17). Convection was increasingly suppressed over Indonesia and around the Date Line (Fig. T25). Low-level westerly wind anomalies were evident over the western and east-central Pacific, with some of the strongest anomalies occurring over the

eastern Pacific during the past week (Fig. T20). Upper-level wind anomalies were easterly over the east-central Pacific (Fig. T21). Overall, the oceanic and atmospheric conditions reflected ENSO-neutral, but with recent trends indicative of a developing El Niño.

The majority of models in the IRI/CPC plume predict El Niño to form during the fall and continue through the winter (Figs. F1-F13). The official forecast favors the formation of a weak El Niño, consistent with the recent strengthening of westerly wind anomalies and positive temperature trends in the surface and subsurface ocean. In summary, El Niño is favored to form in the next couple of months and continue through the Northern Hemisphere winter 2018-19 (70-75% chance).

Weekly updates of oceanic and atmospheric conditions are available on the Climate Prediction Center homepage ([El Niño/La Niña Current Conditions and Expert Discussions](#)).

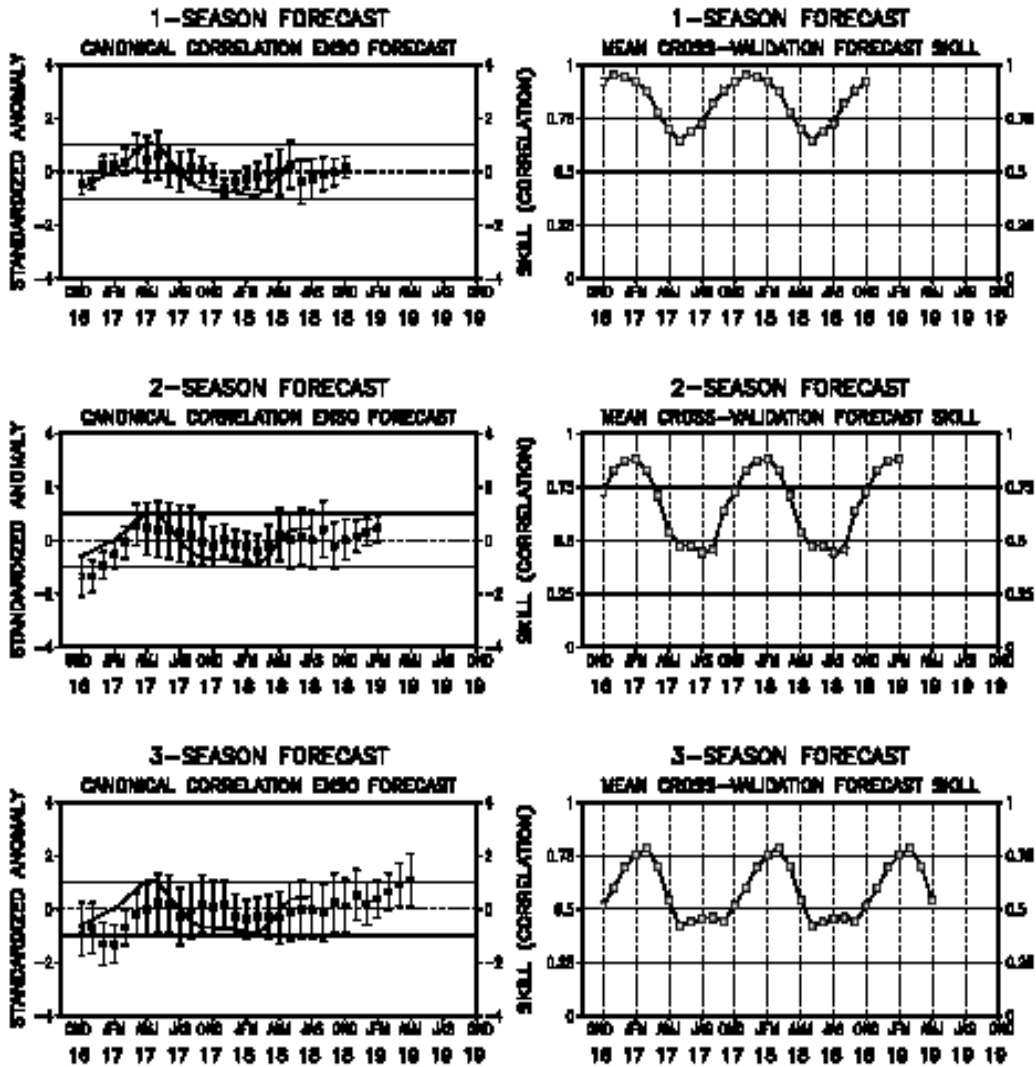


FIGURE F1. Canonical correlation analysis (CCA) sea surface temperature (SST) anomaly prediction for the central Pacific (5°N to 5°S, 120°W to 170°W (Barnston and Ropelewski, 1992, *J. Climate*, 5, 1316-1345). The three plots on the left hand side are, from top to bottom, the 1-season, 2-season, and 3-season lead forecasts. The solid line in each forecast represents the observed SST standardized anomaly through the latest month. The small squares at the mid-points of the forecast bars represent the real-time CCA predictions based on the anomalies of quasi-global sea level pressure and on the anomalies of tropical Pacific SST, depth of the 20°C isotherm and sea level height over the prior four seasons. The vertical lines represent the one standard deviation error bars for the predictions based on past performance. The three plots on the right side are skills, corresponding to the predicted and observed SST. The skills are derived from cross-correlation tests from 1956 to present. These skills show a clear annual cycle and are inversely proportional to the length of the error bars depicted in the forecast time series.

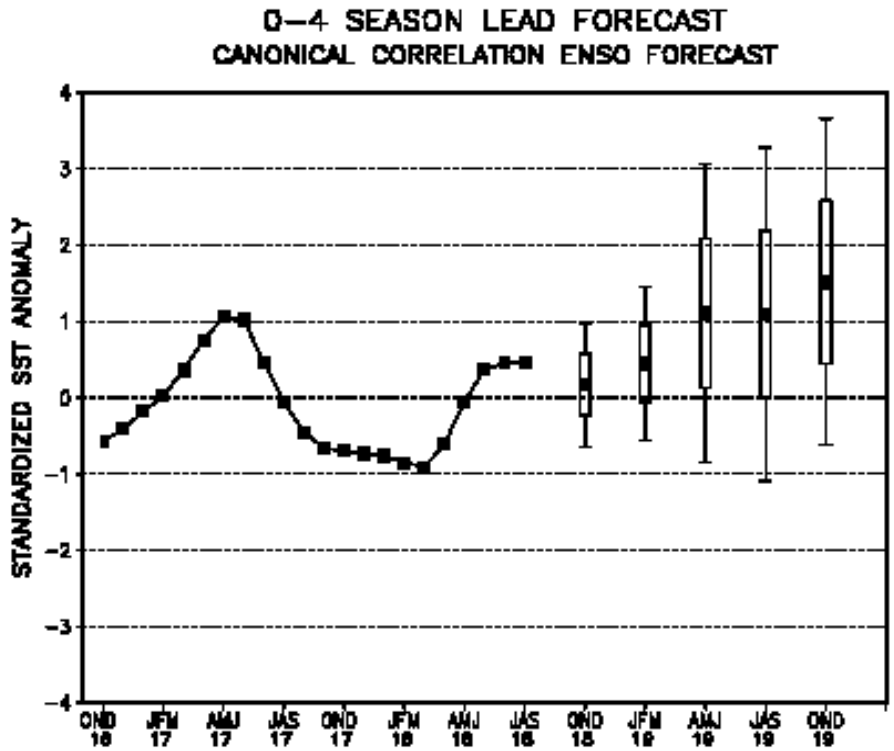


FIGURE F2. Canonical Correlation Analysis (CCA) forecasts of sea-surface temperature anomalies for the Niño 3.4 region (5N-5S, 120W-170W) for the upcoming five consecutive 3-month periods. Forecasts are expressed as standardized SST anomalies. The CCA predictions are based on anomaly patterns of SST, depth of the 20C isotherm, sea level height, and sea level pressure. Small squares at the midpoints of the vertical forecast bars represent the CCA predictions, and the bars show the one (thick) and two (thin) standard deviation errors. The solid continuous line represents the observed standardized three-month mean SST anomaly in the Niño 3.4 region up to the most recently available data.



Last update: Thu Oct 11 2018  
initial conditions: 1Oct2018-10Oct2018

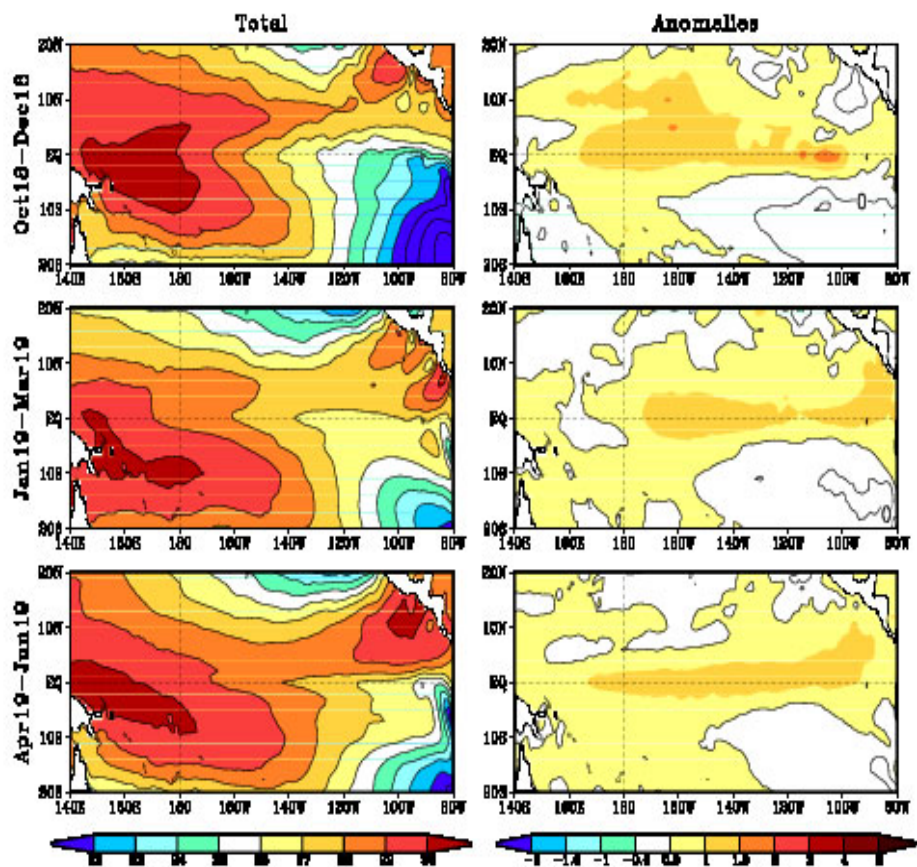


FIGURE F3. Predicted 3-month average sea surface temperature (left) and anomalies (right) from the NCEP Coupled Forecast System Model (CFS03). The forecasts consist of 40 forecast members. Contour interval is 1°C, with additional contours for 0.5°C and -0.5°C. Negative anomalies are indicated by dashed contours.

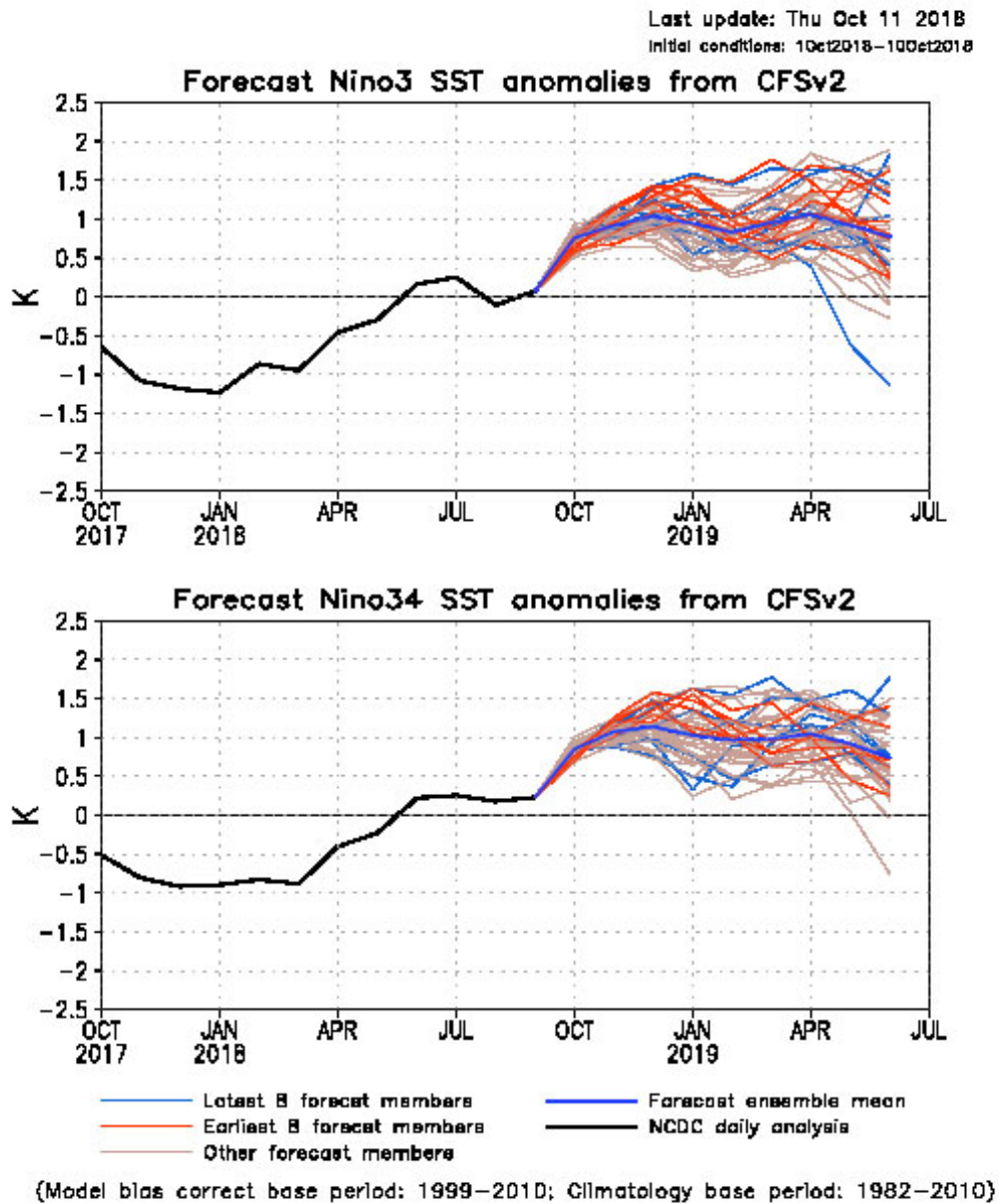


FIGURE F4. Predicted and observed sea surface temperature (SST) anomalies for the Nino 3 (top) and Nino 3.4 (bottom) regions from the NCEP Coupled Forecast System Model (CFS03). The forecasts consist of 40 forecast members. The ensemble mean of all 40 forecast members is shown by the blue line, individual members are shown by thin lines, and the observation is indicated by the black line. The Nino-3 region spans the eastern equatorial Pacific between 5N-5S, 150W-90W. The Nino 3.4 region spans the east-central equatorial Pacific between 5N-5S, 170W-120W.

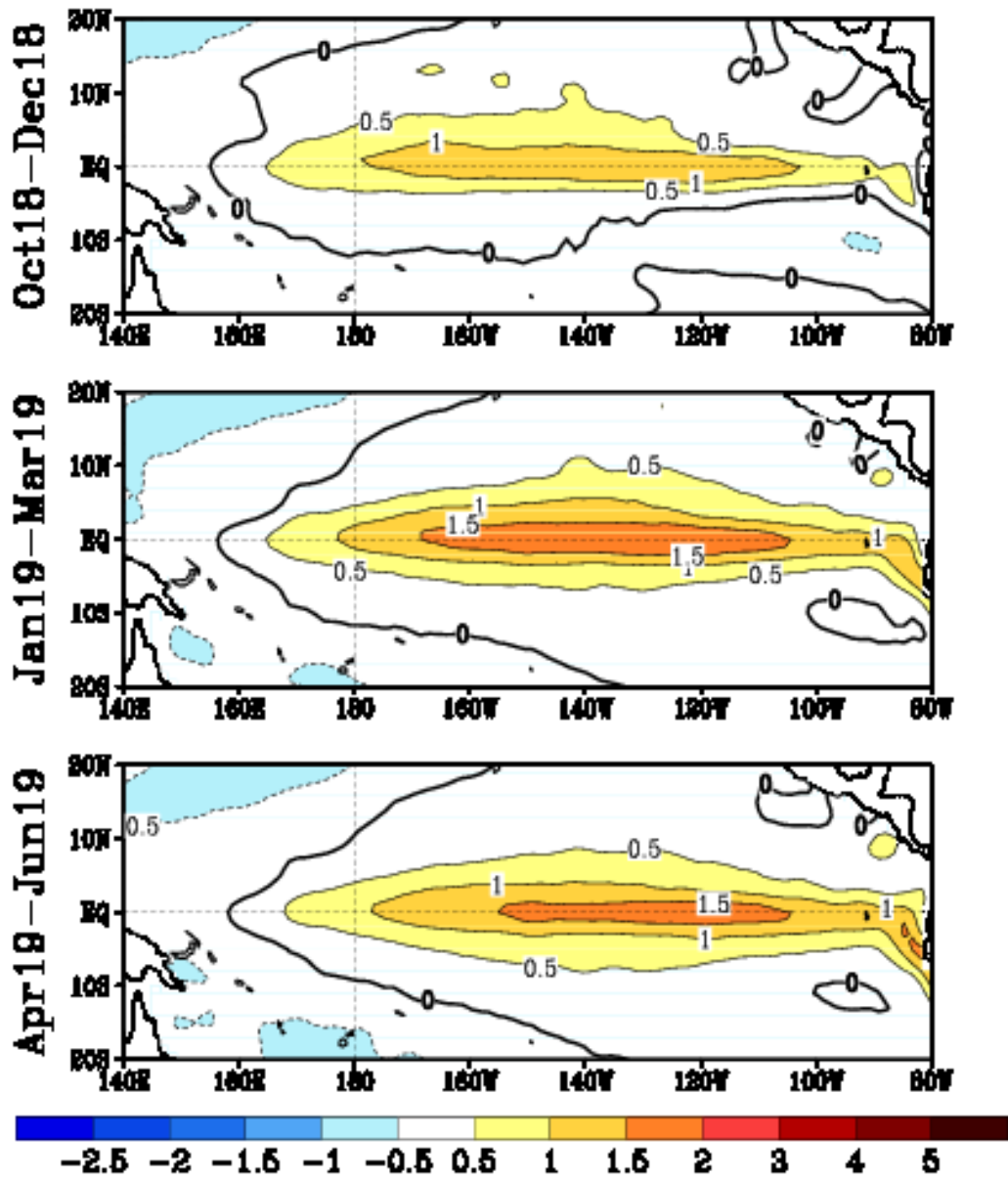


FIGURE F5. Predicted 3-month average sea surface temperature anomalies from the NCEP/CPC Markov model (Xue et al. 2000, *J. Climate*, 13, 849-871). The forecast is initiated in SEP 2018 . Contour interval is 0.3C and negative anomalies are indicated by dashed contours. Anomalies are calculated relative to the 1971-2000 climatology.

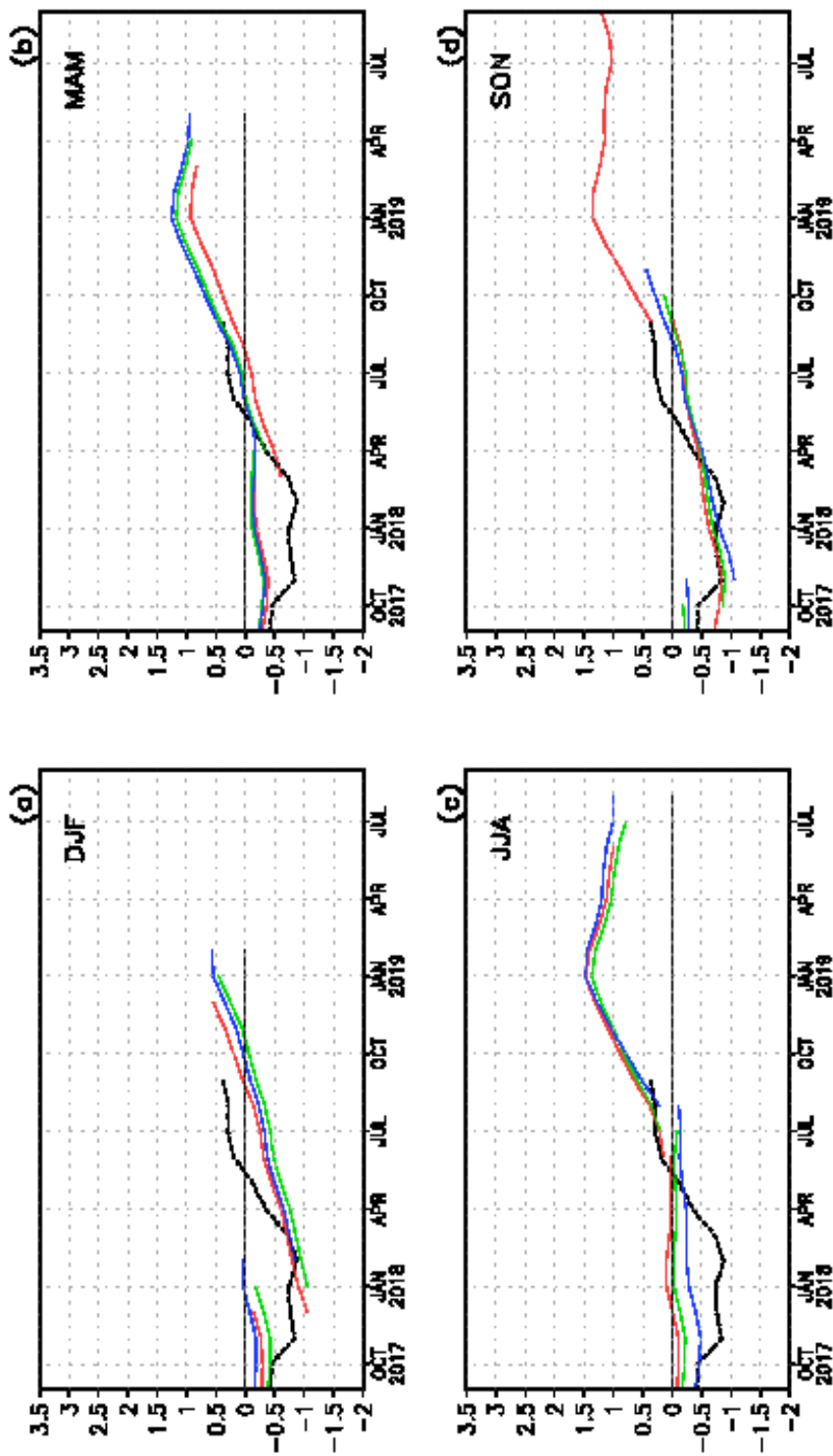
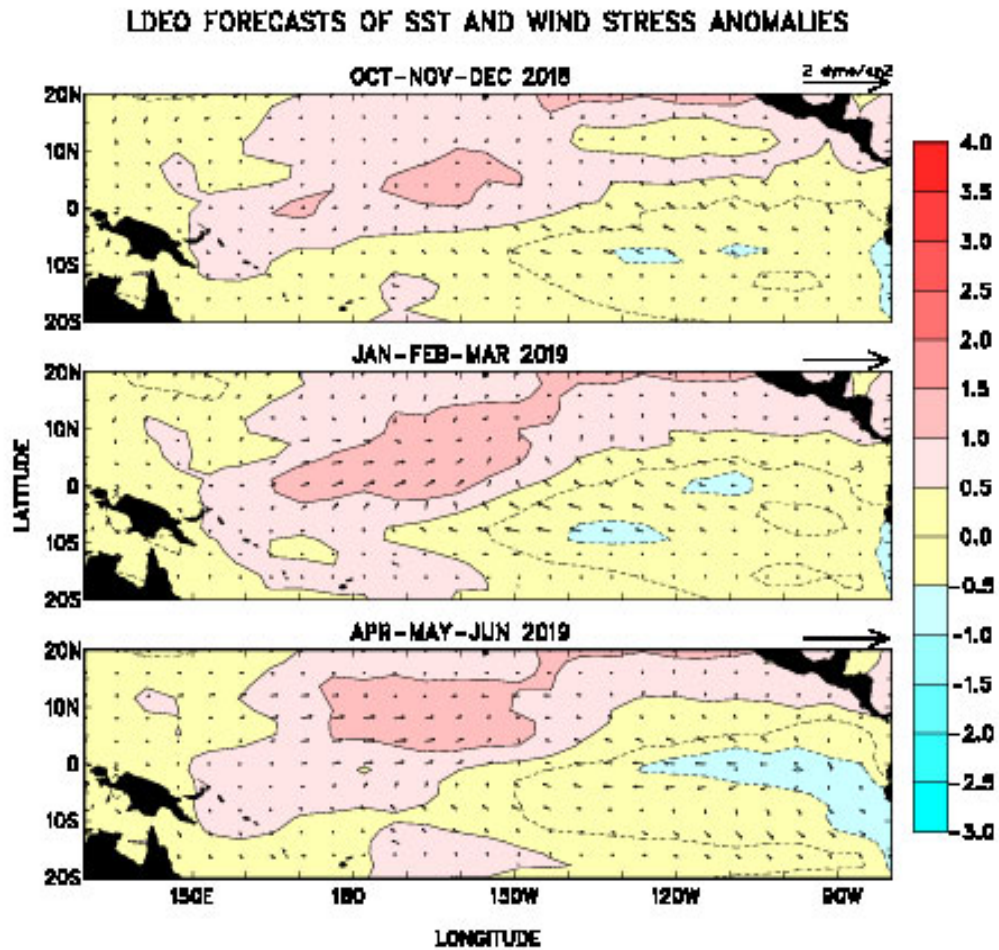
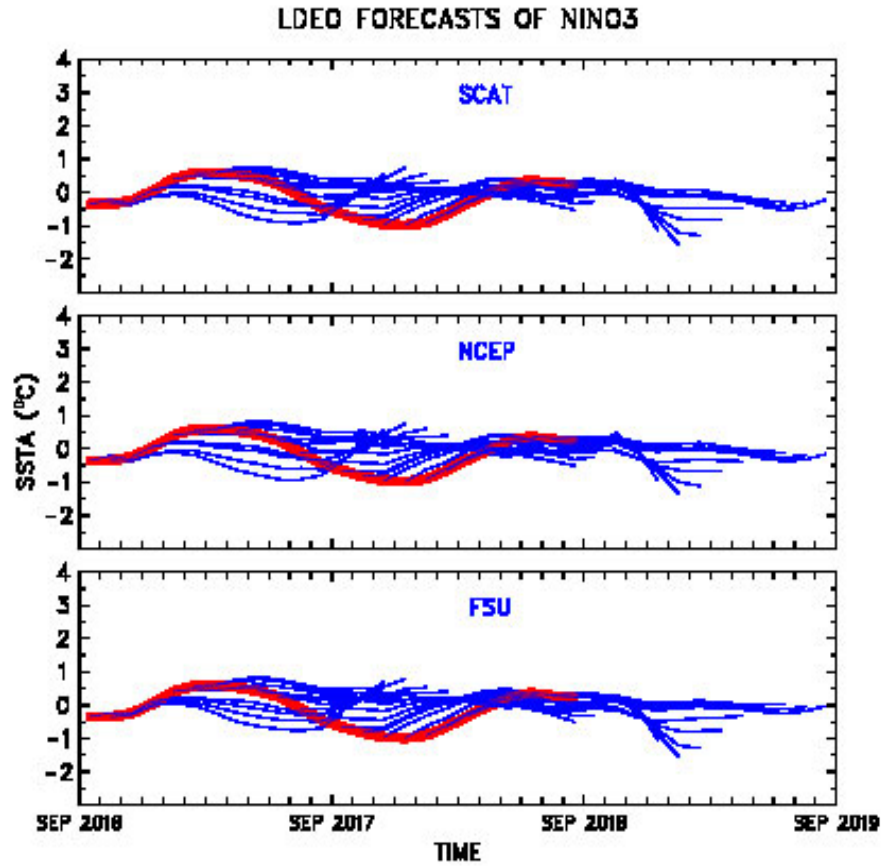


FIGURE F6. Time evolution of observed and predicted SST anomalies in the Niño 3.4 region (up to 12 lead months) by the NCEP/CPC Markov model (Xue et al. 2000, *J. Climate*, **13**, 849-871). Anomalies are calculated relative to the 1971-2000 climatology. Shown in each panel are the forecasts grouped by three consecutive starting months: (a) is for December, January, and February, (b) is for March, April, and May, (c) is for June, July, and August, and (d) is for September, October, and November. The observed Niño 3.4 SST anomalies are indicated by the black dashed lines. The Niño 3.4 region spans the east-central equatorial Pacific between 5N-5S, 170W-120W.



**FIGURE F7.** Forecasts of the tropical Pacific Predicted SST (shading) and vector wind anomalies for the next 3 seasons based on the LDEO model. Each forecast represents an ensemble average of 3 sets of predictions initialized during the last three consecutive months (see Figure F8).



**FIGURE F8.** LDEO forecasts of SST anomalies for the Nino 3 region using wind stresses obtained from (top) QuikSCAT, (middle) NCEP, and (bottom) Florida State Univ. (FSU), along with SSTs (obtained from NCEP), and sea surface height data (obtained from TOPEX/POSEIDON) data. Each thin blue line represents a 12-month forecast, initialized one month apart for the past 24 months. Observed SST anomalies are indicated by the thick red line. The Nino-3 region spans the eastern equatorial Pacific between 5N-5S, 150W-90W.

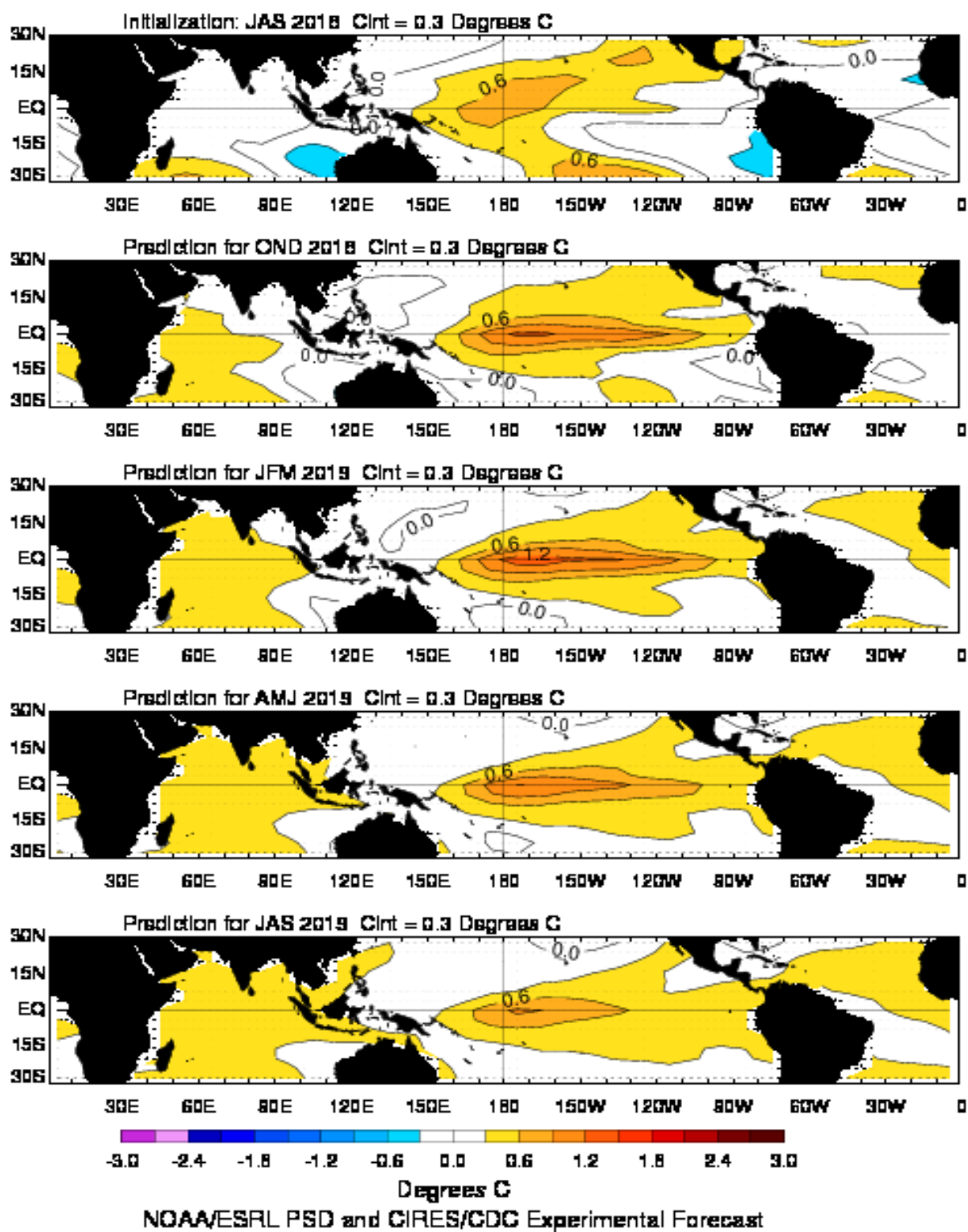


FIGURE F9. Forecast of tropical SST anomalies from the Linear Inverse Modeling technique of Penland and Magorian (1993: *J. Climate*, 6, 1067-1076). The contour interval is 0.3C. Anomalies are calculated relative to the 1981-2010 climatology and are projected onto 20 leading EOFs.

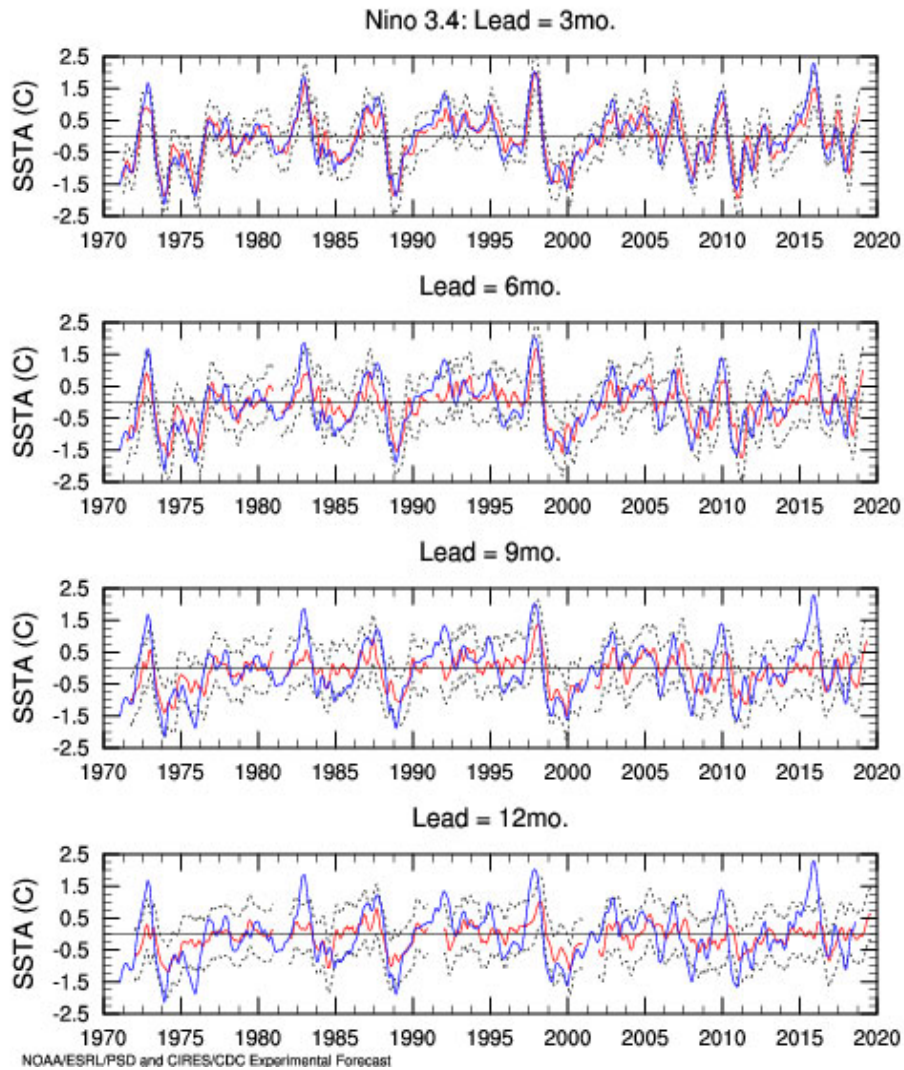


FIGURE F10. Predictions of Niño 3.4 SSTA (blue solid line) and verification (solid red line). The Niño3.4 Index was calculated in the area 6N-6S, 170W-120W. The 1980-2010 climatology was subtracted from ERSST data between 1950 and 2010, after which they were projected onto 20 EOFs containing 90% of the variance. Significant 1950-2010 trends were subtracted from the corresponding PCs, the forecast was made on the detrended anomalies, after which the trend was added to the forecast. The dotted lines indicate the one standard deviation confidence interval for the forecasts based on a perfect adherence to assumption.



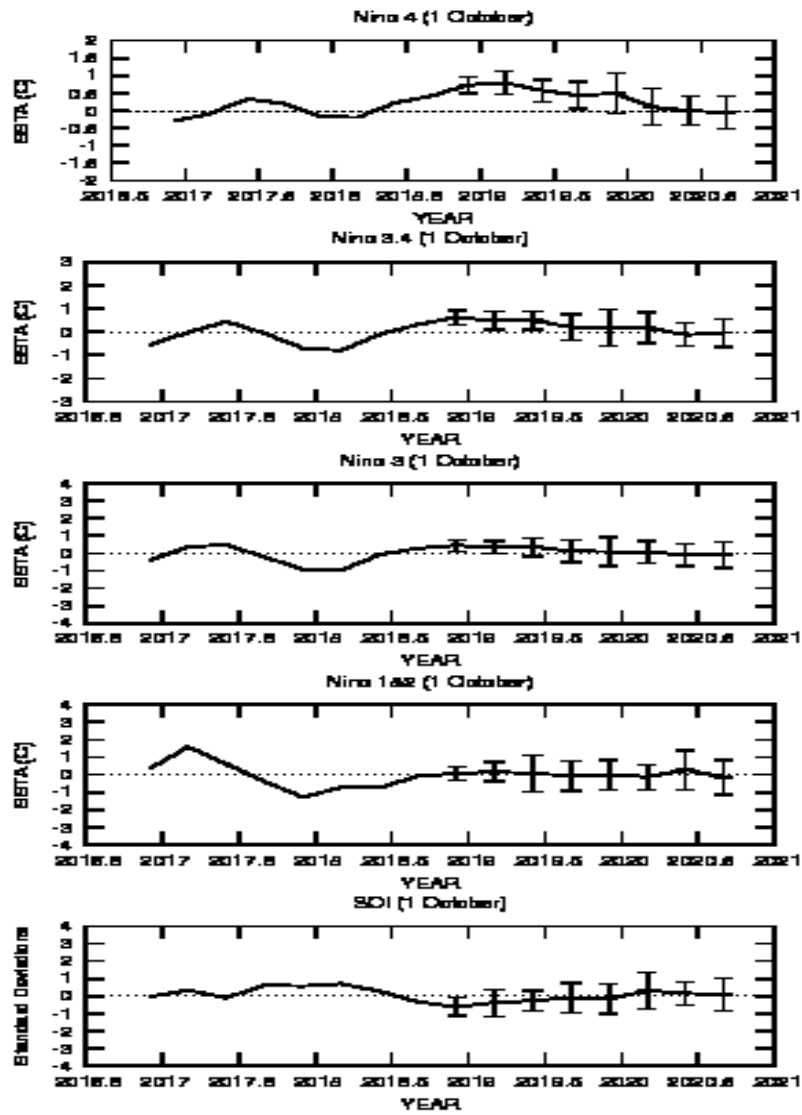


FIGURE F11. ENSO-CLIPER statistical model forecasts of three-month average sea surface temperature anomalies (green lines, deg. C) in (top panel) the Nino 4 region (5N-5S, 160E-150W), (second panel) the Nino 3.4 region (5N-5S, 170W-120W), (third panel) the Nino 3 region (5N-5S, 150W-90W), and (fourth panel) the Nino 1+2 region (0-10S, 90W-80W) (Knaff and Landsea 1997, *Wea. Forecasting*, **12**, 633-652). Bottom panel shows predictions of the three-month standardized Southern Oscillation Index (SOI, green line). Horizontal bars on green line indicate the adjusted root mean square error (RMSE). The Observed three-month average values are indicated by the thick blue line. SST anomalies are departures from the 1981-2010 base period means, and the SOI is calculated from the 1951-1980 base period means.

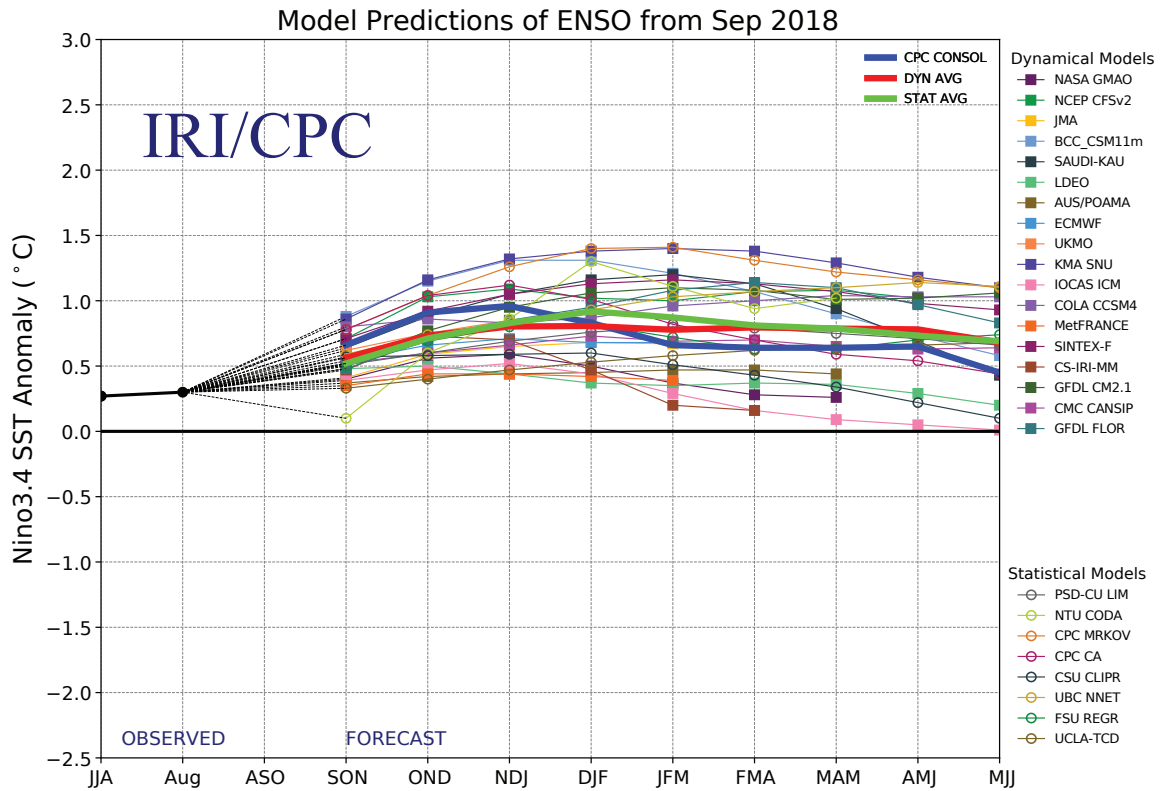


FIGURE F12. Time series of predicted sea surface temperature anomalies for the Nino 3.4 region (deg. C) from various dynamical and statistical models for nine overlapping 3-month periods. The Nino 3.4 region spans the east-central equatorial Pacific between 5N-5S, 170W-120W. Figure provided by the International Research Institute (IRI).

# Extratropical Highlights – September 2018

## 1. Northern Hemisphere

The 500-hPa circulation during September featured above-average heights over the high latitudes of the North Pacific, eastern North America, and Europe, and below-average heights over western Canada and the high latitudes of the North Atlantic (Fig. E9). For the Atlantic, the pattern projected strongly onto the positive phase of the North Atlantic Oscillation (NAO, +1.8 std. dev.) (Fig. E7, Table E1). A strong positive NAO pattern has been present for almost all of 2018.

The main land-surface temperature signals during September included above-average temperatures in both the western and eastern United States and Europe, and below-average temperatures in western Canada (Fig. E1). The main precipitation signals included above-average totals across the central U.S. and eastern Canada, and below-average totals in the northwestern and southeastern U.S. and in much of Europe (Fig. E3).

### a. United States

The 500-hPa circulation during September featured an amplified ridge in the eastern U.S. and a deep trough in the west (Figs. E9, E11). This anomalous wave pattern was associated with well above-average surface temperatures in the eastern half of the U.S., with many areas recording departures of 3+°C and in the upper 90th percentile of occurrences (Fig. E1). Well above-average precipitation occurred across the central U.S., which was situated between the mean trough and ridge axes (Fig. E3). Area-average totals exceeded the 90th percentile of occurrences in the Great Plains, Midwest, Ohio Valley, and Great Lakes regions (Fig. E5). In the Midwest region, rainfall totals have been above the 90th percentile of occurrences for the past two months.

According to the U.S. Drought Monitor, severe-to-exceptional drought continued in the southwestern and northwestern U.S. One of the hardest-hit regions is the 4-corner states of Utah, Colorado, Arizona, and New Mexico. Another major drought area includes the states of Oregon and Washington, with extreme drought evident across central Oregon and moderate or severe drought present elsewhere.

### b. North Atlantic/ Europe

The 500-hPa height pattern featured above-average heights over the central North Atlantic and Europe, and below-average heights over the high latitudes of the North Atlantic (Fig. E9). This pattern reflected a continued strong positive phase of both the NAO (+1.8 std. dev.) (Fig. E7, Table E1). A positive NAO pattern has generally prevailed since January 2018.

The overall circulation contributed to a continuation of exceptionally warm surface temperatures across Europe (Fig. E1), with most of the continent again recording departures in the upper 90th

percentile of occurrences. It also contributed to a continuation of below-average precipitation in northern Europe, an area which has recorded deficits for the last five months (Fig. E4).

### c. West African monsoon

The west African monsoon extends from June through September, with a peak during July-September. During September 2018, the monsoon rains were enhanced (Fig. E3, Fig. T24) with area-average rainfall totals above the 90th percentile of occurrences (see Sahel region, Fig. E4). This region has recorded above-average precipitation for the last four months.

## 2. Southern Hemisphere

The mean 500-hPa circulation during September featured above-average heights over the central portions of the three ocean basins, and below-average heights at high latitudes (Fig. E15). The most significant surface temperature anomalies were present in southern South America, where departures were above the 90th percentile of occurrences (Fig. E1). Much of this area also recorded above-average precipitation (Fig. E3). These conditions were associated with an amplified trough situated over the high latitudes of the South Pacific and located just upstream of continental South America (Fig. E15).

The Antarctic ozone hole typically develops during August and reaches its peak size in September. The ozone hole then gradually decreases during October and November, and dissipates in early December (Fig. S8 top). During the latter half of September 2018, the size of the ozone hole was above average at 23 to 24 million square kilometers. This increased size was associated with larger than average size of the SH polar vortex (Fig. S8 middle), and with an anomalously large area of Polar stratospheric cloud (Fig. S8 bottom).

# TELECONNECTION INDICES

| Month  | North Atlantic |      |      | North Pacific |      |      |               | EURASIA |        |  |
|--------|----------------|------|------|---------------|------|------|---------------|---------|--------|--|
|        | NAO            | EA   | WP   | EP-NP         | PNA  | TNH  | EATL/<br>WRUS | SCAND   | POLEUR |  |
| SEP 18 | 1.8            | 0.1  | -1.8 | -0.8          | 1.2  | ---  | -1.8          | -0.7    | 0.5    |  |
| AUG 18 | 2.4            | 1.8  | -1.4 | -0.8          | 1.2  | ---  | -0.5          | -1.1    | 0.0    |  |
| JUL 18 | 1.4            | 2.4  | -0.8 | -0.2          | -0.8 | ---  | -2.2          | 2.3     | -0.1   |  |
| JUN 18 | 1.4            | -0.5 | -0.4 | 0.1           | 0.7  | ---  | -0.2          | -0.8    | -0.9   |  |
| MAY 18 | 2.0            | -0.1 | -0.2 | -1.0          | -1.1 | ---  | -1.4          | 1.7     | -0.3   |  |
| APR 18 | 1.2            | 1.1  | -0.7 | -0.2          | -1.1 | ---  | 0.5           | 0.3     | -1.3   |  |
| MAR 18 | -1.4           | -0.6 | 0.8  | 0.3           | -1.2 | ---  | 4.0           | -0.8    | 0.1    |  |
| FEB 18 | 1.3            | -1.4 | 0.4  | 0.2           | -1.7 | 2.2  | -1.4          | 0.4     | -2.2   |  |
| JAN 18 | 1.2            | 0.5  | 0.4  | 0.7           | -0.1 | -0.3 | -1.6          | 0.4     | -1.5   |  |
| DEC 17 | 0.7            | -0.5 | 0.3  | ---           | 0.6  | 1.0  | -1.6          | -0.5    | -1.9   |  |
| NOV 17 | -0.1           | 0.1  | 0.7  | 0.4           | -2.0 | ---  | -1.2          | -0.1    | -2.2   |  |
| OCT 17 | 0.7            | 0.6  | 0.7  | -0.6          | -0.3 | ---  | -0.0          | 0.3     | -1.2   |  |
| SEP 17 | -0.5           | 1.6  | -1.2 | -0.5          | -0.3 | ---  | -2.5          | 0.5     | -1.7   |  |

TABLE E1-Standardized amplitudes of selected Northern Hemisphere teleconnection patterns for the most recent thirteen months (computational procedures are described in Fig. E7). Pattern names and abbreviations are North Atlantic Oscillation (NAO); East Atlantic pattern (EA); West Pacific pattern (WP); East Pacific - North Pacific pattern (EP-NP); Pacific/North American pattern (PNA); Tropical/Northern Hemisphere pattern (TNH); East Atlantic/Western Russia pattern (EATL/WRUS)-called Eurasia-2 pattern by Barnston and Livezey, 1987, *Mon. Wea. Rev.*, **115**, 1083-1126); Scandinavia pattern (SCAND-called Eurasia-1 pattern by Barnston and Livezey 1987); and Polar Eurasia pattern (POLEUR). No value is plotted for calendar months in which the pattern does not appear as a leading mode.

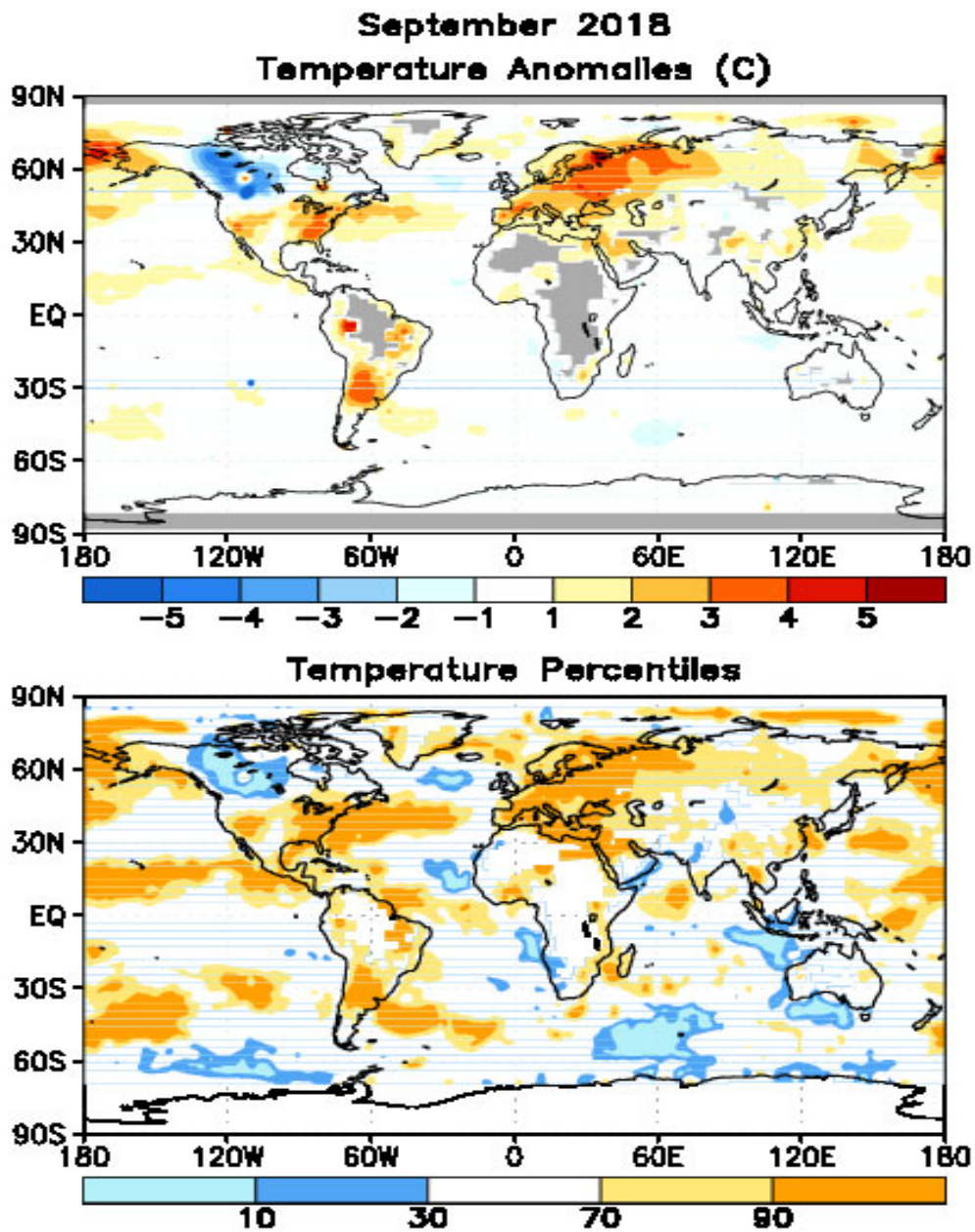


FIGURE E1. Surface temperature anomalies ( $^{\circ}\text{C}$ , top) and surface temperature expressed as percentiles of the normal (Gaussian) distribution fit to the 1981–2010 base period data (bottom) for SEP 2018. Analysis is based on station data over land and on SST data over the oceans (top). Anomalies for station data are departures from the 1981–2010 base period means, while SST anomalies are departures from the 1981–2010 adjusted OI climatology. (Smith and Reynolds 1998, *J. Climate*, **11**, 3320-3323). Regions with insufficient data for analysis in both figures are indicated by shading in the top figure only.

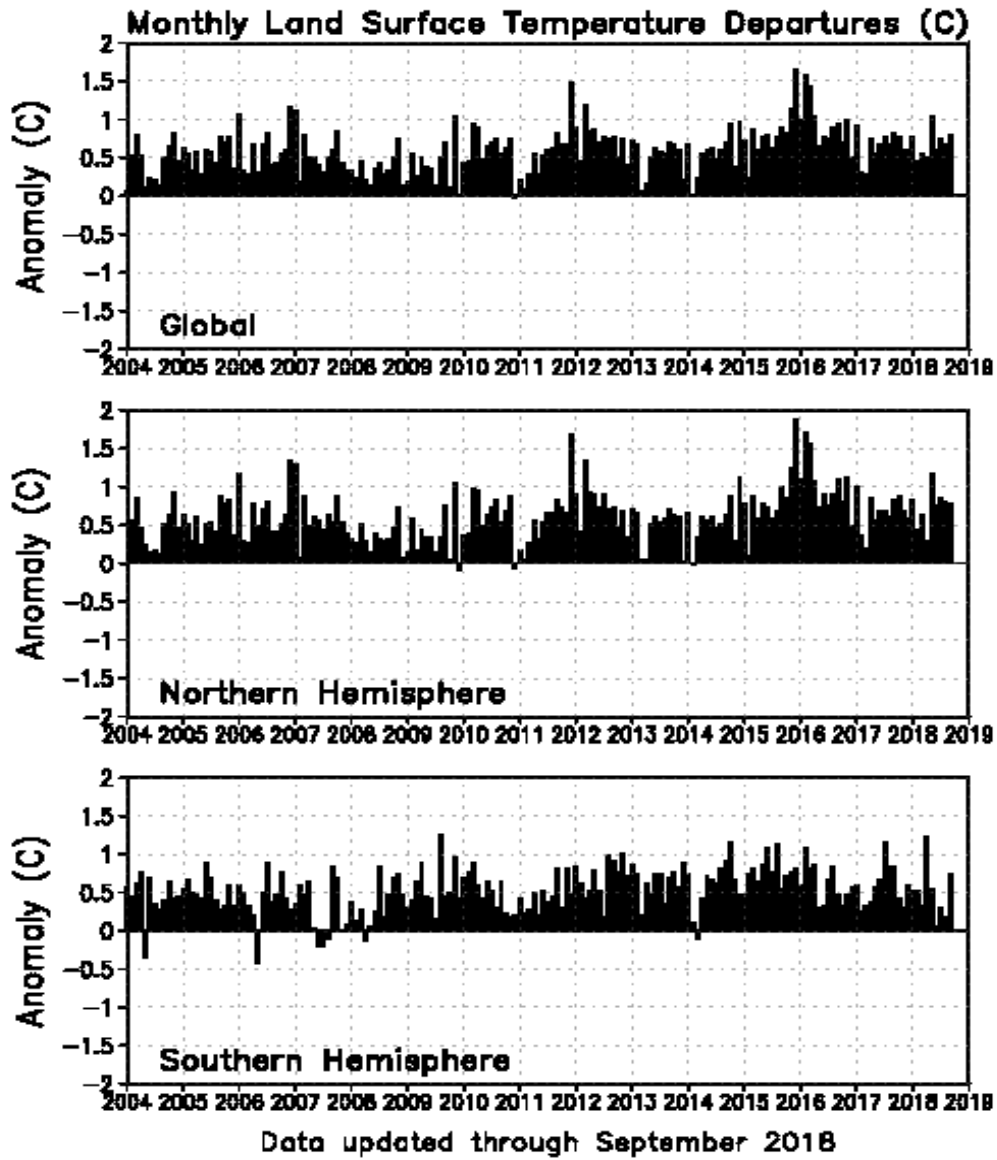


FIGURE E2. Monthly global (top), Northern Hemisphere (middle), and Southern Hemisphere (bottom) surface temperature anomalies (land only, °C) from January 1990 - present, computed as departures from the 1981–2010 base period means.

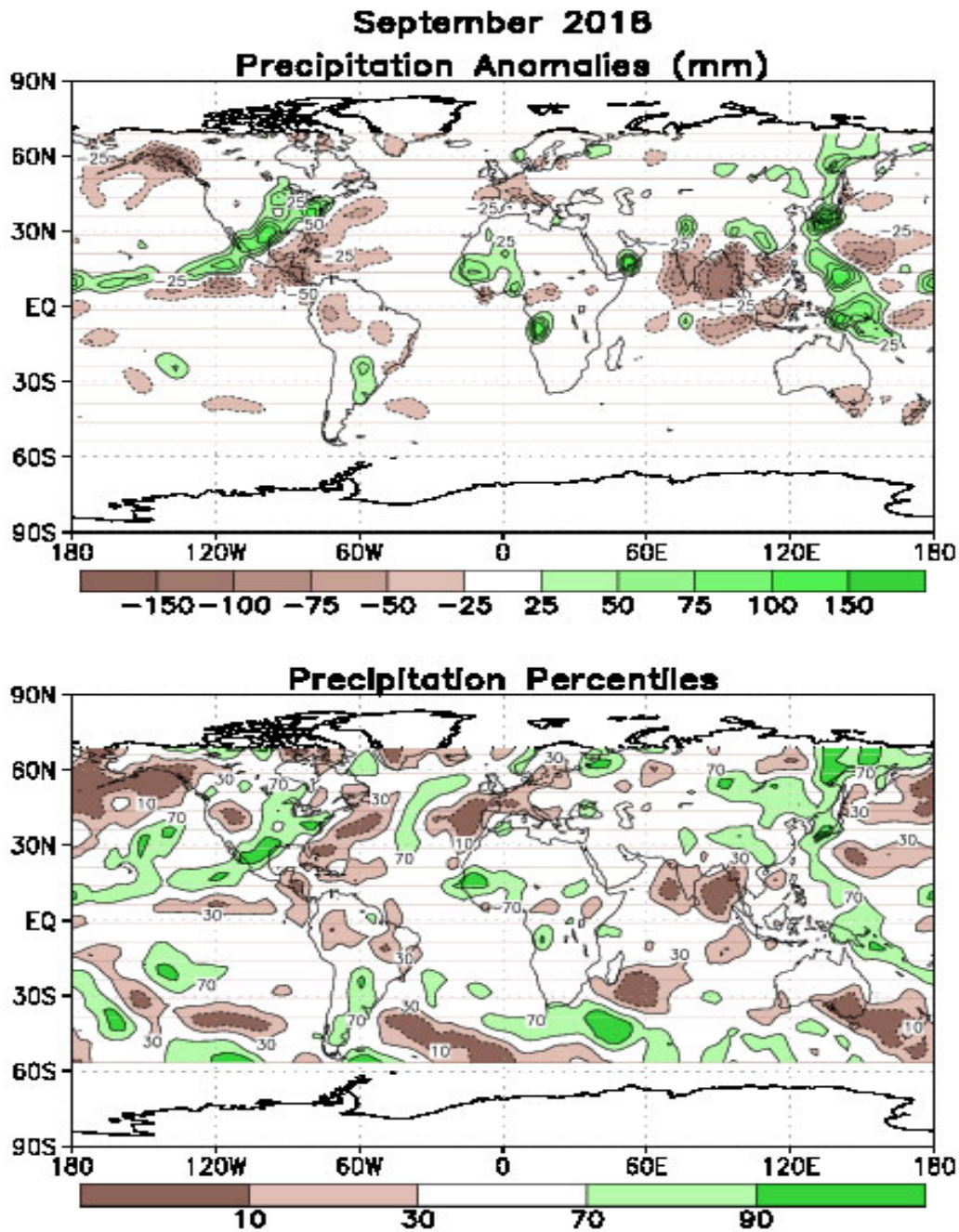


FIGURE E3. Anomalous precipitation (mm, top) and precipitation percentiles based on a Gamma distribution fit to the 1981–2010 base period data (bottom) for SEP 2018. Data are obtained from a merge of raingauge observations and satellite-derived precipitation estimates (Janowiak and Xie 1999, *J. Climate*, 12, 3335–3342). Contours are drawn at 200, 100, 50, 25, -25, -50, -100, and -200 mm in top panel. Percentiles are not plotted in regions where mean monthly precipitation is <5mm/month.



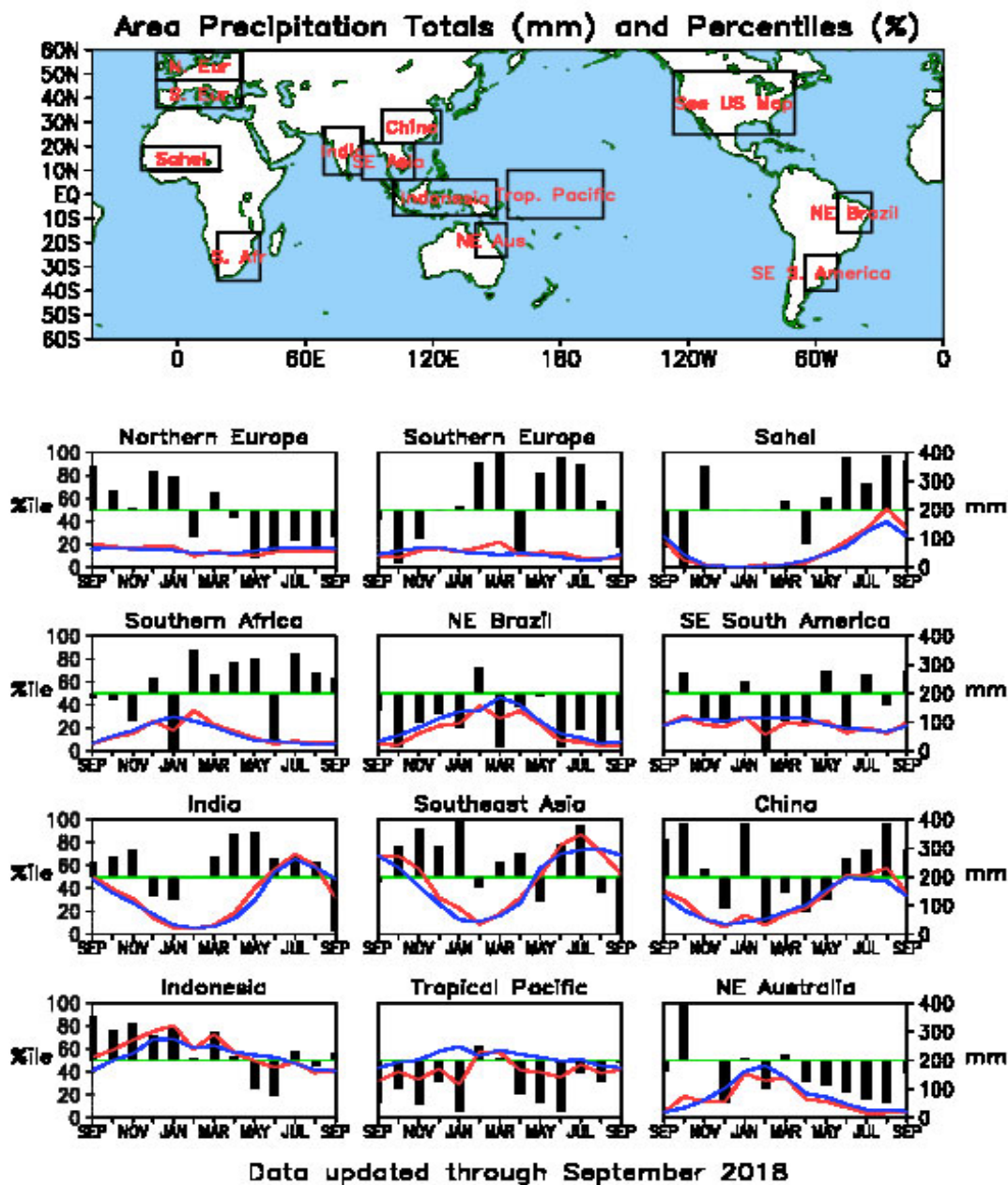


FIGURE E4. Areal estimates of monthly mean precipitation amounts (mm, solid lines) and precipitation percentiles (%) for the most recent 13 months obtained from a merge of raingauge observations and satellite-derived precipitation estimates (Janowiak and Xie 1999, *J. Climate*, 12, 3335–3342). The monthly precipitation climatology (mm, dashed lines) is from the 1981–2010 base period monthly means. Monthly percentiles are not shown if the monthly mean is less than 5 mm.

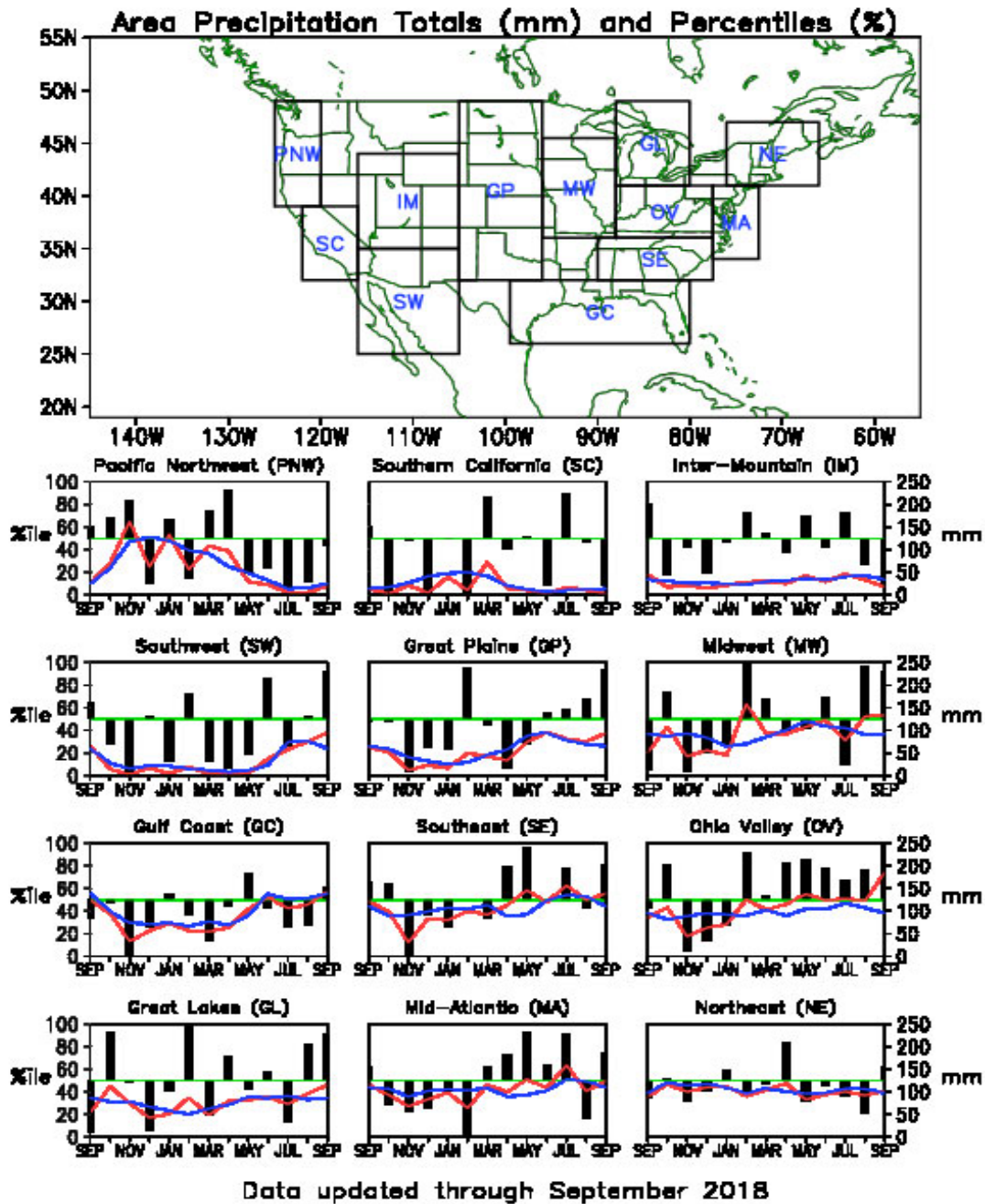


FIGURE E5. Areal estimates of monthly mean precipitation amounts (mm, solid lines) and precipitation percentiles (%) for the most recent 13 months obtained from a merge of raingauge observations and satellite-derived precipitation estimates (Janowiak and Xie 1999, *J. Climate*, 12, 3335–3342). The monthly precipitation climatology (mm, dashed lines) is from the 1981–2010 base period monthly means. Monthly percentiles are not shown if the monthly mean is less than 5 mm.

Monthly Accumulation -- September, 2018

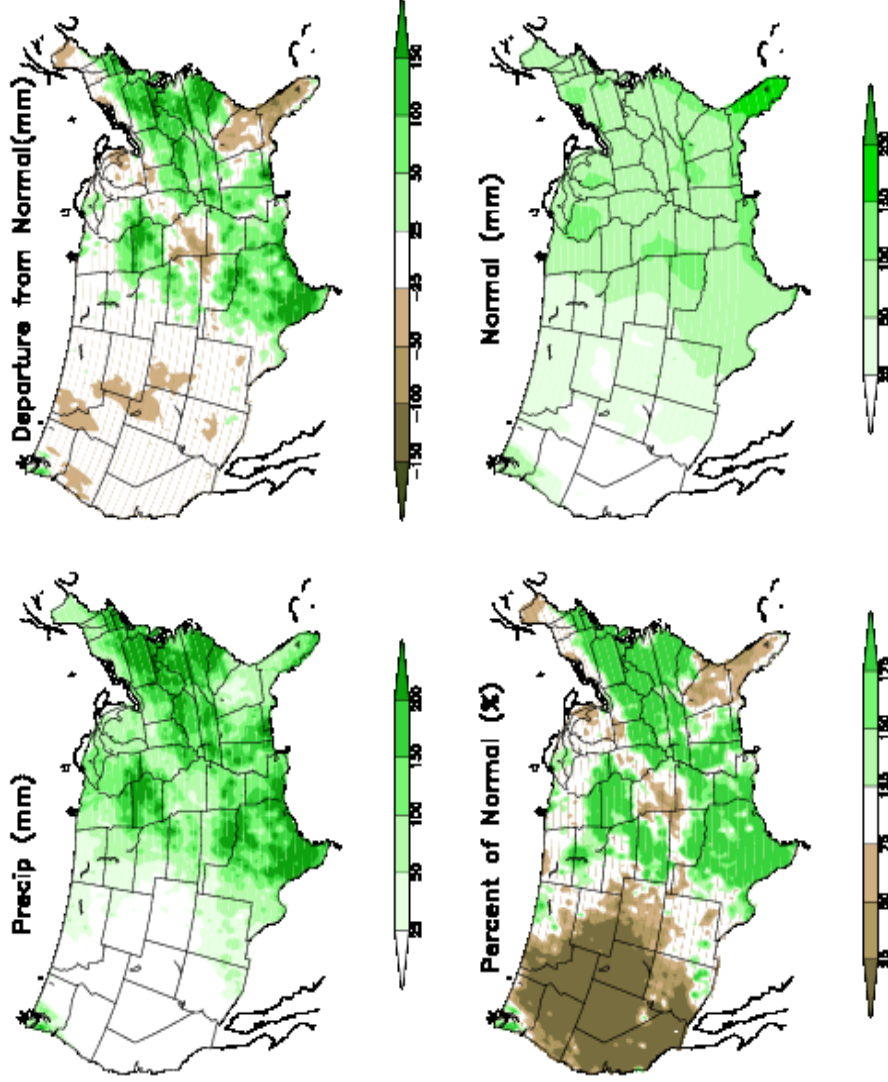
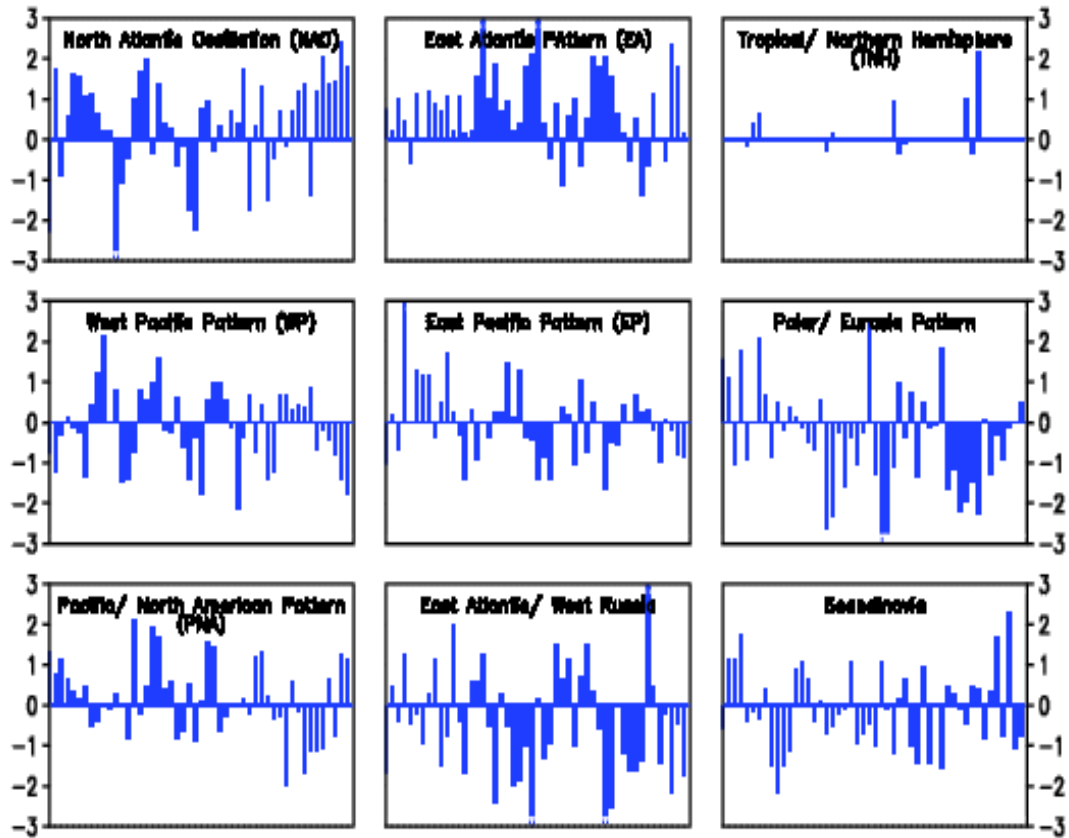


FIGURE E6. Observed precipitation (upper left), departure from average (upper right), percent of average (lower left), and average precipitation (lower right) for SEP 2018. The units are given on each panel. Base period for averages is 1981–2010. Results are based on CPC’s U. S. daily precipitation analysis, which is available at <http://www.cpc.ncep.noaa.gov/products/precip/realtime>.

## Monthly Teleconnection Indices



**Data updated through September 2018**

FIGURE E7. Standardized monthly Northern Hemisphere teleconnection indices. The teleconnection patterns are calculated from a Rotated Principal Component Analysis (RPCA) applied to monthly standardized 500-hPa height anomalies during the 1981-2010 base period. To obtain these patterns, ten leading un-rotated modes are first calculated for each calendar month by using the monthly height anomaly fields for the three-month period centered on that month: [i.e., The July modes are calculated from the June, July, and August standardized monthly anomalies]. A Varimax spatial rotation of the ten leading un-rotated modes for each calendar month results in 120 rotated modes (12 months x 10 modes per month) that yield ten primary teleconnection patterns. The teleconnection indices are calculated by first projecting the standardized monthly anomalies onto the teleconnection patterns corresponding to that month (eight or nine teleconnection patterns are seen in each calendar month). The indices are then solved for simultaneously using a Least-Squares approach. In this approach, the indices are the solution to the Least-Squares system of equations which explains the maximum spatial structure of the observed height anomaly field during the month. The indices are then standardized for each pattern and calendar month independently. No index value exists when the teleconnection pattern does not appear as one of the ten leading rotated EOF's valid for that month.

**September 2018**  
**Sea-Level Pressure and Anomaly**

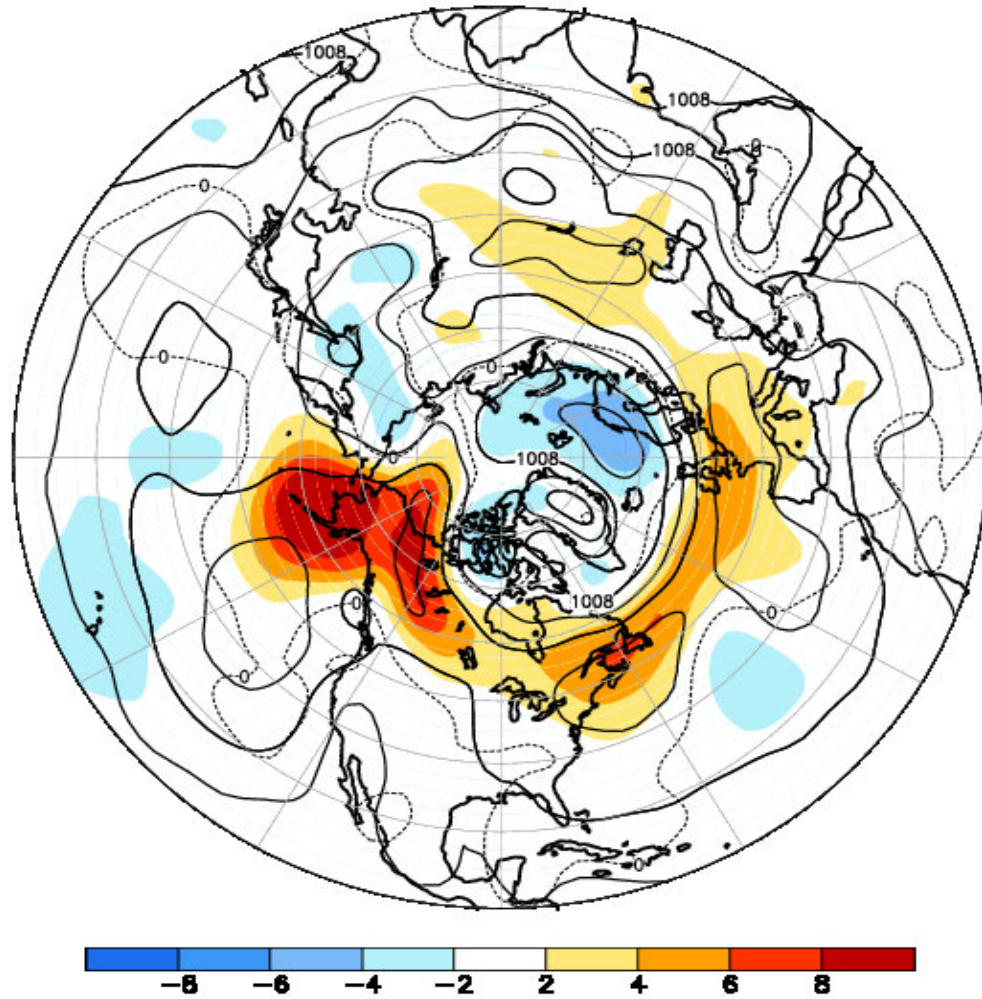


FIGURE E8. Northern Hemisphere mean and anomalous sea level pressure (CDAS/Reanalysis) for SEP 2018. Mean values are denoted by solid contours drawn at an interval of 4 hPa. Anomaly contour interval is 2 hPa with values less (greater) than -2 hPa (2 hPa) indicated by dark (light) shading. Anomalies are calculated as departures from the 1981-2010 base period monthly means.

September 2018  
500-hPa Height and Anomaly

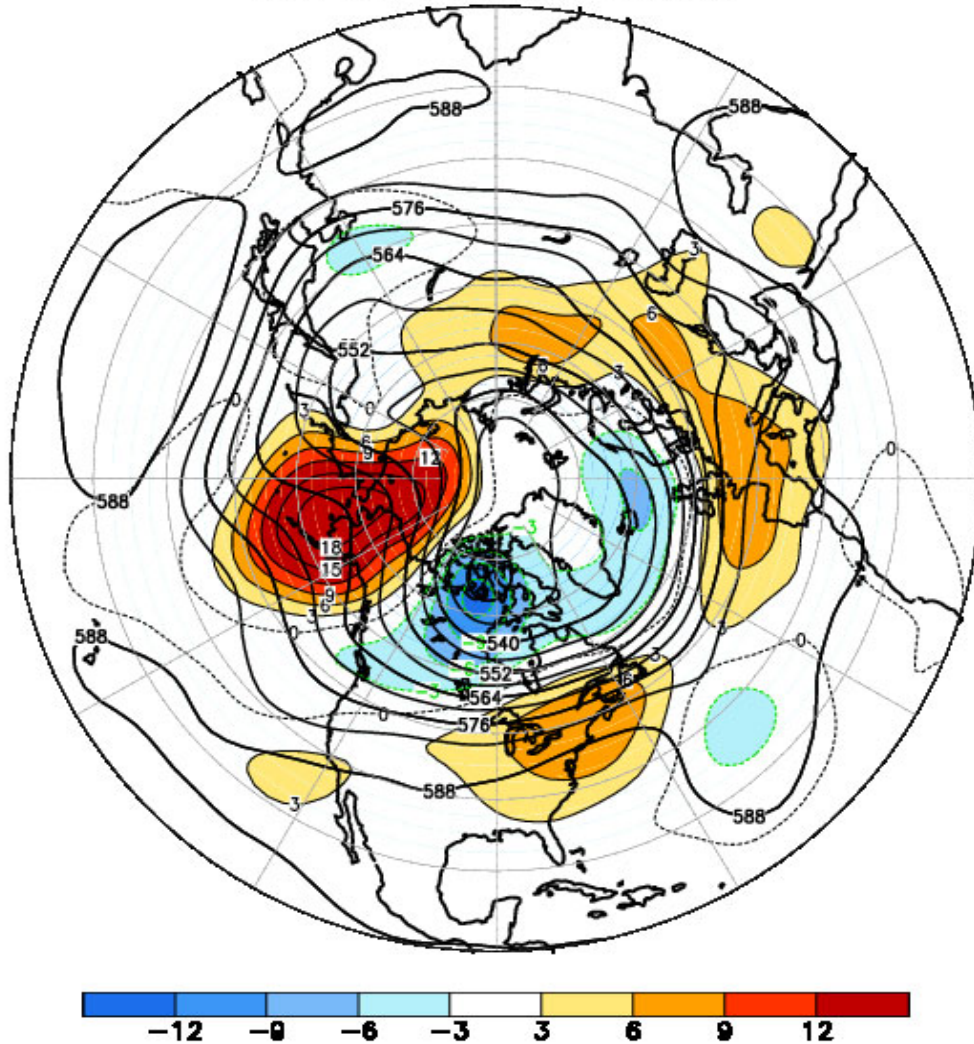


FIGURE E9. Northern Hemisphere mean and anomalous 500-hPa geopotential height (CDAS/Reanalysis) for SEP 2018. Mean heights are denoted by solid contours drawn at an interval of 6 dam. Anomaly contour interval is 3 dam with values less (greater) than -3 dam (3 dam) indicated by dark (light) shading. Anomalies are calculated as departures from the 1981-2010 base period monthly means.

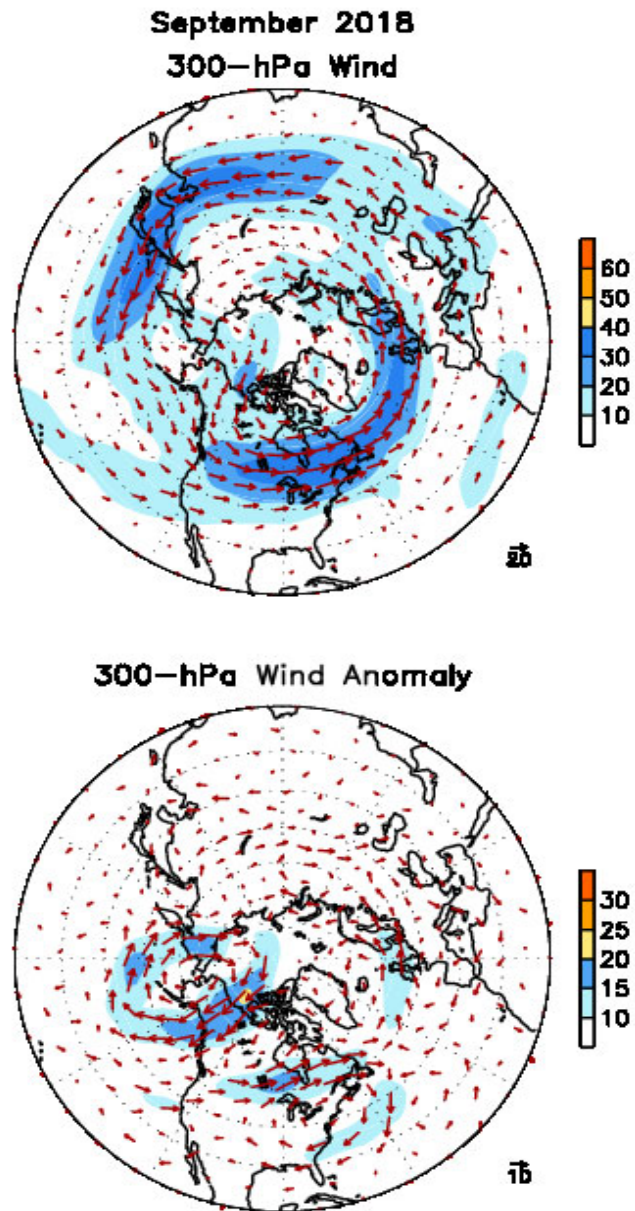


FIGURE E10. Northern Hemisphere mean (left) and anomalous (right) 300-hPa vector wind (CDAS/Reanalysis) for SEP 2018. Mean (anomaly) isotach contour interval is 10 (5)  $\text{ms}^{-1}$ . Values greater than 30  $\text{ms}^{-1}$  (left) and 10  $\text{ms}^{-1}$  (rights) are shaded. Anomalies are departures from the 1981-2010 base period monthly means.

**September 2018**  
**500-hPa: Percentage of Anomaly Days**

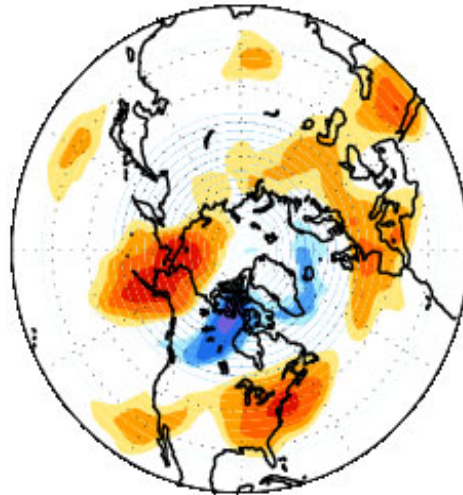


FIGURE E11. Northern Hemisphere percentage of days during SEP 2018 in which 500-hPa height anomalies greater than 15 m (red) and less than -15 m (blue) were observed. Values greater than 70% are shaded and contour in-



**September 2018**  
**500-hPa Height Anomalies: 40°N**

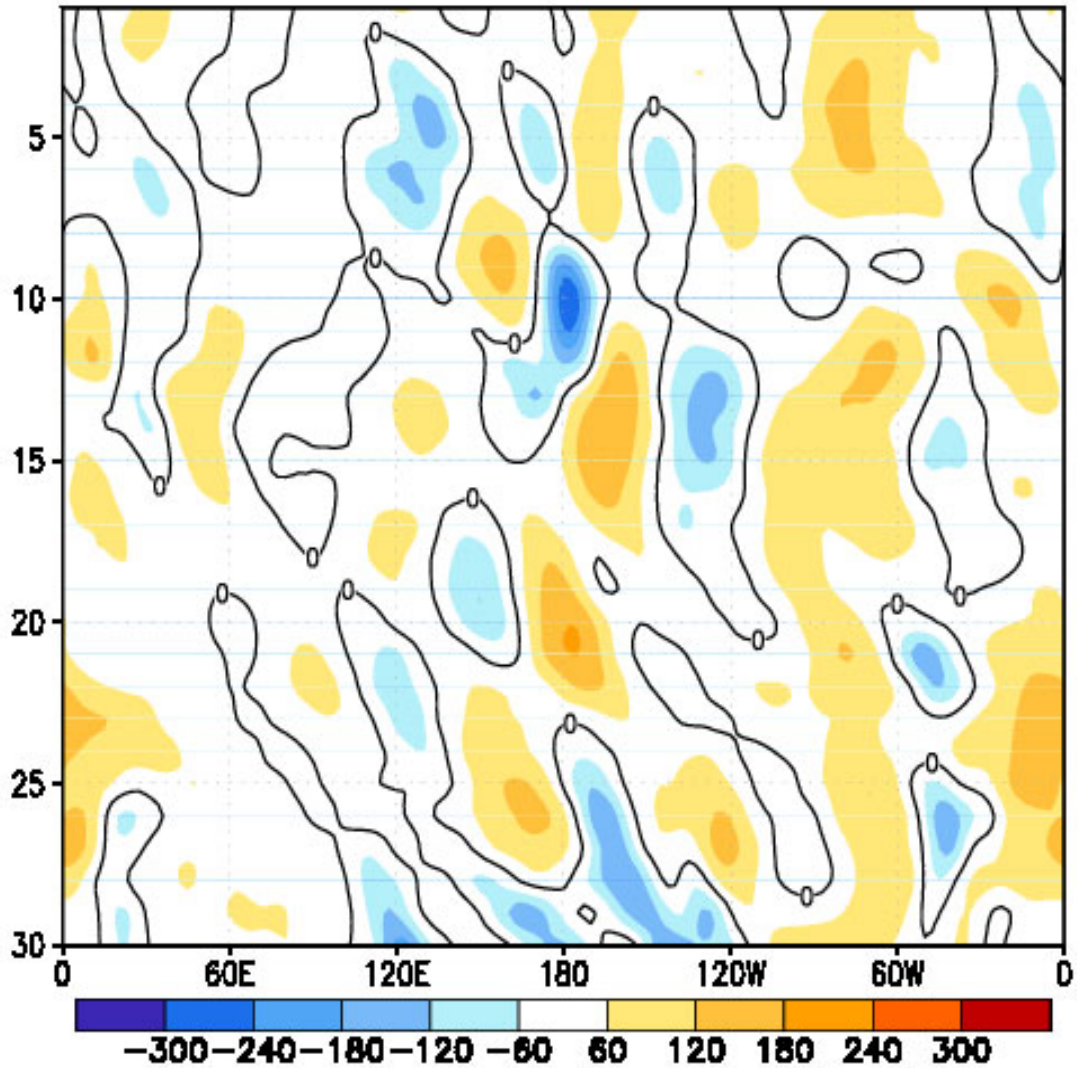
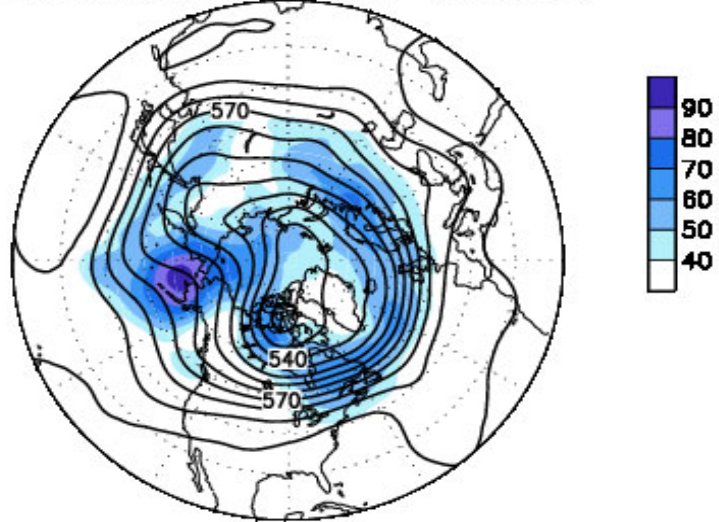


FIGURE E12. Northern Hemisphere: Daily 500-hPa height anomalies for SEP 2018 averaged over the 5° latitude band centered on 40°N. Positive values are indicated by solid contours and dark shading. Negative values are indicated by dashed contours and light shading. Contour interval is 60 m. Anomalies are departures from the 1981-2010 base period daily means.

**September 2018**  
**500-hPa Heights (Contours)**  
**High Frequency Std. Dev. (Shading)**



**500-hPa Heights (Contours)**  
**Normalized High Frequency Variance (Shading)**

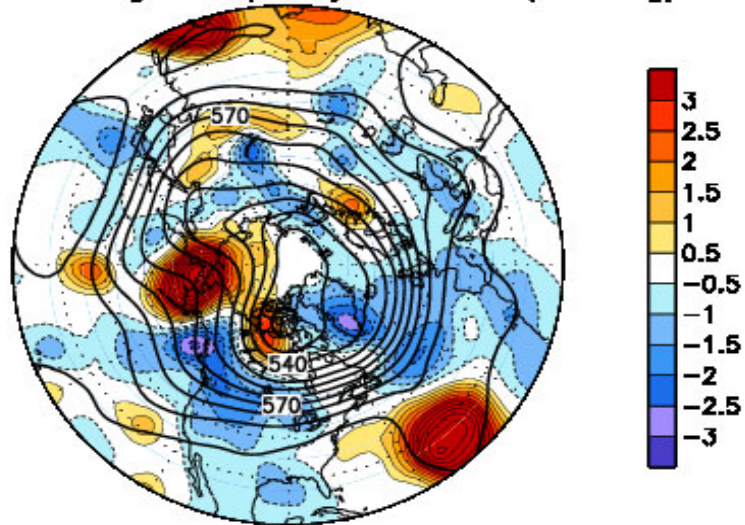


FIGURE E13. Northern Hemisphere 500-hPa heights (thick contours, interval is 6 dam) overlaid with (Top) Standard deviation of 10-day high-pass (HP) filtered height anomalies and (Bottom) Normalized anomalous variance of 10-day HP filtered height anomalies. A Lanczos filter is used to calculate the HP filtered anomalies. Anomalies are departures from the 1981-2010 daily means.

**September 2018**  
**Sea-Level Pressure and Anomaly**

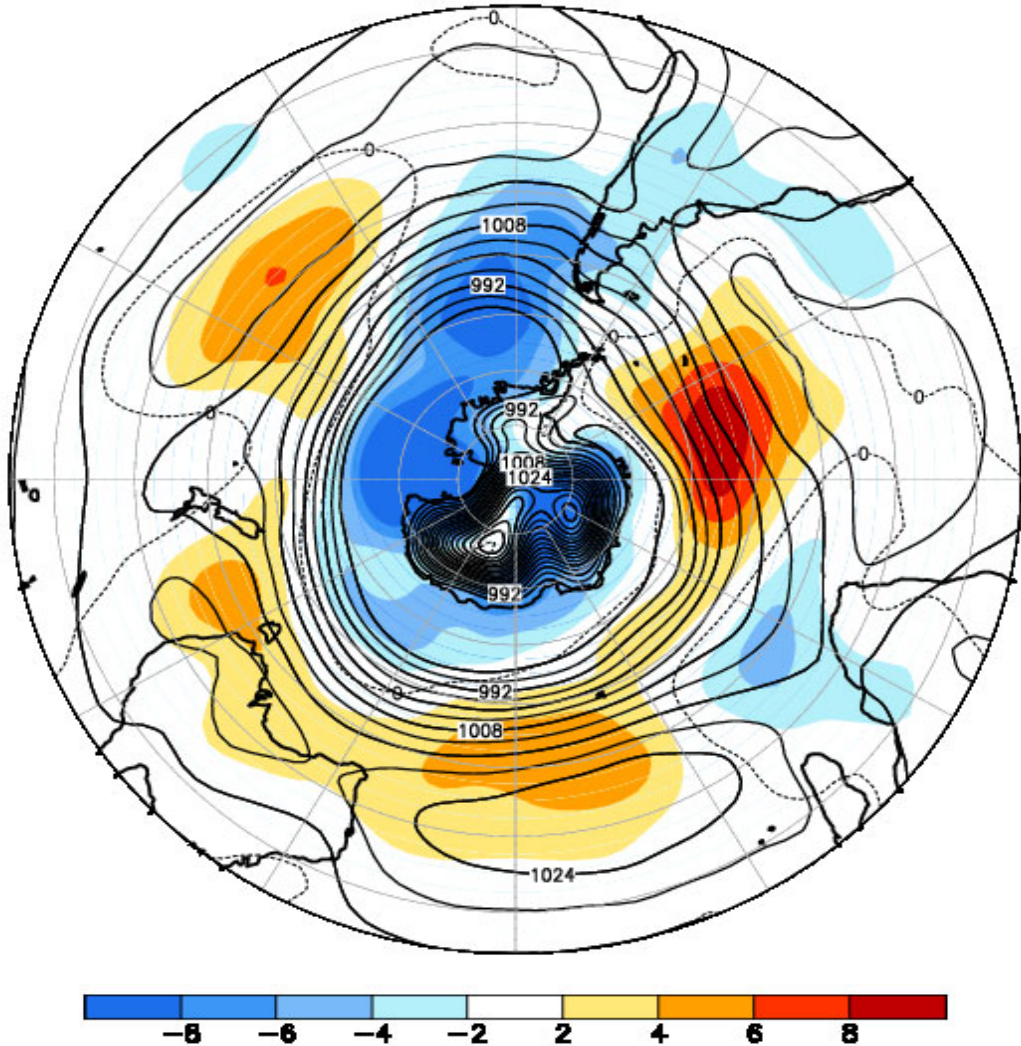


FIGURE E14. Southern Hemisphere mean and anomalous sea level pressure(CDAS/Reanalysis) for SEP 2018. Mean values are denoted by solid contours drawn at an interval of 4 hPa. Anomaly contour interval is 2 hPa with values less (greater) than -2 hPa (2 hPa) indicated by dark (light) shading. Anomalies are calculated as departures from the 1981-2010 base period monthly means.

**September 2018**  
**500-hPa Height and Anomaly**

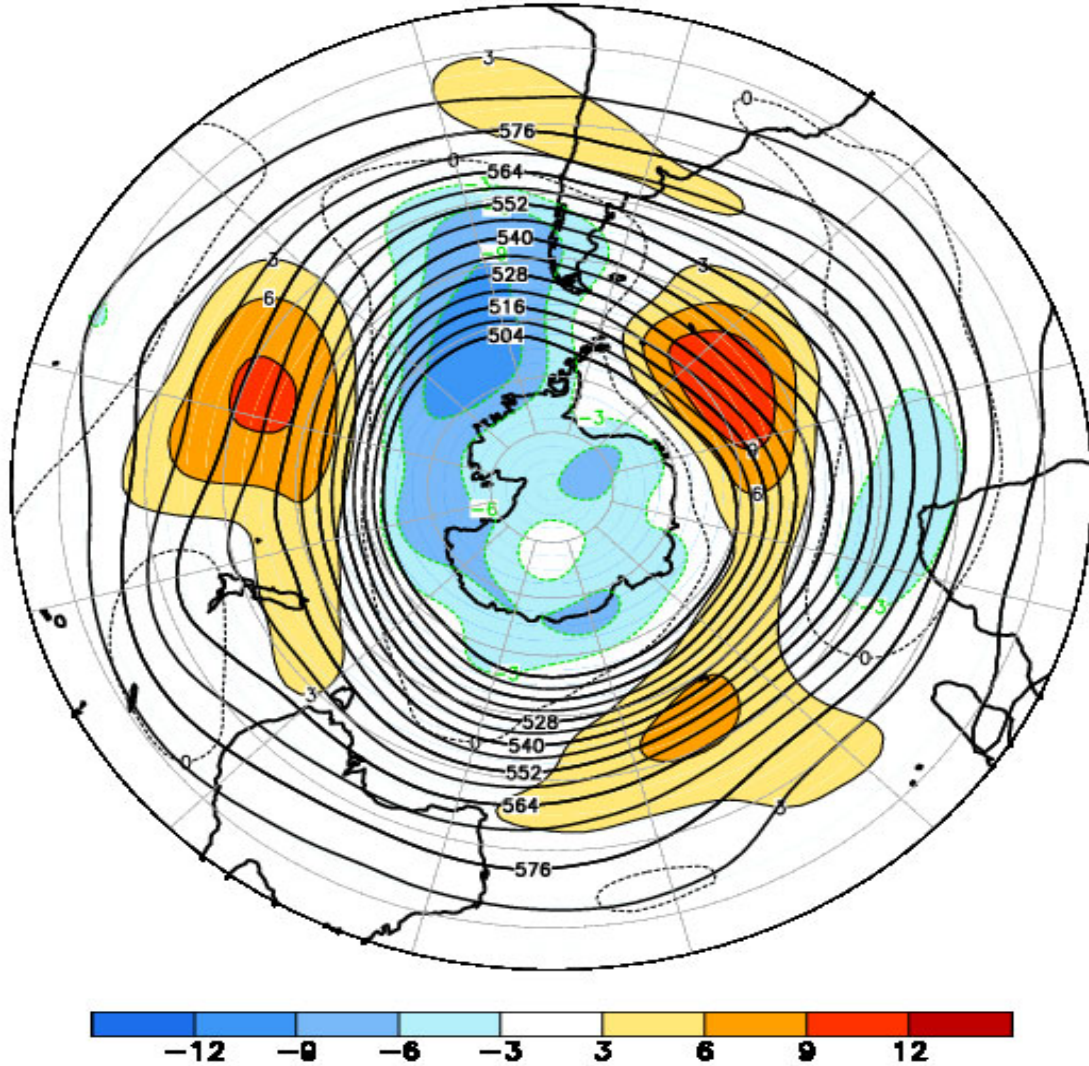


FIGURE E15. Southern Hemisphere mean and anomalous 500-hPa geopotential height (CDAS/Reanalysis) for SEP 2018. Mean heights are denoted by solid contours drawn at an interval of 6 dam. Anomaly contour interval is 3 dam with values less (greater) than -3 dam (3 dam) indicated by dark (light) shading. Anomalies are calculated as departures from the 1981-2010 base period monthly means.

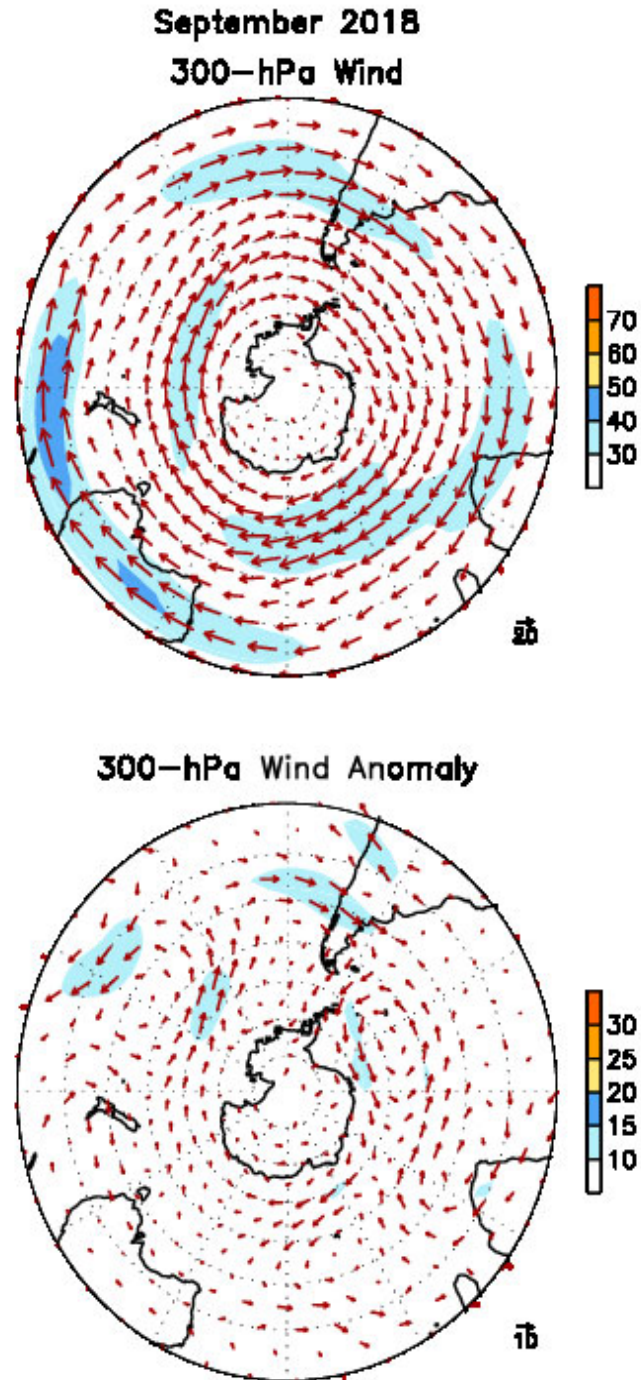


FIGURE E16. Southern Hemisphere mean (left) and anomalous (right) 300-hPa vector wind (CDAS/Reanalysis) for SEP 2018. Mean (anomaly) isotach contour interval is 10 (5)  $\text{ms}^{-1}$ . Values greater than 30  $\text{ms}^{-1}$  (left) and 10  $\text{ms}^{-1}$  (rights) are shaded. Anomalies are departures from the 1981-2010 base period monthly means.

**September 2018**  
**500-hPa: Percentage of Anomaly Days**

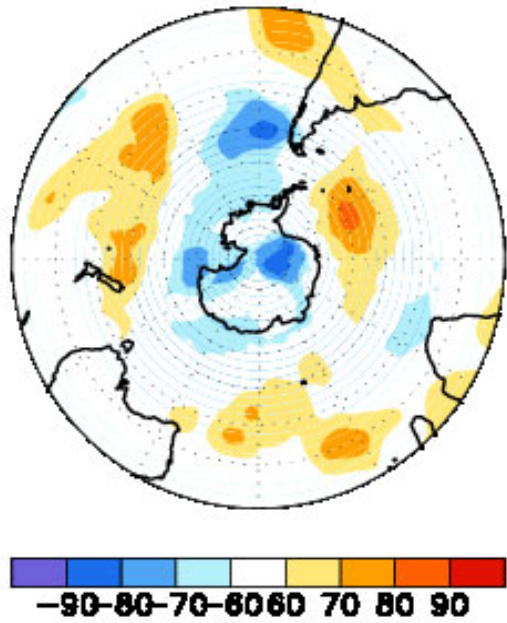


FIGURE E17. Southern Hemisphere percentage of days during SEP 2018 in which 500-hPa height anomalies greater than 15 m (red) and less than -15 m (blue) were observed. Values greater than 70% are shaded and contour in-

**September 2018  
500-hPa Height Anomalies: 40°S**

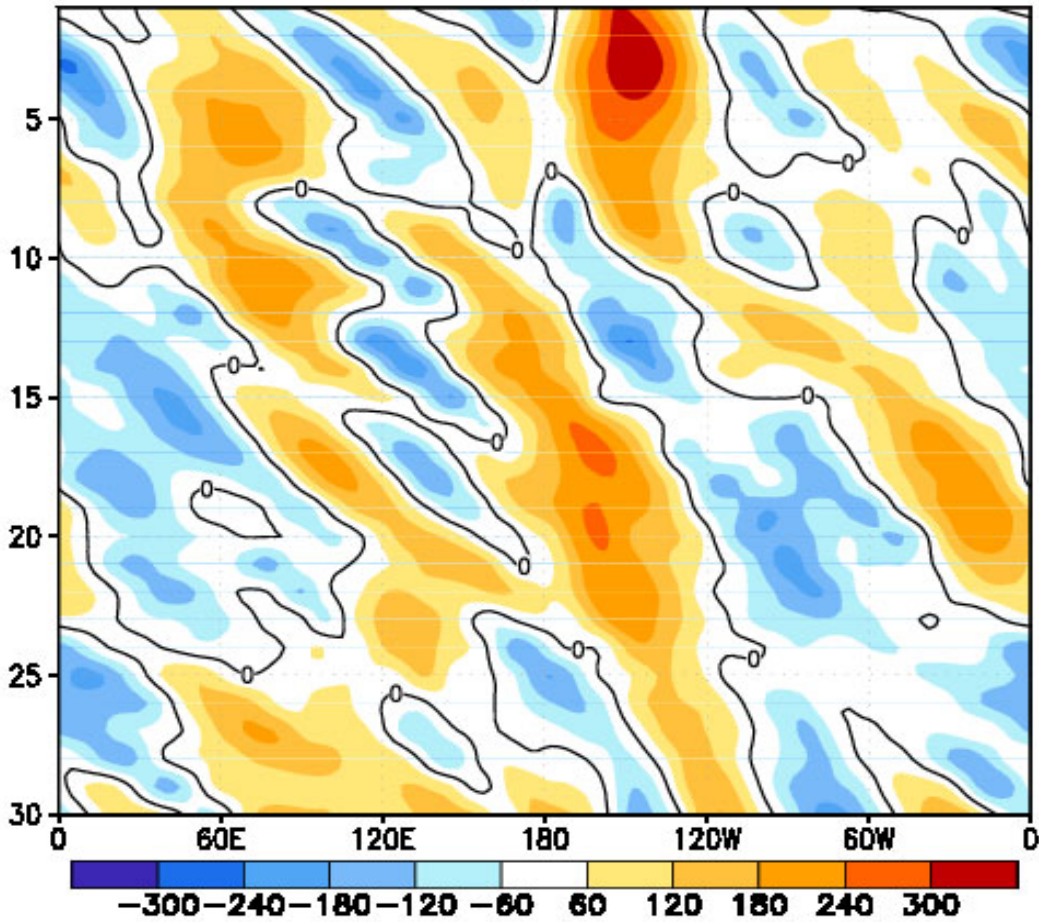


FIGURE E18. Southern Hemisphere: Daily 500-hPa height anomalies for SEP 2018 averaged over the 5° latitude band centered on 40°S. Positive values are indicated by solid contours and dark shading. Negative values are indicated by dashed contours and light shading. Contour interval is 60 m. Anomalies are departures from the 1981-2010 base period daily means.

**September 2018  
Height Anomalies**

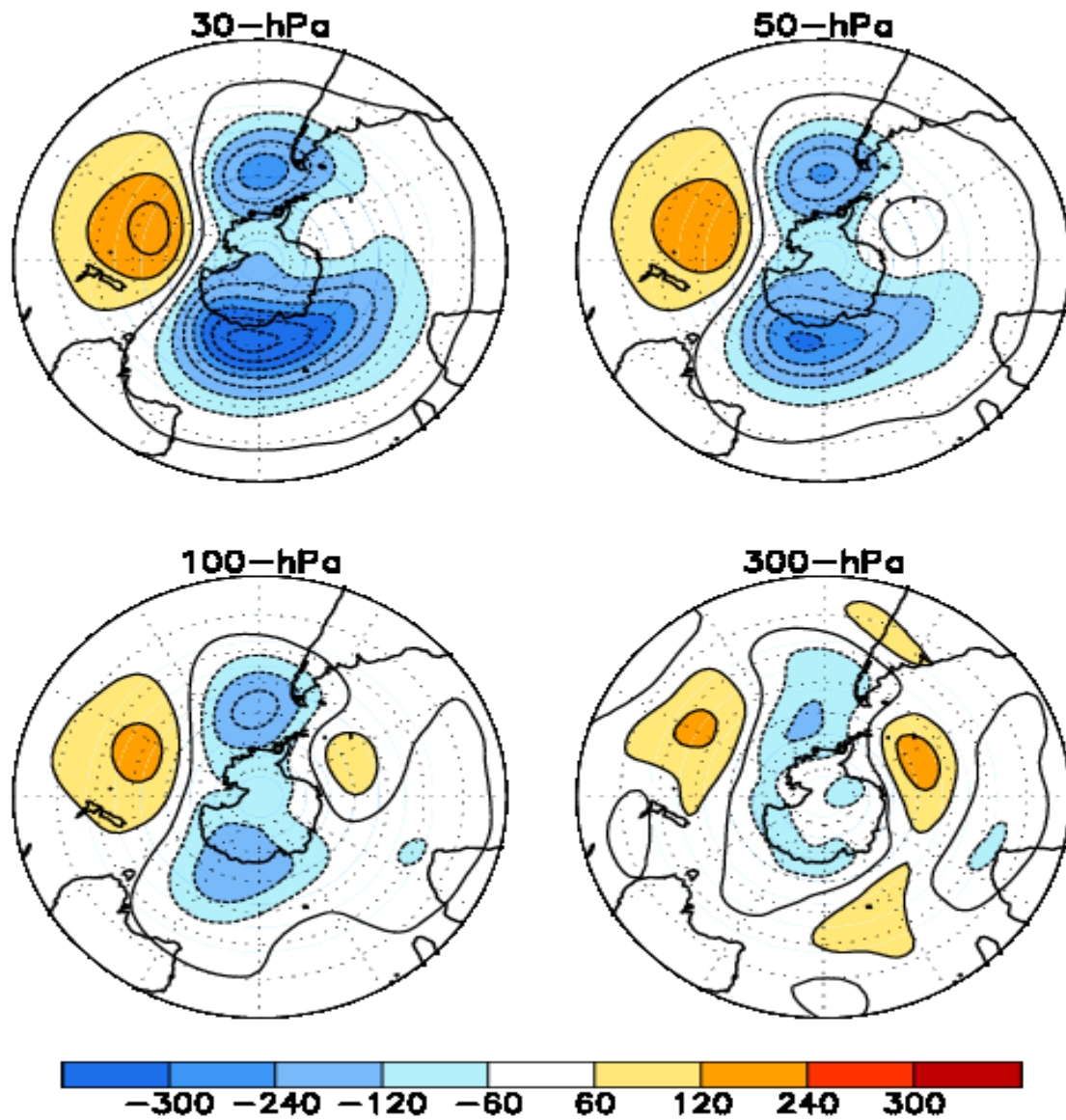


FIGURE S1. Stratospheric height anomalies (m) at selected levels for SEP 2018. Positive values are indicated by solid contours and dark shading. Negative values are indicated by dashed contours and light shading. Contour interval is 60 m. Anomalies are calculated from the 1981-2010 base period means. Winter Hemisphere is shown.



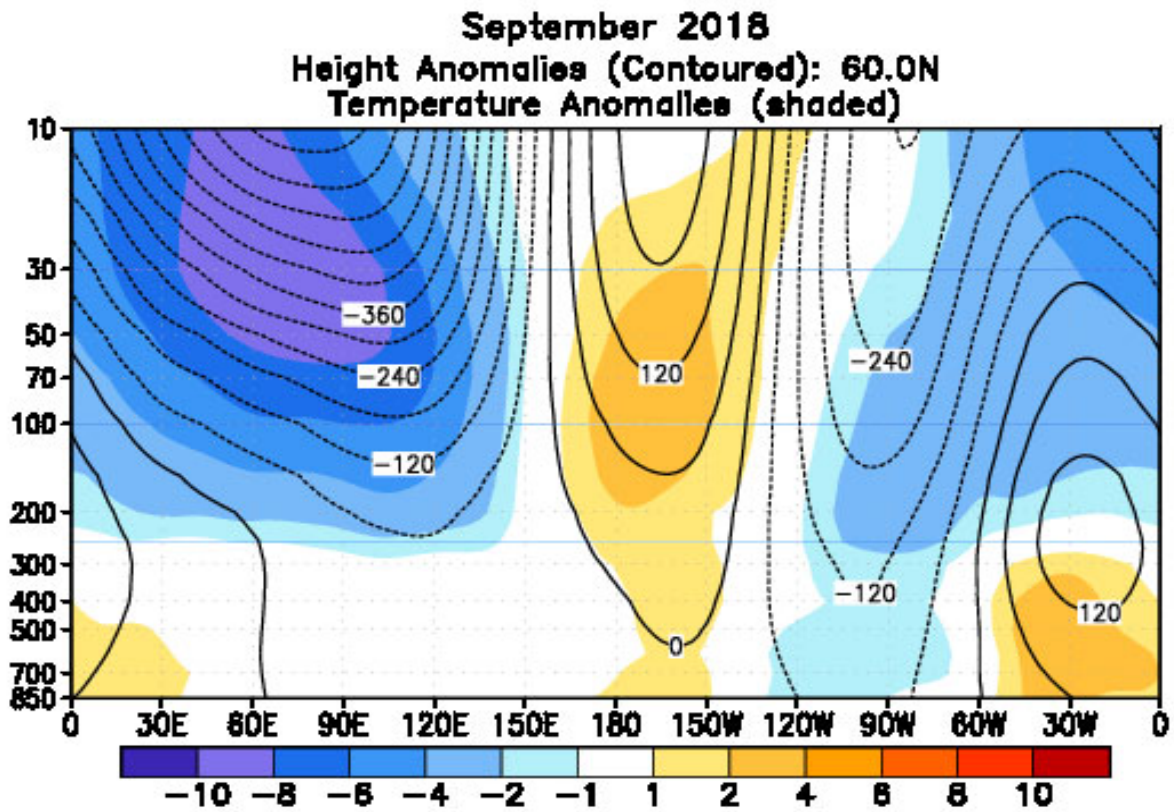


FIGURE S2. Height-longitude sections during SEP 2018 for height anomalies (contour) and temperature anomalies (shaded). In both panels, positive values are indicated by solid contours and dark shading, while negative anomalies are indicated by dashed contours and light shading. Contour interval for height anomalies is 60 m and for temperature anomalies is 2°C. Anomalies are calculated from the 1981-2010 base period monthly means. Winter Hemisphere is shown.

## 50hPa JAS Mean Temperature Anomalies

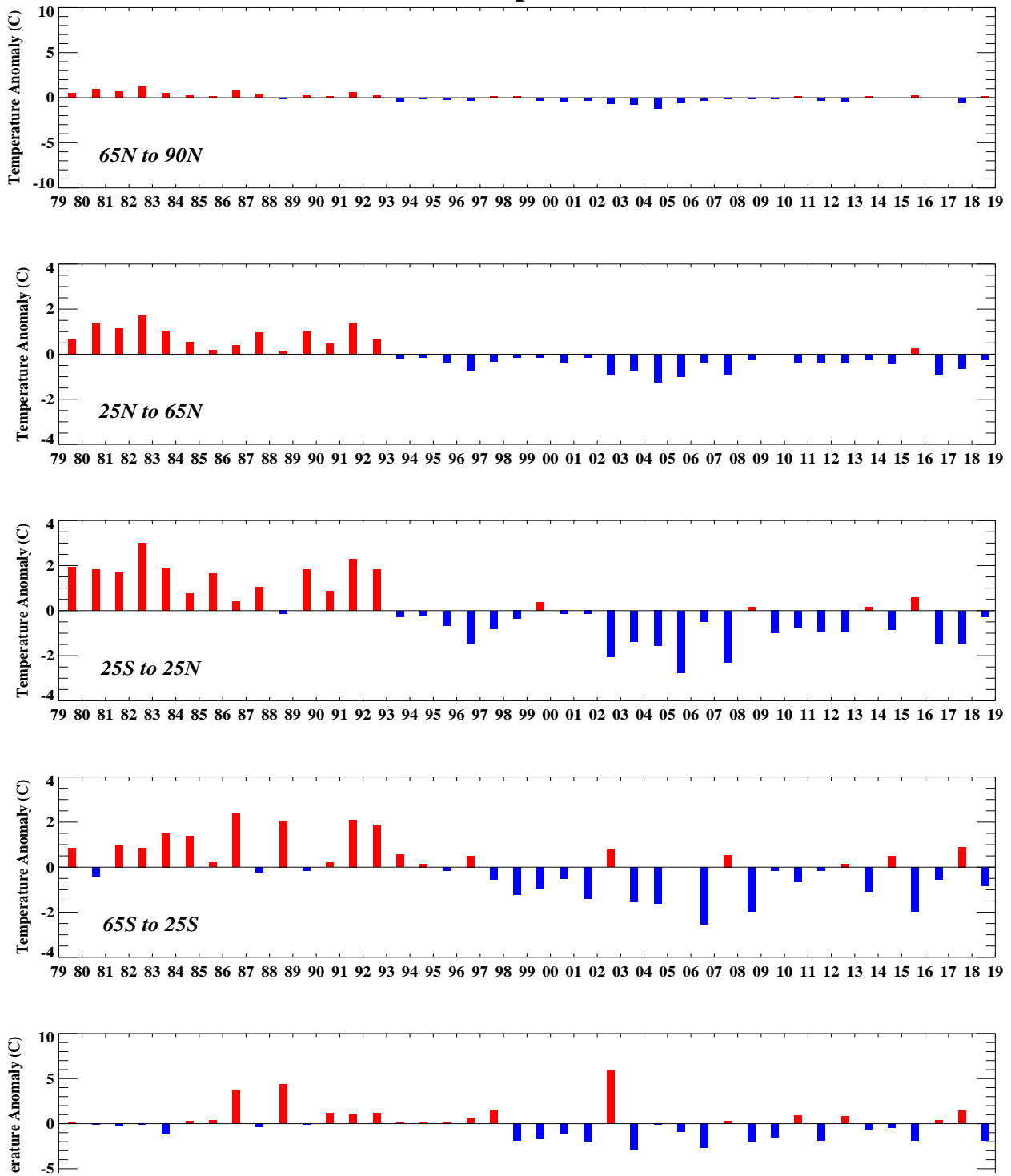


FIGURE S3. Seasonal mean temperature anomalies at 50-hPa for the latitude bands 65°–90°N, 25°–65°N, 25°N–25°S, 25°–65°S, 65°–90°S. The seasonal mean is comprised of the most recent three months. Zonal anomalies are taken from the mean of the entire data set.

### Zonal Mean Temperature for 2017 & 2018

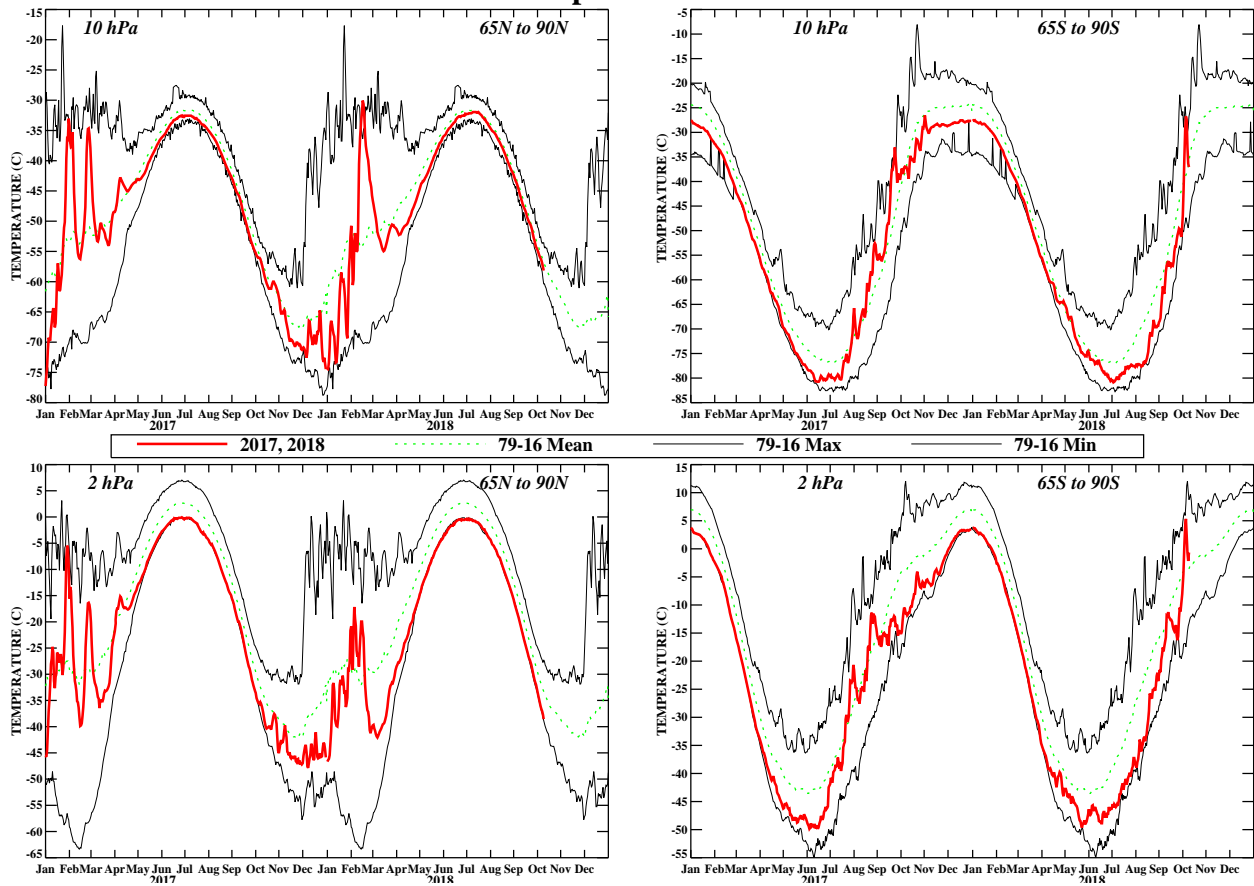


FIGURE S4. Daily mean temperatures at 10-hPa and 2-hPa (thick line) in the region 65°–90°N and 65°–90°S for the past two years. Dashed line depicts the 1981–2010 base period daily mean. Thin solid lines depict the daily extreme maximum and minimum temperatures.

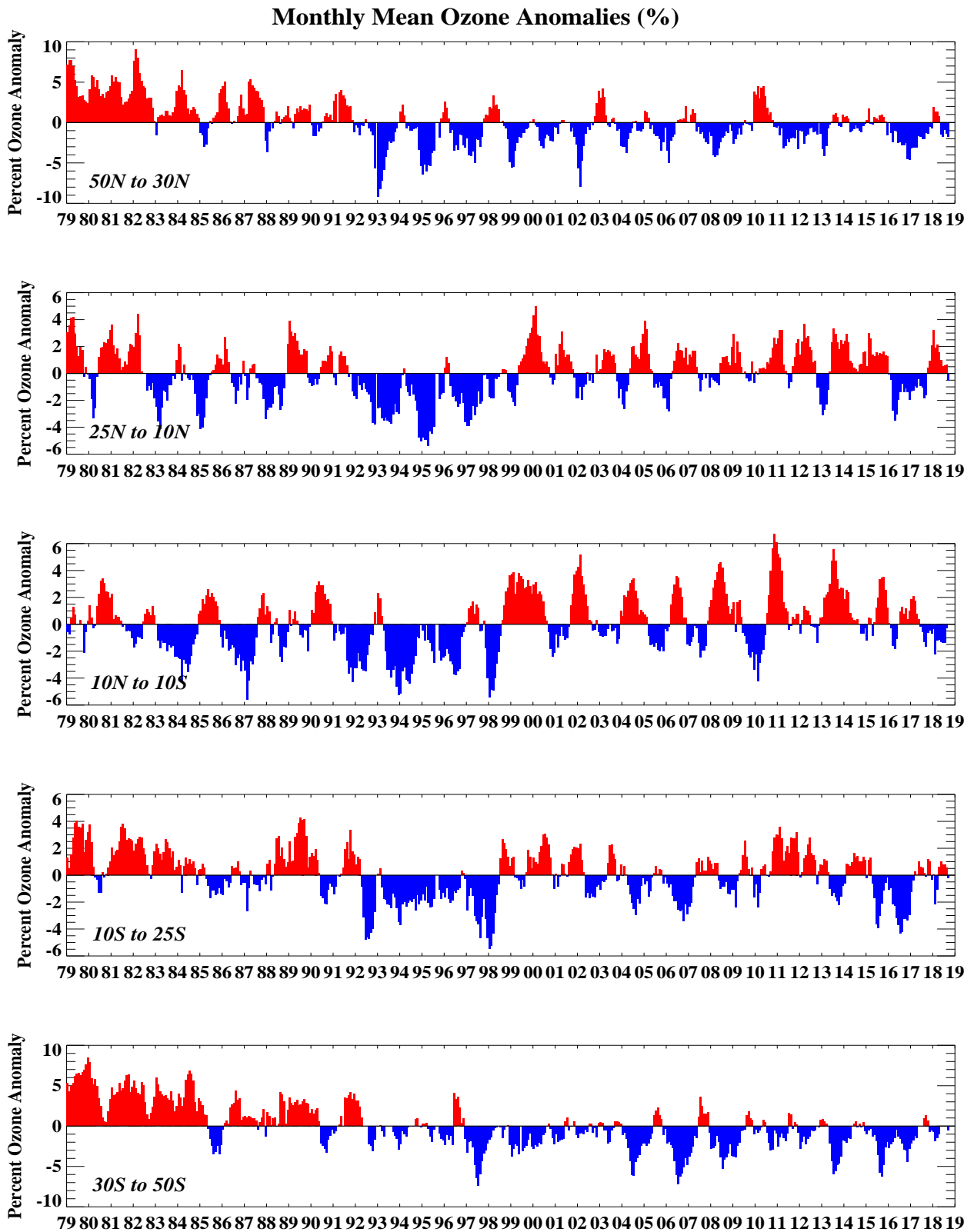


FIGURE S5. Monthly ozone anomalies (percent) from the long term monthly means for five zones: 50N-30N (NH mid-latitudes), 25N-10N (NH tropical surf zone), 10N-10S (Equatorial-QBO zone), 10S-25S (SH tropical surf zone), and 30S-50S (SH mid-latitudes). The long term monthly means are determined from the entire data set

**SEPTEMBER PERCENT DIFF (2018 - AVG[79-86])**

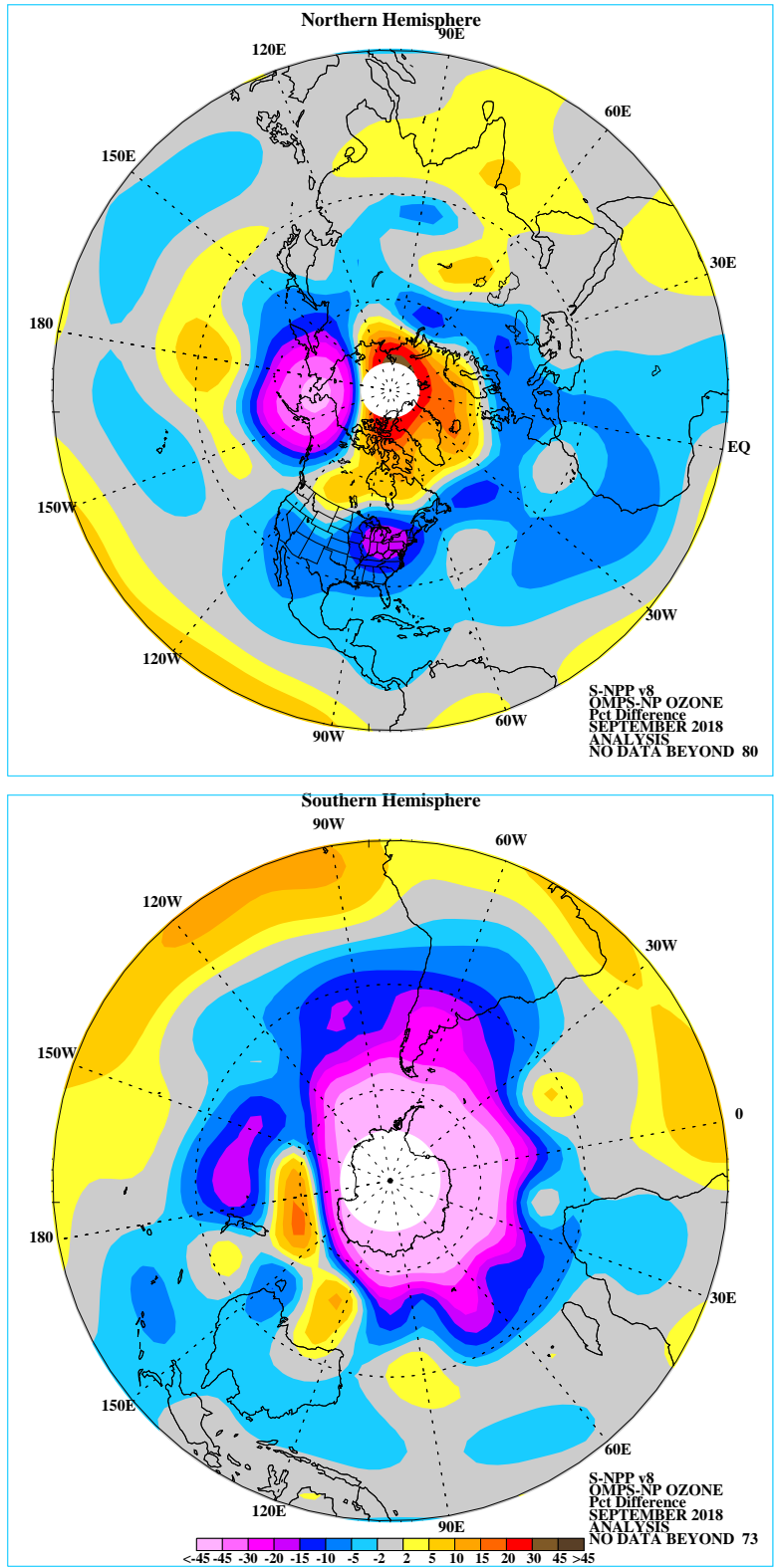


FIGURE S6. Northern (top) and Southern (bottom) Hemisphere total ozone anomaly (percent difference from monthly mean for the period 1979-1986). The region near the winter pole has no SBUV/2 data.

# Fz at 100 hPa (Sep. 2018)

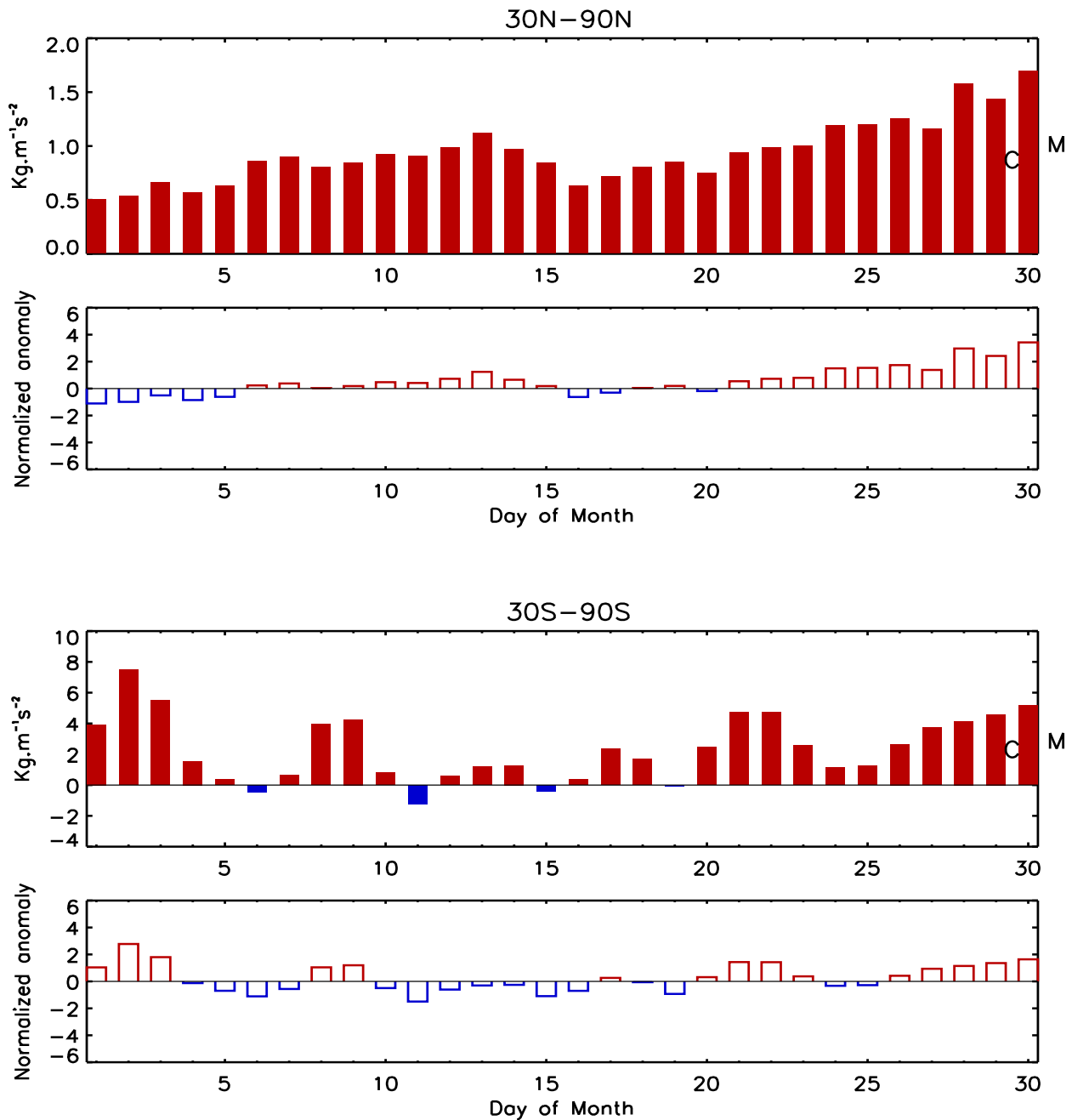


FIGURE S7. Daily vertical component of EP flux (which is proportional to the poleward transport of heat or upward transport of potential energy by planetary wave) at 100 hPa averaged over (top) 30°N–90°N and (bottom) 30°S–90°S for SEP 2018. The EP flux unit ( $\text{kg m}^{-1} \text{s}^{-2}$ ) has been scaled by multiplying a factor of the Brunt Vaisala frequency divided by the Coriolis parameter and the radius of the earth. The letter ‘M’ indicates the current monthly mean value and the letter ‘C’ indicates the climatological mean value. Additionally, the normalized departures from the monthly climatological EP flux values are shown.

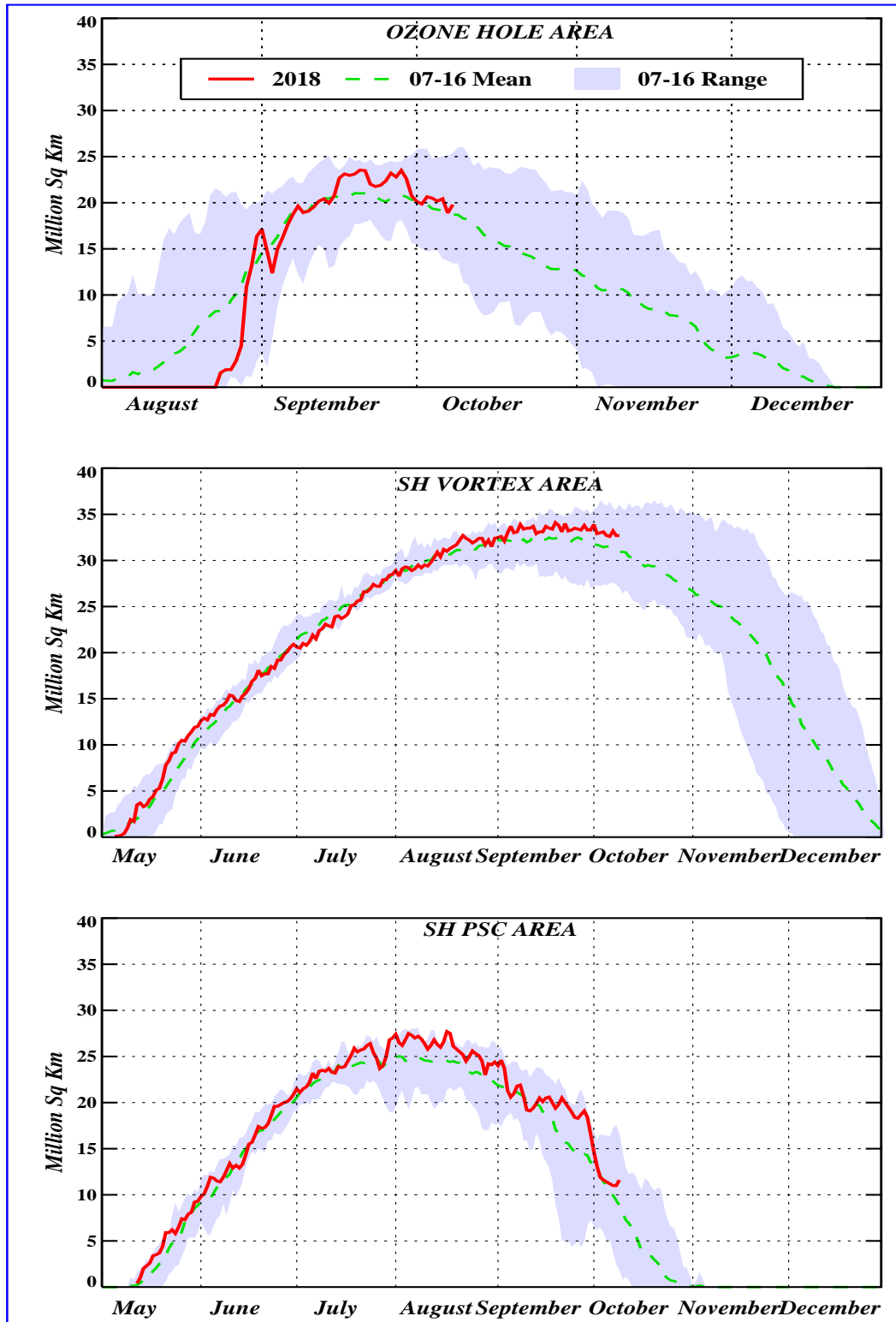


FIGURE S8. Daily time series showing the size of the SH polar vortex (representing the area enclosed by the 32 PVU contour on the 450K isentropic surface), and the areal coverage of temperatures < -78C on the 450K isentropic surface.

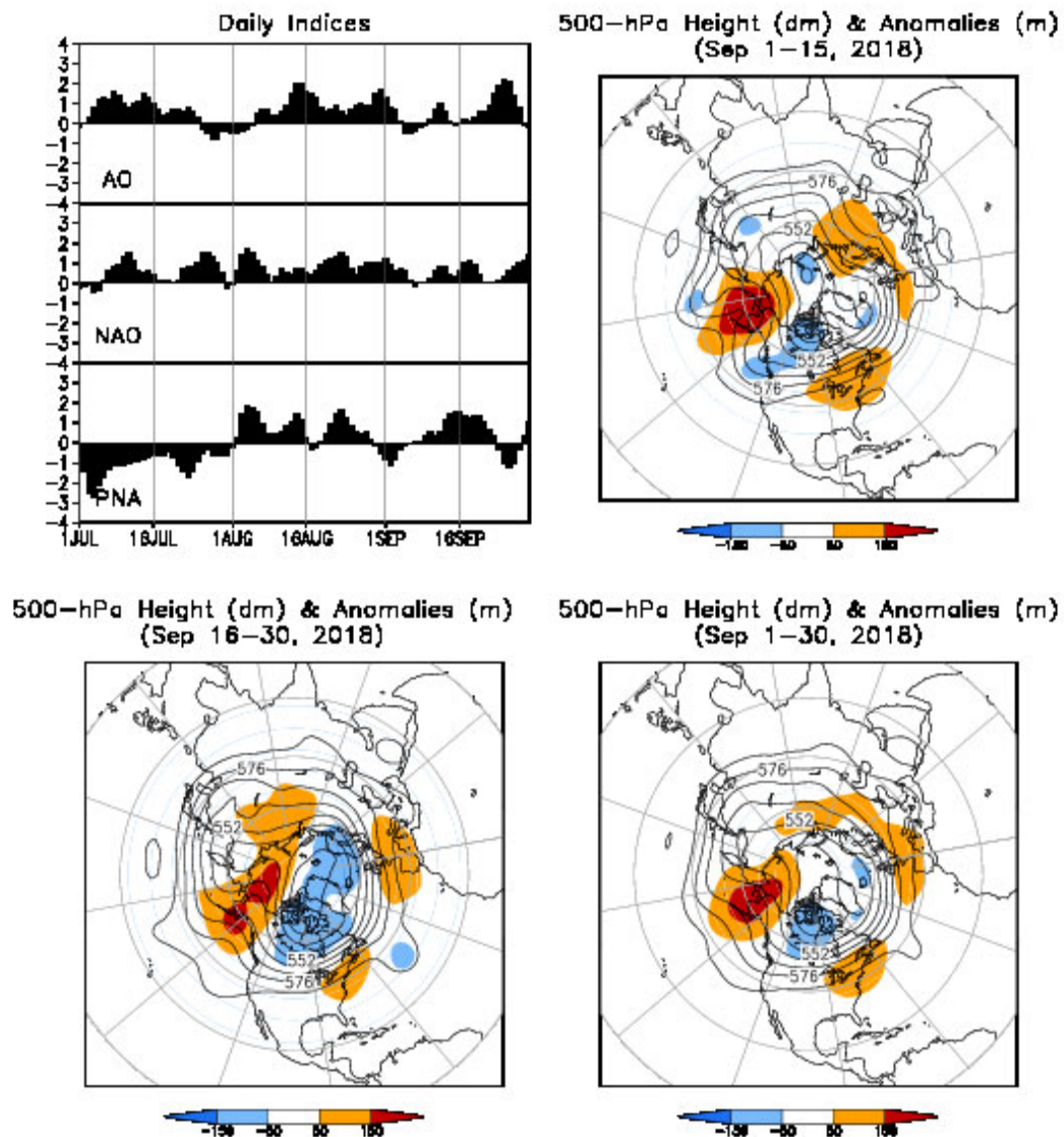


FIGURE A2.1. (a) Daily amplitudes of the Arctic Oscillation (AO) the North Atlantic Oscillation (NAO), and the Pacific-North American (PNA) pattern. The pattern amplitudes for the AO, (NAO, PNA) are calculated by projecting the daily 1000-hPa (500-hPa) height anomaly field onto the leading EOF obtained from standardized time-series of daily 1000-hPa (500-hPa) height for all months of the year. The base period is 1981–2010.

(b-d) Northern Hemisphere mean and anomalous 500-hPa geopotential height (CDAS/Reanalysis) for selected periods during SEP 2018 are shown in the remaining 3 panels. Mean heights are denoted by solid contours drawn at an interval of 8 dam. Dark (light) shading corresponds to anomalies greater than 50 m (less than -50 m). Anomalies are calculated as departures from the 1981-2010 base period daily means.



**SSM/I Snow Cover for Sep 2018  
anomaly based on departure from 1987-2010 baseline**

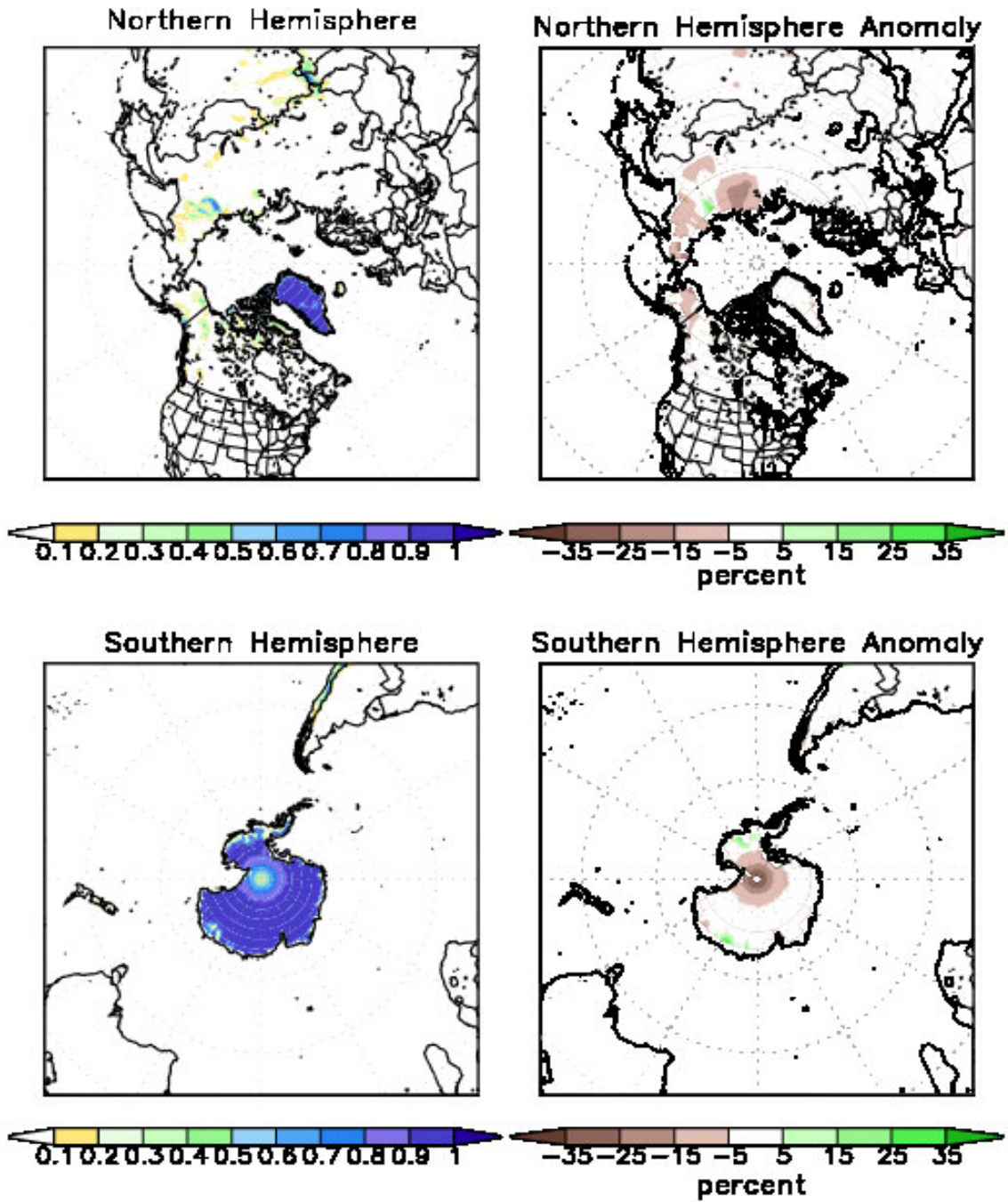


FIGURE A2.2. SSM/I derived snow cover frequency (%) (left) and snow cover anomaly (%) (right) for the month of SEP 2018 based on 1987 - 2010 base period for the Northern Hemisphere (top) and Southern Hemisphere (bottom). It is generated using the algorithm described by Ferraro et. al, 1996, Bull. Amer. Meteor. Soc., vol 77, 891-905.